INVESTIGATION OF LUNAR AND TERRESTRIAL MATERIALS FOR ALKALI METAL DEGRADATION

A DISSERTATION SUBMITTED TO THE GRADUATE DIVISION OF THE UNIVERSITY OF HAWAII IN PARTIAL FULFILLMENT OF THE REQUIREMENTS FOR THE DEGREE OF

DOCTOR OF PHILOSOPHY

IN CHEMISTRY

DECEMBER 1970

By

James Victor Derby

Dissertation Committee:

John J. Naughton, Chairman
Robert W. Buddemeier
Arthur T. Hubbard
Richard G. Inskeep
Gordon A. Macdonald

We certify that we have read this dissertation and that in our opinion it is satisfactory in scope and quality for the degree of Doctor of Philosophy in Chemistry.

DISSERTATION COMMITTEE

John J. Vaughan
Chairman

Gordon A. Macdonald

Richard G. Brabeep

Arthur Hubbard

Robert W. Buddemeier

TABLE OF CONTENTS

Page

Page

Page

LIST OF TABLES

LIST OF ILLUSTRATIONS

I. INTRODUCTION

A. Purpose of Research

For centuries, scientists and philosophers have been intrigued by the cosmogony of the earth. Men realized that much of the earth's early features and the geochemical processes causing them have been obliterated by the action of the hydrosphere, atmosphere, and biosphere, and they have looked to the heavens for additional information. In recent years technological advances have enabled scientists to examine lunar material, which may provide the key to understanding the fundamental processes of planetary accretion. The distribution of lunar material to the scientific community led to many studies of the properties and characteristics of this material. The purpose of this research was to probe the enigma of the lunar regolith, or soil layer, using basic analytical techniques as the mode of inquiry.

Of particular interest was the possibility that alkali comminution played a role in lunar erosion. By investigating lunar samples and similar terrestrial materials, it was anticipated that information would be derived which would lead to a partial evaluation of the following points:

1) the mechanism of release of alkalis from volcanic materials under vacuum at various temperatures,
2) the vapor composition of the released alkalis
3) the mechanism of alkali metal comminution of polycrystalline rocks,

4) consideration of the extent to which alkali erosion may have occurred on the lunar surface.

Finally, the development of analytical techniques of sample treatment and analysis have been an important and necessary part of this investigation.

B. Historical Review and Background

1. Familiar Processes Acting on the Lunar Surface

Prior to the Apollo 11 and 12 missions, several conclusions concerning the nature of the lunar surface were drawn from indirect measurements. The loss of crater clarity with age was one of the earliest observations that showed that one or several processes were fragmenting the lunar surface (1). Trask and Rowan (2), in their observations of the lunar orbiter photographs, reported that fresh craters were gradually destroyed and darkened with time. Six mechanisms were commonly accepted as playing a role in the fragmentation of the lunar surface: meteorite impact, micrometeorite infall, radiation effects, internal seismic shock, volcanism, and thermal fracture.

Terrestrial meteorite craters and hypervelocity impact experiments demonstrate the scope of possible pulverization from meteorite impact. Impacting pulverized the target material and ejected a portion of the breccia to form a crater. In the laboratory, Moore and Gault (3) found that ejecta mass was approximately 10^2 times the mass of the projectile. Bjork's calculations (4) of the mass of the projectile that produced Meteor Crater, Arizona show ejecta:mass ratios of 10^3 at a

meteorite velocity of 11km./sec. and $10^{3.4}$ at a velocity of 73km./sec. Whipple (5) suggested 10^3 was a good estimation of the ejecta:mass ratio for lunar meteorite impacts on a soil surface at a median velocity of 15-20km./sec. Though meteoritic impact was a potent mechanism for pulverization, examination of the lunar fines indicate that it contained only a very small percentage of meteoritic and brecciated materials (6). This amount of material probably could not completely account for a lunar maria regolith of 3 to 6 meters thick (7).

Simple micrometeorite infall, as opposed to impact pulverization, was proposed as an explanation for a fine-grain blanket of material on the lunar surface. This seemed highly unlikely, as a source of soil, since most of the lunar fines appeared to be degradation products of the crystalline rocks present on the lunar surface (6).

Gold (8) proposed that X-rays and ultraviolet radiation acted in such a way as to break down rock grains into particles of minute size, but there was no experimental evidence given. Pulverization of certain minerals by particular radiation was reported by Fairbairn and Hurley (9), but this phenomena occurred from internal sources of radiation. Atomic sputtering rather than comminution could be produced by particulate bombardment, but Wehner (10) reported that most of the sputtered atoms should escape into space. Fisher's study (11) of the space erosion of meteorites concluded that neither particulate nor electromagnetic radiation is significant as an erosive agent.

Seismic shock produced by internal lunar disturbances had been suggested by Gilvarry (12) as an erosion mechanism. Although Sutton (13) reported that seismic shocks were present and would tend to reduce steep slopes to the angle of repose, the amount of pulverization over the entire lunar surface could not be large, because crustal movement and brecciation should be localized along linear fracture zones. From the geometry of the lunar crustal fractures surrounding the circular maria, it appeared that much of the lunar seismic activity must have been related to meteorite impact.

Green (14) proposed a surface layer composed of volcanic ash and other volcanic ejecta. Though the Apollo 11 findings (7) showed the importance of volcanism early in the lunar history, e.g. during the formation of the maria, there was no evidence of widespread recent volcanism. Alter (15) pointed out, that Kozynov's observation of a gas cloud in Alphonsus was not an observation of a volcanic eruption in the generally accepted sense. Kozynov estimated gas pressures of 10^{-9} atmospheres at the vortex of the crater, which was indicative of internal degassing rather than an erupting volcano. The Apollo 12 mission (6) returned an anomalous sample (#12013) which was judged by some to be a volcanic ash sample. However, this was exceptional and was not generally observed on the lunar surface. It should be understood, that though volcanism was not an active agent on the lunar surface in recent times, it could have been the major stimulus for the soil-producing mechanism during the lunar past.

The rapid and extreme changes in lunar surface temperature permitted by the lack of a detectable atmosphere suggested thermal fracture as an effective pulverization mechanism. However, Ryan's experimental evidence (16) showed that such temperature changes would not produce appreciable thermal fracture. Under terrestrial conditions a much more limited temperature range resulted in rock breakage only because of the presence of water, which undergoes a relatively darge volume change at 0°C. The presence of water in the primeval lunar atmosphere was postulated (17) which would make possible effective thermal fracturing on the moon at that time. This mechanism is not currently operative in lunar soil production, and has not been so for perhaps 4×10^9 years. The Apollo investigations found no water or hydroxyl compounds to indicate water as an erosive agent on the lunar surface (6,7).

2. Evidence for Another Mechanism

The discussion of the six mechanisms commonly called upon to produce a lunar surface layer demonstrated that meteorite impact was the most important of these mechanisms. However, not all of the lunar regolith characteristics could be accounted for by this, or by any combination of all of these mechanisms.

Findings at the Apollo 11 and 12 landing sites (6,7) revealed that rock fragments had a wide variety of shapes and were buried to varying degrees in the lunar fines. A vast majority of the rocks were rounded to subrounded on their

exposed surface. Many of the rounded rocks, were flat or of an irregular angular shape on the buried portions.

Minute, deep pits were found on the rounded surfaces of most rocks. These pits were distinguishable from vesicles and many were lined with glass. Impact pits produced in the laboratory did not resemble these pits, which were probably formed by the same process causing surface rounding.

The impact pits on the coarse to medium-grained rocks were glass-lined and raised above the surface. Apparently, meteoritic impact caused localized melting, followed by some surface process which eroded away the surface, leaving the more resistant glass-lined pits raised above the surface. Some of these glass-lined pits were surrounded by a "halo" of light-colored material that probably arose from condensation or spraying of the volatiles, which emerged during the localized melting caused by impact.

The lunar fines are predominately fine-grained materials that exhibited a certain amount of cohesiveness. The astronauts found that the fines were able to maintain a deformed shape and that clumps of fines were hard to distinguish from rock fragments. In general, the stickiness of the fines proved to be a nuisance during the extravehicular lunar surface activities. Chemical similarity of the fines and rocks indicated that the fines were probably to a large extent degradation products of the crystalline rocks. One important chemical difference which has been noted was the higher potassium content in the fines and breccias.

In summary, the Ranger and Orbiter photographs revealed the existence of an unknown erosion process on the lunar surface. These pictures showed very fresh craters interspersed among smoothed older craters. Surveyor photographs revealed abrasion and rounding of individual rocks on the surface. The surface morphology, glass-lined, raised pits, and splashs of molten material seen on both hard and fragmented rocks during the Apollo missions, suggest that there is a widespread erosional mechanism that is unlike any process previously considered.

3. A Lunar Erosion Hypothesis

In the lunar environment, gaseous alkali metal could be produced from a basaltic surface at elevated temperatures. Widespread magma flooding from volcanism or localized heating from meteorite impact would serve as the heat source. The low partial pressure of oxygen and the large mean free path of the molecules in the lunar atmosphere would insure widespread distribution of the alkali metal over the lunar surface.

Certain volatiles may escape into space from the heated surface materials, but reactive substances such as the alkalis, with large accommodation or sticking coefficients, would remain. Once distribution of alkalis had occurred, it has been found from laboratory experiments that the lunar diurnal temperature cycle would be sufficient to produce significant comminution of surface rocks.

4. Justification of Hypothesis

a. Heat Sources

Prior to the United States lunar program, Naughton (18) argued that volcanism, or lava flooding, under the conditions which existed on the surface of the moon would have given rise to unique reactions. These reactions involved selective volatilization of rock components and a form of rock differentiation which was unlike similar terrestrial phenomena. Eruptions in the lunar vacuum would have been more spectacular than terrestrial volcanism and a great increase in the rate of volatilization would have occurred. The lunar volatiles would have been in a highly reduced state and the large mean free path of molecules in the lunar vacuum would have caused widespread distribution of materials emanating from a molten source. These assumptions were based on laboratory observations of alkali release on vacuum melting of volcanic rocks, the nature of volatilization observed in terrestrial volcanoes and its enhancement under lunar conditions, thermodynamic calculations of the vapor pressures and volatilization rates of rock components, and speculations on observable lunar features.

Early proponents of the view that volcanism and lava flooding existed at some stage during the evolution of the lunar surface included Whipple (19), Kuiper (20), Green (14), and Kozynov (21). They closely examined the lunar features and were struck by the similarity of these structures to terrestrial volcanic features. The apparent lava-flooded maria

and crater-capped peaks on the lunar surface were two that could probably be associated with volcanism.

The photographic evidence of the early Surveyor missions (22) and the remote controlled alpha-backscatter analyzer on the later Surveyor missions (23,24) substantiated the igneous nature of the maria rocks. Conclusions drawn from the telemetric data, indicated that the maria regions were basaltic in composition and very similar to terrestrial basaltic regions such as the Columbia River Plateau, the Snake River Plains, the Hudson River Palisades, the Great Plateau of Brazil, a large part of India, Iceland, and the Hawaiian Islands. The Apollo 11 findings (25) and preliminary investigations of the Apollo 12 rocks (6) confirmed that the maria samples were similar to terrestrial basalts. Geologic examination and K-Ar dating of Apollo 11 samples, indicated that rock solidification took place in certain areas of the lunar surface approximately 2.5 to 3.5 x 10^9 years ago.

Localized surface melting could have been accomplished by meteorite impact. Evidence for this was found in the Apollo 11 and 12 samples described earlier. Also, Gold (26) has reported a remarkable glazing phenomena on the lunar surface, which he ascribed to radiation heating. This glazing was found on protruding sharp edges and points of clumps of soil located in the centers of small craters. The explanation offered by Gold for the phenomena attributed it to a giant solar outburst in geologically recent times, which could cause radiation melting

only in crater centers. The analysis of Buhl, et al. (27) showed that the absolute temperature in the bottom of a hemispherical crater must be expected to rise about 11 percent above that of the surroundings. Therefore, sub-molten temperatures on the flat surface might cause melting in the centers of craters.

b. Volatilization of Alkalis

The release of alkalis from basalts was observed in the laboratory (28). During the vacuum melting step in the K-Ar dating technique, alkalis are frequently observed to be released from molten basalts and to be condensed as metals on cooler regions of the quartz reaction chamber. When exposed to the atmosphere, the alkali layer rapidly oxidized. O'Hara, et al. (29) prepared synthetic silicates for petrographic experimental comparisons with Apollo 11 samples. Samples held near liquidus in a vacuum furnace at 1200°C, 10^{-5} torr for 14 days lost 3.4 percent by weight. Analysis after the experiment showed a reduction of total alkalis from 3.6 to 2.2 percent.

c. Distribution of Alkalis

Though the alkali contents of the lunar maria samples were quite low, many geologists believe the parent magma was considerably higher in these elements. During the initial surface formation, release of the volatile alkalis would have occurred and they would have distributed over vast areas. The maximum density of the lunar atmosphere consistent with the measurements of Elsmore (30) yielded a mean free path of the order of 10^4 km. This was sufficient to use ballistic

trajectories for the mechanism of molecular transport in the lunar atmosphere, since the average jump length for molecules in equilibrium with the lunar surface would be approximately 10^2 km. (31). The lunar highlands should act as a larger sink for redeposited volatiles than the flat maria regions. The presence of condensed volatiles might account for the high electrical conductivity and radar reflectivity of the highlands (32).

d. Alkali Metal Degradation

So far, the source and distribution of alkali metals in the lunar environment has been indicated. However, of particular interest, is the interaction of alkali metals with surface materials under the conditions of high temperature and low pressure. The majority of earlier work on alkali interaction with various materials was sponsored by the Atomic Energy Commission during their development of liquid-metal-cooled fast breeder reactors (33). The disintegration of ceramic bodies by grain-boundary attack by liquid sodium was studied (34). Stapleton and Snavely (35) qualitatively observed the effects of exposing potassium vapor at 850°C to 91 insulating materials and metal coatings. Tarpinian (36) reported on insulation materials exposed to sodium at 510°C.

Until the preliminary study conducted by Naughton, et al. (37), it appears that little or no work was carried out to study rock degradation by alkali metals. They used the technique for the separation of chondrules from chondritic meteorites and suggested this as a nonmechanical method of rock

comminution for special applications by mineralogists. X-ray examination by the powder technique indicated no significant difference between a degraded sample and the parent material.

When alkali metals and rock samples were sealed in a vacuum and held at 100°C, disintegration of rock to a powder became evident after two weeks. At 350°C, there was evidence of disintegration after only 12 hours. Their work was mostly qualitative, but revealed that basic rocks disintegrated more readily than siliceous or acidic rocks. However, polycrystalline aggregates of a single mineral (quartz or synthetically prepared forsterite) were not disrupted.

It was evident that the alkali vapor was effective as a penetrating agent. When samples exposed to alkali vapor were treated with alcohol or water, microbubbles of hydrogen were released at grain boundaries and surface cracks. No similar attack of rocks occurred when aqueous or molten alkali ionic media were used as the attacking agents. These substances were known to cause swelling in silicates (38,39). Iron(III) chloride and bromine, which along with the alkali metals, form nonstoichiometric intercalation compounds with graphite, did not affect the rocks. Various natural and synthetic glasses showed no evidence of disintegration by alkali vapor attack.

C. Modes of Inquiry

1. High Temperature Mass Spectrometry

Mass spectrometry has proven to be one of the most versatile tools for the study of the vaporization process. It

has been used to investigate the thermodynamics of gas-solid and gas-liquid equilibria at high temperatures. The use of Knudsen and Langmuir methods as a source of the vapor species has given us a modified picture of the stability of gaseous inorganic molecules and has added to the knowledge of the existence and properties of many new molecules.

Grimley (40) reported that N.I. Ionov initiated mass spectrometric vaporization studies in 1948 when he investigated the vapor species over a number of alkali halides. The experimental techniques and procedures used for the past decade and a half were developed by Chupka and Inghram (41) and by Honig (42) with their studies of the vaporization of carbon. Thereafter, the research extended rapidly to other elements, to intermetallic compounds, to oxides, sulfides, selenides, tellurides, halides, hydroxides, and nitrates (43,44).

With proper instrumental design, mass spectrometry at high temperatures can simultaneously determine the composition of the gaseous phase, the pressure of each of the vapor species, and the variation of each pressure with temperature. To do this, the system must produce a molecular beam characteristic of the vapor under investigation and produce ions which reflect the true composition of the molecular beam. Finally, these ions must be resolved into their various mass components to enable a study of each species in the vapor from the sample.

Mass spectrometers are usually operated at pressures below 10^{-5} torr, so any system used must satisfy the requirements

needed to produce and maintain such pressures. Both the Knudsen (45) and the Langmuir (46) vapor pressure methods provide a suitable source of vapor species for the mass spectrometer. During Langmuir evaporation, molecules evaporate directly from the surface of the sample. However, this does not necessarily establish thermodynamic equilibrium between the condensed and the gaseous phase, or between the different components in the gaseous phase. Other disadvantages of the Langmuir method include the difficulty in achieving uniform sample temperatures, the almost non-existent knowledge of evaporation coefficients, and the complex calibration procedures necessary for determining absolute pressures. Sample-container interactions and the observation of vapor species over pure elements and metal oxides are typically studied using the Langmuir method. Specific examples are the studies of barium oxide (47), copper (48), and germanium (49).

Because of the difficulties involved with the Langmuir method, most sample chambers have incorporated the Knudsen method. With this design, a molecular beam effuses from a container with a small orifice, such that thermodynamic equilibrium exists within the cell and the flow from the orifice gives a representative sample of the equilibrium vapor. This method was used in the collection of thermodynamic data for many inorganic systems. The determination of the heat of sublimation of carbon (41), the study of the gaseous species at high temperatures in the aluminum-aluminum oxide system (50),

and the vapor pressure measurements of the lithium and sodium metaborates (51) exemplify the use of the Knudsen technique.

Ideally, Knudsen cells should be constructed of materials of low vapor pressures which cause no interactions with the sample. Tungsten, molybdenum, tantalum, platinum, and nickel are typical cell materials that have been used. Resistance or Joule, induction, and high intensity image arc heating are all used as heat sources, but Joule heating has an advantage because it avoids difficulties produced when vapors evaporating from the crucible surface cause electrical discharge breakdown when the pressure becomes too high. Temperatures can be accurately measured with thermocouples or optical pyrometers.

Instrument ion sources with the mass spectrometer must give a representative picture of the qualitative and the quantitative composition of the entering molecular beam. These limitations permit the use of electron impact or photoionization sources. At the present time, the intensity limitations of photoionization sources make them less competitive than electron impact sources. Looking to the near future, it is likely that laser sources may overcome these intensity limitations (52). When photoionization sources are applied to thermodynamic property measurements, dissociation energies are determined directly, rather than from thermodynamic equations (53).

Electron impact has proved to be the most versatile source of ions for high temperature mass spectrometry. Dempster (54) introduced this technique which was further developed by

Bleakney (55), Tate and Smith (56), and Nier (57). There are three common source configurations. The molecular, electron, and ion beams are all at right angles to each other, with the electron beam parallel to the ion beam exit slits; the molecular, electron, and ion beams are at right angles to each other, with the electron beam perpendicular to the ion exit slits: and the molecular beam is parallel to the electron beam, but opposite in direction (48). The parallel beam geometry has the disadvantage that reflection and dissociation of molecular components on the electron source filament complicates the interpretation of data results. Since the molecules with the high kinetic energy cross the ionization region in a shorter time than those with thermal energy, their relative ionization probabilities are reduced in any type of ionization source.

Inghram and Hayden (58) reviewed the different types of mass analyzers used in high temperature work, but most investigators have used the single-focusing magnetic type. The ideal instrument should have high accelerating voltages for high sensitivity, high resolving power, a large mass range, high sensitivity over a large detector current range, and minimal residual gas pressures to minimize background interferences and ion beam scattering.

Next, the steps of data collection and evaluation must be considered. High temperature studies of inorganic materials seldom produce one species in an equilibrium vapor phase. At each temperature, the difference of individual intensity data collected from the Knudsen cell with and without a sample yields

the relative ion intensity of the vapor species. The identity of the ion species must be established and the identity of the neutral species from which the ions originate should be ascertained.

Having established the nature of the components in the gas phase, it is still necessary to determine their pressures. One of the easiest ways to calculate absolute pressure from ion intensity is by the method of vaporization of a standard substance (40). The value of the absolute pressure for each species can be determined according to the equation:

at temperature T,

$$P_u = \frac{I_u^+ / \sigma_u}{I_s^+ / \sigma_s} P_s \; ; \qquad \text{(I-1)}$$

where, P is the pressure, σ is the relative ionization cross section, I^+ is the relative ion intensity, s represents the standard substance, and u represents the unknown substance.

The method requires the estimation of the relative ionization cross sections of the vapor species. Otvos and Stevenson (59) calculated the relative atomic ionization cross sections for elements with $1 \leq Z \leq 56$ and $Z = 80, 81, 82$. Furthermore, they have shown that total ionization cross sections of molecules are constitutive molecular properties, i.e. the sum of the atomic cross sections. With this data and the ion intensities of the vapor species, absolute pressures can be calculated.

Most high temperature mass spectrometric studies of vaporization processes used relatively simple inorganic systems. The work the Bendix Corporation carried out for the Manned Spacecraft Center was the first evidence of any similar work having been done with geologic samples (60). They studied fourteen geologic samples under lunar conditions and part of the study included the use of a time-of-flight mass spectrometer to measure the loss of water as temperature increased. Vapor pressures were calculated by the methods developed for simple inorganic systems. Muenow (61) reported on the work of Margrave, et al. at Rice University. They measured the release of organic materials from tektites by step-wise heating. In their work, a single-focusing mass deflection mass spectrometer was used with an electron impact ion source and a Knudsen sample chamber.

Mass spectrometry was one of the major analytical tools used by the Apollo 11 investigators. A brief survey of the uses of mass spectrometry for lunar analysis shows the versatility and importance of this method for geochemical investigations. Wanless, et al. (62) made age determinations and isotopic abundance measurements on lunar samples. Spark source mass spectrometry and isotopic dilution methods were used to quantitatively determine the elemental composition of lunar material (63). Solar wind gases, cosmic ray spallation productions and irradiation history studies were conducted (64). Abell, et al. (65) sought organic materials in the lunar rocks.

chloride with the sample and heating to 1400°C. With some modifications, this technique could be used to analyze the elements sublimed from basalts at various temperatures.

Most sublimation studies are carried out under conditions of equilibrium between the solid and vapor in order to obtain thermodynamic data for the vaporization reaction. However, these experiments do not give information about the reaction paths of volatilization. Information about the release mechanism of volatiles at various temperatures could best be obtained from free vaporization studies, i.e. sublimation into vacuum (70).

Volatilization processes in minerals seem to be diffusion controlled. The surfaces of minerals are heterogeneous with several atomic positions which differ in the number of neighbors surrounding them. These atoms in the different surface sites have different binding energies. Sublimation seems to be a multi-step process where atoms break away from stronger bound sites and diffuse along the surface sites until they are ready to vaporize, most likely from low energy sites. Once surface sites are depleted of the volatile components, further sublimation will be dependent on replenishing surface sites from internal sources.

At temperatures near the liquidus point, lattice self-diffusion is common in many materials. For polycrystalline materials, there are certain high diffusivity paths which cause significant diffusion at lower temperatures (71). These

paths are due to the cracks, dislocations, and grain boundaries prevalent in multi-component materials. Activation energies from grain boundary diffusion are less than for lattice diffusion. A grain boundary increases the apparent diffusivity in the plane of the boundary, while the randomly oriented dislocations in single crystals increase the apparent diffusivity in all directions.

Rybach and Laves (72) observed that alkali ions diffuse through quartz when stimulated by only a concentration gradient. Later, diffusion of radioactive sodium in a commercial SiO_2 glass was investigated from 179° to 1000°C by Frischat (73). The temperature dependence curves had discontinuities at about 573° and 250°C. The two anomalies were explained in terms of quartz-like and cristobalite-like precrystalline elements in the structure of the glass causing diffusion of sodium by an interstitial rather than a vacancy methanism. Frischat pointed out that the ternary nature of the glass causing boundary diffusion was very similar to the results of Haven and Verkerk in their work with binary glasses. Sodium tracer studies with quartz crystals revealed that sodium diffusion in the c-axis direction was about two orders of magnitude faster than sodium diffusion in more open silica glass (74).

Early in their investigations, geologists recognized that many well-known features of igneous rocks are the result of diffusion (75). The growth of crystals is accomplished largely by diffusion of material to crystal nuclei. Inclusions often

exhibit solution at their borders and some diffusion of their material into the surrounding magma takes place. For magmas, Wood (76) cited crystallographic evidence that cation diffusion occurs more readily than recrystallization during certain types of metamorphism. Apparently, this was because all bonds of an atom have to be broken in order to remove it from one crystal and add it to another, whereas at no point during the diffusion process must all bonds be broken simultaneously.

Fisher (77) showed that diffusion occurs more rapidly along grain boundaries, or internal surfaces, in natural minerals than lattice diffusion. These findings indicated that the activation energy for grain boundary and surface diffusion is less than that for lattice diffusion; so surface and grain boundary diffusion will increase relative to lattice diffusion with decreasing temperature. Sippel (78) determined sodium self-diffusion coefficients in nine natural minerals. He recognized the need for diffusion studies of natural minerals which may have entirely different diffusion behavior than synthetic materials and realized that grain boundaries, fractures, parting cracks, inclusions, twin lamellae, and other kinds of internal surfaces may significantly contribute to diffusive transfer.

Most geochemical diffusion studies have been made in connection with studies of factors affecting age dating determinations. Many investigators attempted to classify the most important minerals as to their ability to retain radiogenic

inert gases such as helium and argon (79,80,81). Since transport phenomena in solids was usually given by more than one activation energy, they concluded that mechanisms operating at high temperatures (lattice diffusion) may not be operating at lower temperatures. Fechtig and Kalibitzer (82) reported that fractions of weakly-bound argon were sometimes found in polycrystalline materials. At lower temperatures, flat curves for Arrhenius plots were observed, which yielded low activation energies. They concluded that this could occur in minerals where potassium is not a regular lattice ion and that radiogenic argon would be found at grain boundaries and consequently be loosely bound. In crystals containing potassium as a regular constituent, loosely-bound argon could be due to structural defects. For example, this was observed in experiments with synthetic single crystals of potassium chloride.

The basic description of the diffusion phenomena is given by Fick's Law:

$$J = -D\, dc/dx \quad ; \qquad \text{(I-2)}$$

where J is the flow, or diffusion current; D is the diffusion coefficient; and dc/dx is the concentration gradient. This relation is dependent on the temperature and structure of the substance under investigation.

Certain assumptions can be made to solve Fick's Law for physical situations. Let the structure of the substance be a sphere and the amount of volatile materials at time zero be homogeneously distributed. Let the concentration of volatile

material outside the sphere be zero. This condition can be met experimentally by condensing the volatiles on a cold region of the reaction furnace during a diffusion run. With these assumptions, Carslaw and Jaeger (83) derived the exact solution of the equation for this system:

$$F = 1 - \frac{6}{\pi^2} \sum_{n=1}^{\infty} \frac{1}{n^2} \exp(-n^2 Bt) \quad ; \qquad \text{(I-3)}$$

where F is the fraction of material lost, B is equal to $\pi^2 D/a^2$, t is time, D is the diffusion coefficient, and a is the radius of the sphere.

More practical forms of this equation were found by Reichenburg (84). For small loses, $F \leq 0.10$:

$$F = \frac{6}{\pi^{3/2}} (Bt)^{1/2} \quad ; \quad D = \frac{F^2 \pi a^2}{36t} \qquad \text{(I-4,I-5)}$$

For losses, $F \leq 0.90$:

$$F = \frac{6}{\pi^{3/2}} (Bt)^{1/2} - \frac{3}{\pi^2} Bt \quad ; \qquad \text{(I-6)}$$

$$D = \frac{a^2}{\pi^2 t} \left[2\pi - \frac{\pi^2}{3} - 2\pi\left(1 - \frac{\pi}{3} F\right)^{1/2} \right] \qquad \text{(I-7)}$$

The experimentally observed temperature dependence on the diffusion constant is given by the Arrhenius equation (85):

$$D = D_o \exp(-E/RT) \quad ; \qquad \text{(I-8)}$$

where E is the activation energy, R is the gas constant, T is the absolute temperature, and D_o is a characteristic constant. The activation energies for the various diffusion transport

mechanisms can be calculated from plots of Log D/a^2 versus 1000/T.

Since the diffusion equations were based on certain assumptions and ideal models, some complications may result when working with natural samples. Naturally occurring crystals are only approximate spheres and samples are usually of a variety of grain sizes. When samples are heated at various temperatures simple diffusion profiles are disturbed (83). The activation energies determined for multi-component materials have fairly nebulous values. Being realistic, these really are values of all the energy factors involved in the release of a volatile from a material by some transport mechanism. However, the problems encountered with natural samples can be tolerated if only relative comparisons of the calculated quantities are desired.

3. Electron Microprobe Analysis

Bombardment of matter by a focused electron beam, coupled with the measurement of the energy and number of emitted X-ray quanta, permits fine-scale chemical analysis. The technique, colloquially known as electron microprobe analysis, is of fundamental importance in mineralogy and petrology because tedious and often incomplete mineral separations can be avoided and because the high spatial resolution (approximately 1-5 microns for primary excitation) permits detailed study of zoned materials and tiny inclusions (86). The high speed, relative accuracy, and non-destructive nature of the analysis

make the electron microprobe particularly useful for the stody of small, valuable samples. Shock effects (87), impact features (88), elemental zoning (89), distribution of α-emitting nuclides (90), as well as the analysis of individual mineral phases (91), is a partial list of some of the Apollo 11 lunar investigations conducted by microprobe analysis.

In 1960, Castaing (92) summarized the development of this technique which resulted from his earlier doctoral studies. His work showed that an electron microscope could be converted into a useful X-ray emission spectrograph for point-to-point exploration on a micron scale. The conversion involved the addition of a second electrostatic lens to obtain a smaller electron beam and the attachment of an external spectrometer for analysis of the spectrum and measurement of analytical line intensity. Outstanding features of the technique were the small size of sample (about a 1 micron cube); and the absence of pronounced adsorption and enhancement effects, which is characteristic of electron excitation.

The essential elements of an X-ray emission electron microprobe include: equipment for producing and controlling the electron beam, a mechanism for moving the sample so as to accomplish scanning by the electron beam, an optical system for examining the surface of the sample and locating the area under electron bombardment, and spectrometers for analysis of the X-radiation. The requirements imposed on the power supply and the electrical equipment are considerably more demanding

for successful operation of such a microprobe than of an ordinary X-ray spectrograph. The sample in the probe approaches being a point source, and therefore the X-ray beam is strongly divergent. This requires the use of curved crystal spectrometers to prevent the loss of intensity arising from collimation and the use of flat crystals. Also, the sample surface must be conducting, otherwise the electron beam might be deflected enough by a surface charge to excite X-rays in the wrong part of the sample.

The importance of correct sample preparation must be emphasized since the quality of microprobe analysis is dependent greatly on the characteristics and degree of perfection of the sample preparation. This is particularly true when geologic samples are to be prepared for microprobe work. Polishing must not cause edge rounding, distortion, pitting, or relief of the sample surface which can arise because of the varying degrees of hardness of different minerals.

In his Ph.D. dissertation, Taylor (93) presented detailed procedures for the preparation of ore minerals, ores, grain concentrates, and fine-grained powdered materials for microprobe analysis. The methods are applicable to all types of ores, including those containing malleable and ductile minerals such as native gold, electrum, silver, and copper; and those containing the hard brittle minerals such as pyrite, magnetite, chromite, and cassiterite. Taylor's instructions for the mounting and polishing of different types of mineral specimens

include: polished sections of liberated grains from, for example, heavy media separations and flotation concentrates; polished sections of ore specimens which contain opaque, translucent, and transparent minerals; polished thin sections of rocks which contain minor amounts of opaque minerals associated with transparent to translucent minerals; polished sections of single particles ranging in size from six to several hundred microns; and powdered minerals or submicron clay-like materials which have been cleaned and concentrated.

After a mineralogical sample has been properly mounted and polished, it must be coated with a conducting material. Early investigators (94) coated the surface of nonmetallic samples with about 50Å of manganese or copper to provide sufficient electrical conductivity. Later, a 200Å graphite layer proved effective to give good sample conductivity, while not significantly masking the X-radiation. Carbon coating in a vacuum deposition apparatus must be carefully controlled to insure uniformity of the coating from sample to sample. A piece of polished brass has been used as a control, and the color of the surface was seen to change successively due to interference from lemon yellow to orange, red, purple, blue, gray, and finally black. It was found that when the purple color on the polished brass was reached the carbon coat is sufficient for good electrical conduction (86).

Sample preparation must still be considered in the category of an "art form," but the "state-of-the-art" of

commercial microprobes now permit detection of all elements with atomic number greater than 5. The new instruments have multi-spectrometers which enable simultaneous analysis of more than one element. Many instruments have incorporated an X-ray emission electron microprobe and a medium resolution scanning electron microscope into one instrument. The advantages of not having to use two instruments, one for analysis, and one for imaging are obvious. The latest instruments are being computer interfaced, for automatic analysis, programmed scanning, and teletype print-out (95).

II. EXPERIMENTAL WORK

A. Mass Spectrometry

1. Construction of High Temperature Sample Chamber

The chamber (Figure 1) consisted of a Knudsen cell in a furnace enveloped by a bell jar on a baseplate. This plate had fittings for two resistance-heater feedthroughs, an evacuation port, a thermocouple port, and a port for molecular beam entry into the ion source. The stainless steel baseplate was drilled and machined smooth to provide vacuum-tight surfaces for the Viton seals for the feedthroughs and bell jar.

A platinum sample bucket was suspended from an inverse Knudsen cell made of nickel sheet with a 0.030 inch escape orifice. Entry to the cell was accomplished by a removable top which was clipped into place.

A platinum, platinum-rhodium thermocouple served not only as a means to measure temperature, but also as a support for the Knudsen cell. A tungsten-to-glass feedthrough was constructed so that the thermocouple could be used in vacuum with the measuring potentiometer outside. The calibration procedures used were those of Seybolt and Burke (96). Emf values for the thermocouple were compared with a similar thermocouple standardized by the National Bureau of Standards. The thermocouples were put in a resistance heater with the measuring junctures of each in a heat sink to insure uniform temperatures. Below 500°C, the thermocouple had the same emf values as the standard. Above 500°C, the thermocouple gave lower emf values;

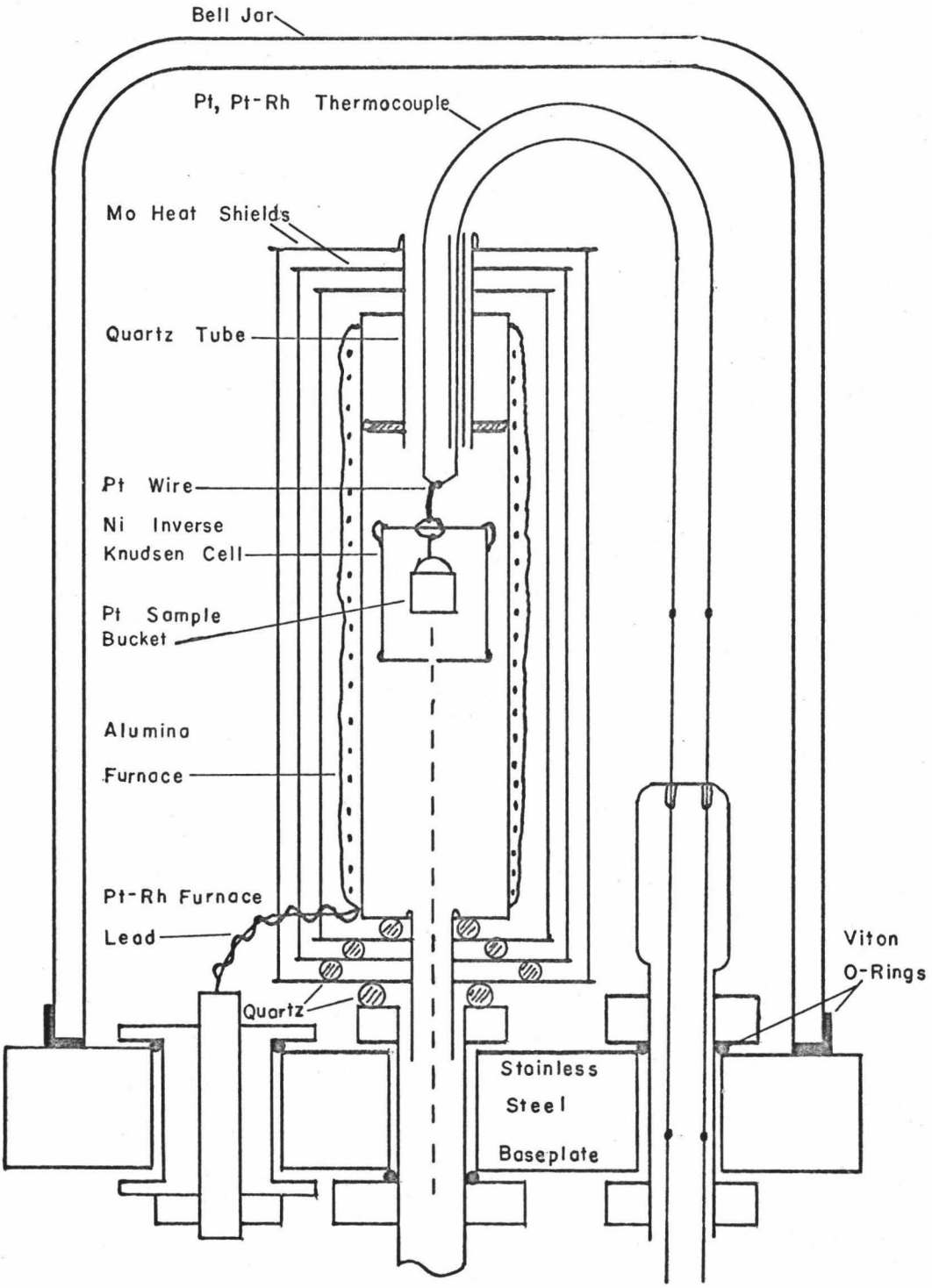

Figure 1: High Temperature Sample Chamber

but even at 1100°C, the working thermocouple was within 0.73 percent of the standard.

A high-purity alumina furnace tube wound with platinum-rhodium wire served as the heat source. Furnace leads were a twisted double-strand of the winding wire attached to the machined steel rod extensions of the heater feedthroughs. Three molybdenum heat shields surrounded the furnace with quartz rods acting as spacers.

Supplementary equipment for the sample chamber included a furnace power supply constructed from a heavy duty variac, a potentiometer for temperature measurement, and an implosion shield. The implosion shield was fitted to the laboratory air line so that a stream of cool air could be applied to the bell jar.

2. Construction of the Mass Spectrometer

a. Description of Tube and Supporting Electronics

The mass spectrometer as a whole was originally designed by Nier, and later modified by Schaeffer (97) and Moore (98). It was a 60° sector single-focusing, single collector instrument, utilizing an electron impact ion source. The radius of curvature was approximately six inches.

Supporting electronics for the instrument were either purchased commercially or constructed in the laboratory, and were standard power supplies except for the modifications enumerated below.

Moore wound the magnet coils according to the specifications of Nier (57). They required about twenty watts of power under normal operation conditions.

b. Ion Source Modifications

Although the mass spectrometer ion source was designed to incorporate a slit system for collimation of the electron beam, there was none in the mass spectrometer tube as received. Therefore, Moore (98) designed and constructed a set of slits approximately following the system described by Schaeffer (97). Schaeffer's desire for a pressurized source to decrease the hot filament contributions to the background led to a design with unusually small slits. In an effort to attain better stability and resolution, Moore made the slits larger to allow a stronger (but collimated) flux of ionizing electrons resulting in a commensurate increase in ion intensity.

The entrance port for the molecular beam has been modified for this work. Originally, the molecular beam, electron beam, and ion beam were mutually perpendicular. The new arrangement put the molecular beam at 120° to the plane of the electron and ion beams. This enabled a direct lead-in of the molecular beam from the sample chamber to the electron beam, theoretically giving more efficient molecule-to-ion conversion.

The repeller plates of the ionization chamber were found to be of an L-shaped design. It appeared that this design would interfere with the new entrance of the molecular beam into the ion source. Therefore, new plates were constructed in a flat, rectangular shape.

In addition, the 0.001 x 0.010 inch tungstem filament was replaced by a more rugged 0.001 x 0.015 inch tungsten filament.

c. Restoration of the Copper Analyzer Tube

The feasibility of cleansing copper by the oxidation of methanol was investigated using copper scrap. Nitrogen was bubbled through methanol and the saturated gas was passed over the copper at 350°C. After two days, the oxide coating was completely reduced. The same procedure was tried on the analyzer tube. Before covering with heating tapes, the glass-to-metal seals at the ends of the tube were wrapped with copper foil and asbestos for even heat transfer. The tube was heated at 395°C for two days, cooled gradually, and stored under a nitrogen atmosphere until evacuation of the vacuum system.

d. Electronic Modifications

Mass separation was accomplished by magnetic sweeping, which was done either manually or by programming the magnet power supply to change linearly with time. Also provided in this system was a two position switch which allowed alteration between two masses. Precision potentiometers were used to vary the magnetic field for specific mass separation. The linear voltage programmer swept approximately 2000 gauss upfield or downfield at times of 0.5, 8, 80, or 160 minutes.

A vibrating reed electrometer (Cary Model 31) was used to moniter and amplify the current generated by the ion beam falling on the collector plate. The electrometer was provided with a calibration unit for range, linear, or external calibration of output signals. This was accomplished by

shorting the electrometer feedback across various voltage dividers. Since the electrometer range positions changed signals by factors of three, which was frequently too large a change, a voltage divider across the recorder output that doubles the electrometer signal was added. A voltage suppressor was used to decrease recorder signals in increments from one to ten millivolts. Of the voltage generated by the electrometer, a small portion was tapped off and fed to a potentiometric recorder in the usual fashion.

Optimization of collector head noise, mass separation, and peak shape was achieved by the use of an adjustable collector slit, by applying a 90-volt potential across the collector plates, and by damping the pre-amplifier and/or varying the pre-amplifier resistance.

A schematic drawing of the mass spectrometer electronics is shown in Figure 2. Of importance was the necessity of a common ground for all electrical units.

e. Range of Instrument

A given mass-to-charge ratio is detected when the force of the magnetic field is equivalent to the centrifugal force of the ion. From this, Kiser (99) has derived the equation:

$$\frac{m}{Z} = \frac{B^2 r^2}{20{,}721\ V} \quad ; \qquad \text{(II-1)}$$

where m is the mass in atomic mass units, Z is the number of electronic charges on the ion, B is the magnetic field strength in gauss, r is the radius of curvature of the analyzer tube in

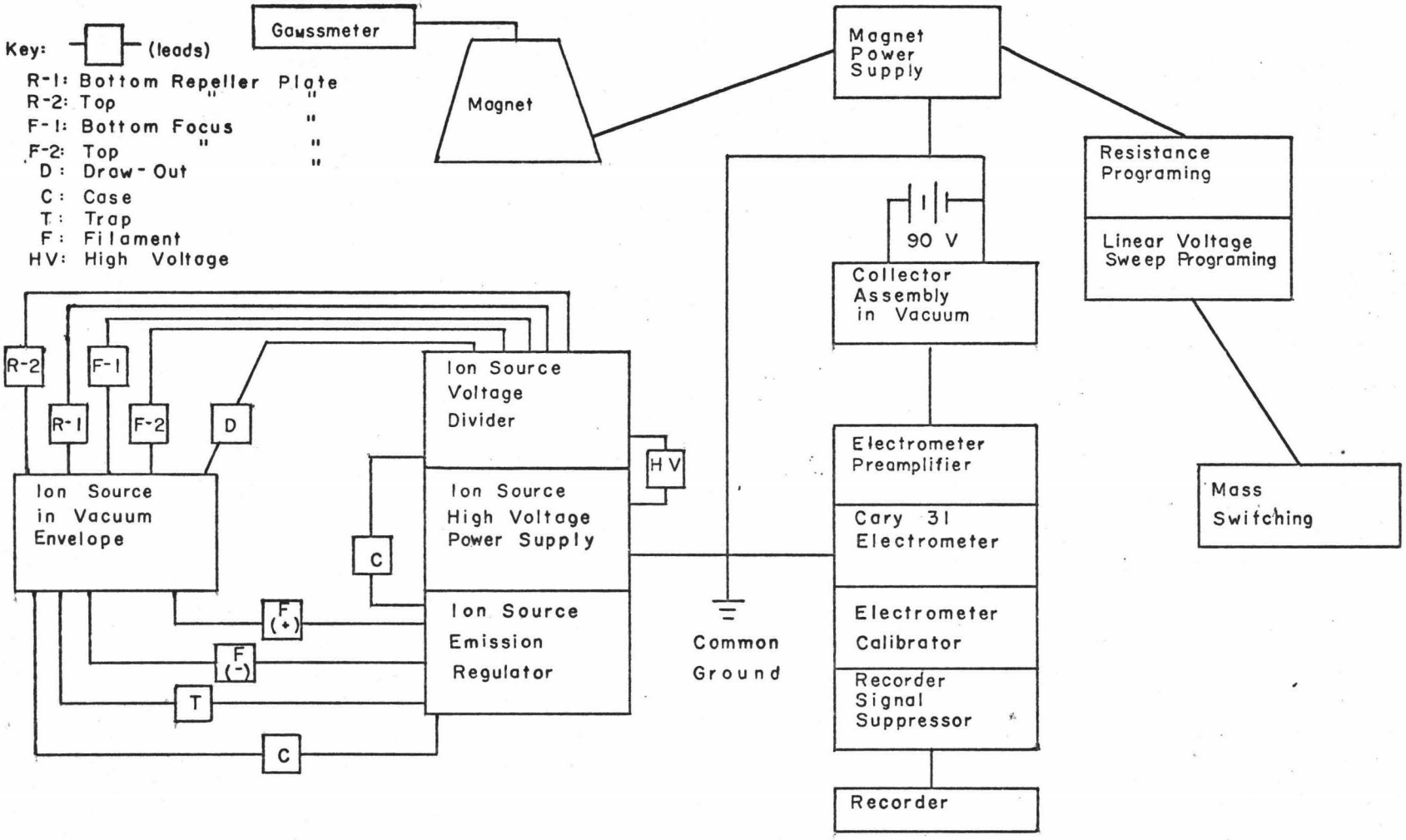

Figure 2: Mass Spectrometer Electronics

centimeters, and V is the ion accelerating voltage.

The electromagnet was capable of a maximum field strength of 7.4 kilogauss and the analyzer tube had a radius of curvature of 15.8 centimeters. Assuming monovalent ions, Table I shows the maximum detectable mass at selected accelerating voltages. At lower accelerating voltages, larger mass detection was possible but mass resolution was less. For this work, 3000 volts gave suitable mass separation and enabled detection of ions past mass 204(Hg^+).

f. Evaluation of the Vacuum and High Temperature Systems

A standard pumping system was used, which employed a 120 liter/second mechanical pump in tandem with a 70 liter/second, three-stage mercury diffusion pump. Liquid nitrogen trapping brought the pressure down in the ion source region to 4×10^{-6} torr, after baking the system at 250°C for 4 hours, and continuous pumping for a period of 3 days.

Stable furnace temperatures within 5°C could be maintained by the variable power supply. With heat shielding, the bell jar reached 50°C at a furnace temperature of 750°C. Above 750°C, air cooling of the sample chamber was used to protect the feedthrough O-rings. Following this procedure, a maximum furnace temperature of 1325°C was obtained. Continuous pumping during heating maintained the pressure in the ion source region below 5×10^{-4} torr which was within mass spectrometric operating limits.

TABLE I. MAXIMUM MASS DETECTION AT SELECTED ACCELERATING VOLTAGES

V(volts)	$m_{max.}$(a.m.u.)	V	$m_{max.}$
500	1317	3000	219
1000	633	3500	188
1500	441	4000	164
2000	331	4500	146
2500	262	5000	132

Figure 3 presents a schematic of the complete high-temperature mass spectrometric vacuum system.

3. Sample Analysis

To insert a sample, the ion source electronics were shut off, stopcock #1 (Figure 3) was closed, stopcocks #2 and #3 were opened to the atmosphere, and the bell was removed. The Knudsen cell was removed from the sample chamber (Figure 1). After removing the previously run sample, the sample bucket was cleaned by heating to yellow-red heat and allowing it to cool to ambient temperature in a desiccator.

A sample weighing approximately 250 milligrams with a grain size of 0.4 to 0.8 millimeters was placed in the sample bucket-Knudsen cell assembly. This was suspended in the furnace tube by the thermocouple and the bell jar was replaced. Stopcock #3 was opened to the rough pump position and the system was evacuated to 10^{-2} torr. When this pressure was obtained, stopcocks #1 and #2 were opened to the high vacuum pumping system and pumping was continued until a pressure of at least 5×10^{-5} torr was achieved. The sample furnace was set at 250°C overnight. If the system pressure was 2×10^{-5} torr or lower, a sample run was begun. If the pressure was higher, the entire system was baked out for 4 hours at 200°C.

The electronic components were turned on and a spectra was run at a sample temperature of 250°C. The ion source parameters were set to obtain a maximum mass 28 (N_2^+) peak. After optimization of the electronic parameters, duplicate

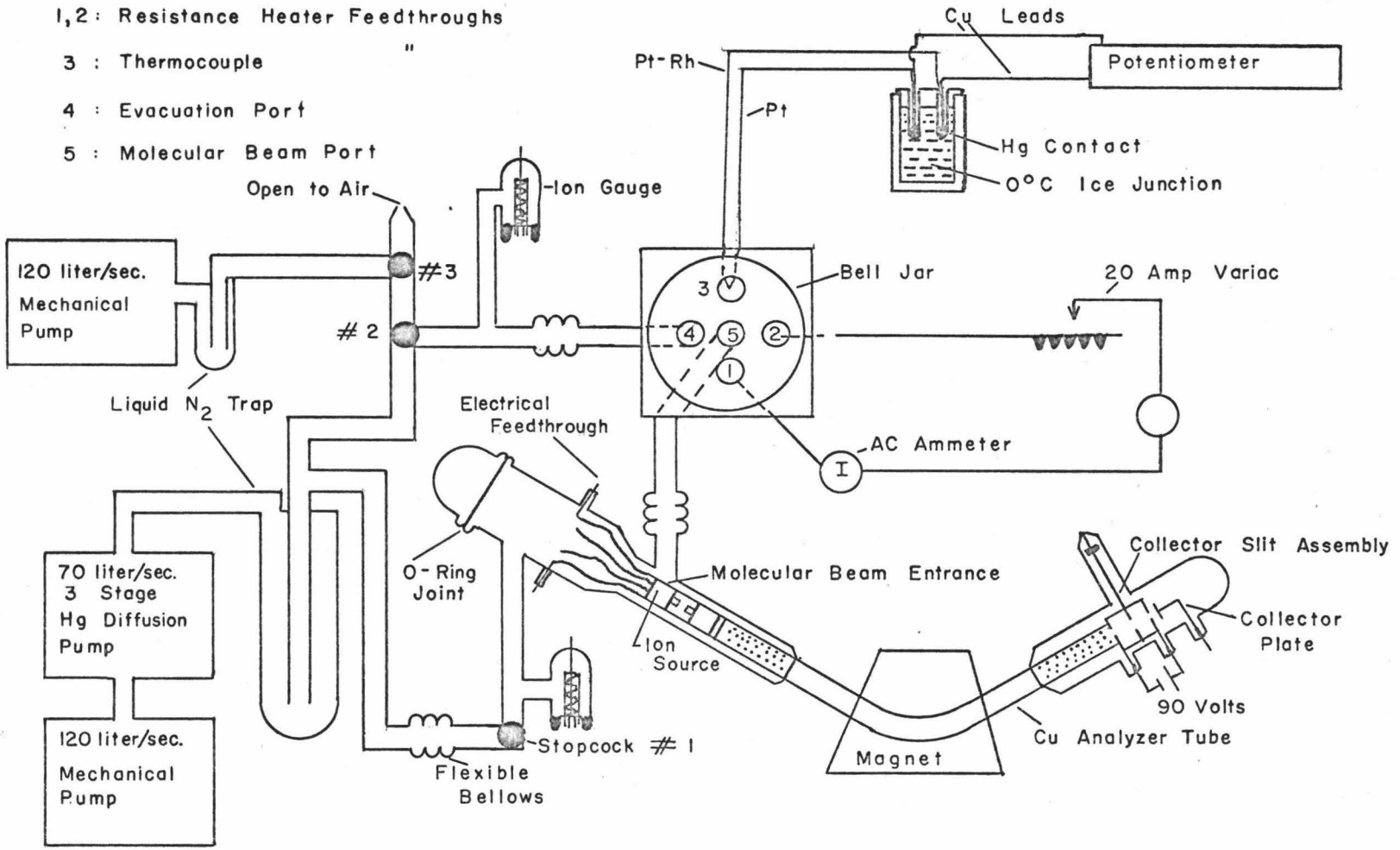

Figure 3: Mass Spectrometer Vacuum and High Temperature System

spectra of masses 20 through 100 were run. This was accomplished in two sets by first recording a mass range of 20 to 64 followed by down-field sweeping of masses 64 to 20; and then, repeating the same procedure for a mass range of 36 to 100. Sweep rates of 250 gauss/minute with a recorder speed of 1 inch/minute gave acceptable spectra.

The ion source filament current was decreased to 1 amp before each temperature increase in the sample chamber. Usually the sample temperature was increased in increments of approximately 75° to 100°C. At each increment, the sample was allowed to equilibrate for 20 minutes, and then the ion source current was returned to its optimum setting. Spectra were recorded at this temperature in the same manner as described above. This process was repeated until a sample temperature of about 1125°C was reached. Around this temperature, the geologic samples were usually melted and the volatiles caused system pressure increases above 5×10^{-4} torr, prohibiting ion source operation.

The procedure required about one hour for data to be collected at each temperature. When it was necessary to leave the sample overnight, the furnace temperature was decreased to 250°C and the electronics were turned down. The sample run would be continued the next day by optimizing the ion source parameters at the previous day's last temperature setting.

Blank spectra for system background were obtained before and after each sample run. The mode of operation was the same

as described above, except that no sample was placed in the Knudsen cell. An effort was made to record blank spectra at the same temperature as the sample spectra.

4. Treatment of data

Plots of relative ion intensity of the volatiles versus temperature were made by subtracting the intensity of the blank spectra from the sample spectra intensities at the same temperature. At each temperature, duplicate peaks were averaged to present a picture of the release of volatiles from each sample. From knowledge of the types of materials likely to be volatilized and the composition of the sample, an effort was made to identify the ions of each mass peak.

Earlier, it was shown taht vaporization of a standard substance could be used to determine vapor pressures from ion intensities. The advantage of this technique was that data from one mass spectrometer could be correlated with data from another instrument, provided that a standard of defined vapor pressure was used. In the past, many workers used silver as the standard substance (40). The advantages being that silver was available in pure form, it volatilized into simple silver ions, and it had significant vapor pressures above 1100°C. For the present work, silver's disadvantages included its high mass number and its low volatility below 1000°C. However, due to the amount of mass spectrometric work done on boron compounds in the early 1960's, boron oxide proved to be a suitable calibration standard. Boron oxide has significant vapor

pressures in the region 800° to 1300°C (Figure 4), it has a lower mass than silver, it can be prepared under vacuum in pure form (100), it volatilizes as $B_2O_3^+$ ions (101), and its ionization cross section is known (59).

Boron oxide was run in exactly the same manner as the geologic samples and blanks to provide a plot of the logrithm of the product of the ion intensity of boron oxide times the absolute temperature, versus the reciprocal of absolute temperature. This data provided the final information needed to calculate the vapor pressures of geologic volatiles by the use of Equation I-1.

B. Vacuum Deposition

1. Design of a Sample Chamber and Vacuum System

The belief that alkali degradation and volatilization were diffusive processes necessitated the design and construction of a system to study these processes. Edwards and Urey's work (69) with a distillation process to determine low alkali contents in meteorites stimulated an idea to try a similar vacuum evaporation and deposition technique.

The initial sample chamber was designed to run 2.50 gram samples. Since this prototype proved the workability of the technique, the sample chamber shown in Figure 5 was built to run smaller samples of 250 milligrams or less. The sample chamber consisted of a cold finger which would condense the volatiles from heated samples. Since the entire chamber was heated, the water-cooled cold finger was the only surface

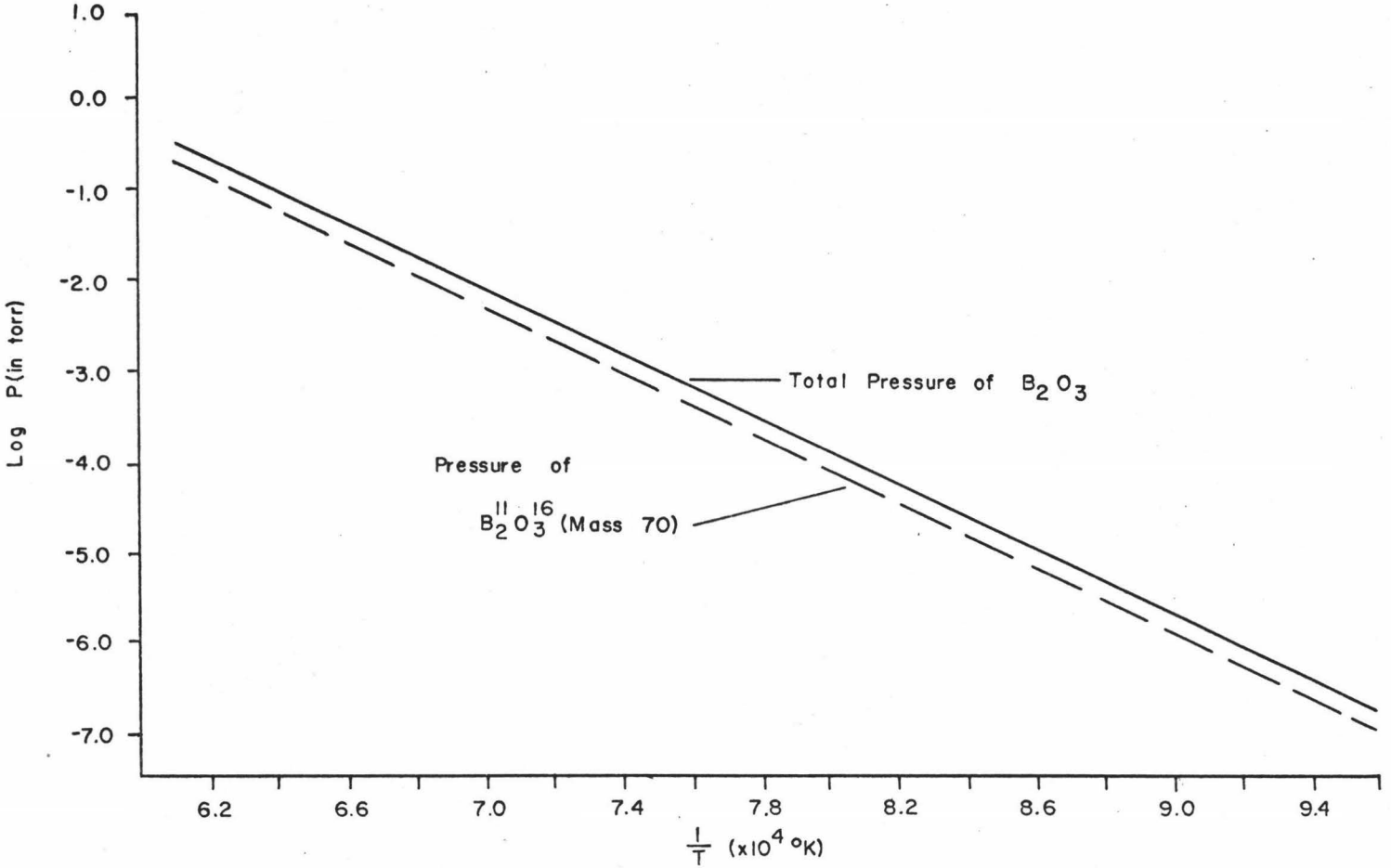

Figure 4: Vapor Pressure of B_2O_3 as a Function of Temperature

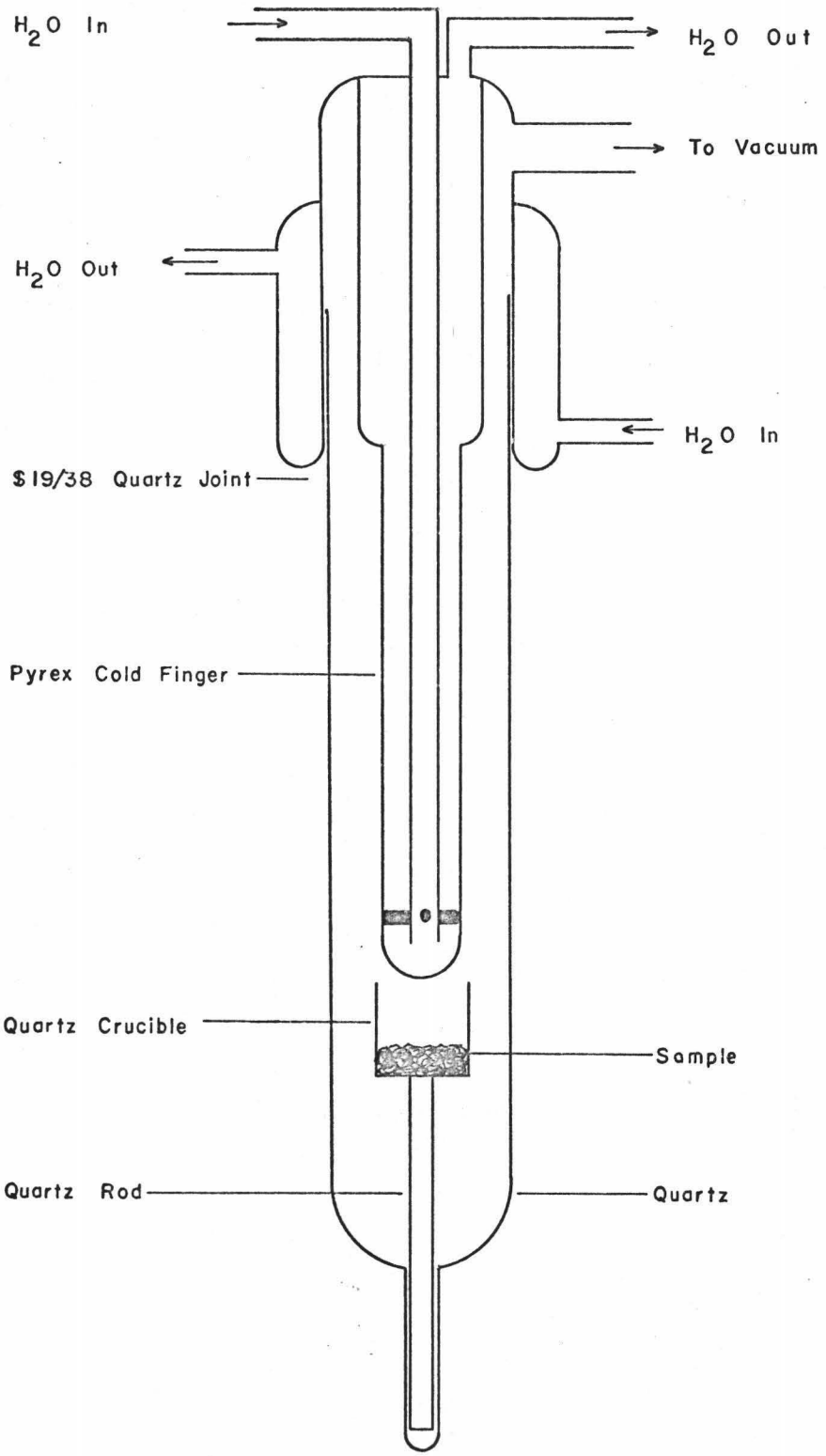

Figure 5: Vacuum Deposition Cold Finger Sample Chamber

available for condensation in the vicinity of the sample. With a flow rate of 2 liters/minute through the cooling system, the water in the cold finger stayed below 30°C up to sample temperatures of 1200°C.

The sample chamber was joined to the vacuum system shown in Figure 6. With liquid nitrogen trapping, the system was capable of pressures of 2×10^{-6} torr. Versatility and rapid pump-down from atmospheric pressure were the important features of the vacuum system.

2. Sample Analysis

A screened (0.4 to 0.8 millimeter diameter) sample weighing approximately 250 milligrams was placed in the quartz crucible and lowered into the reaction tube. The tube was seated in the water-cooled glass joint with Apiezon N stopcock grease. After rough pumping through stopcock #1 (Figure 6) for 5 minutes, liquid nitrogen was placed on the cold trap, followed by 5 minutes of rough pumping. Closing stopcock #1 and opening stopcocks #2 and #3 allowed the system to be pumped to the 10^{-5} torr range. With water flowing in the cold finger, a Kanthal-wound alumina tube furnace was placed around the sample chamber for one hour at a known temperature.

After one hour, the furnace was removed and the sample chamber was cooled to ambient temperature. The liquid nitrogen was removed from the trap and the diffusion pump section was closed. Stopcock #4 was opened slowly to allow atmospheric pressure equilibration and the reaction tube was removed from

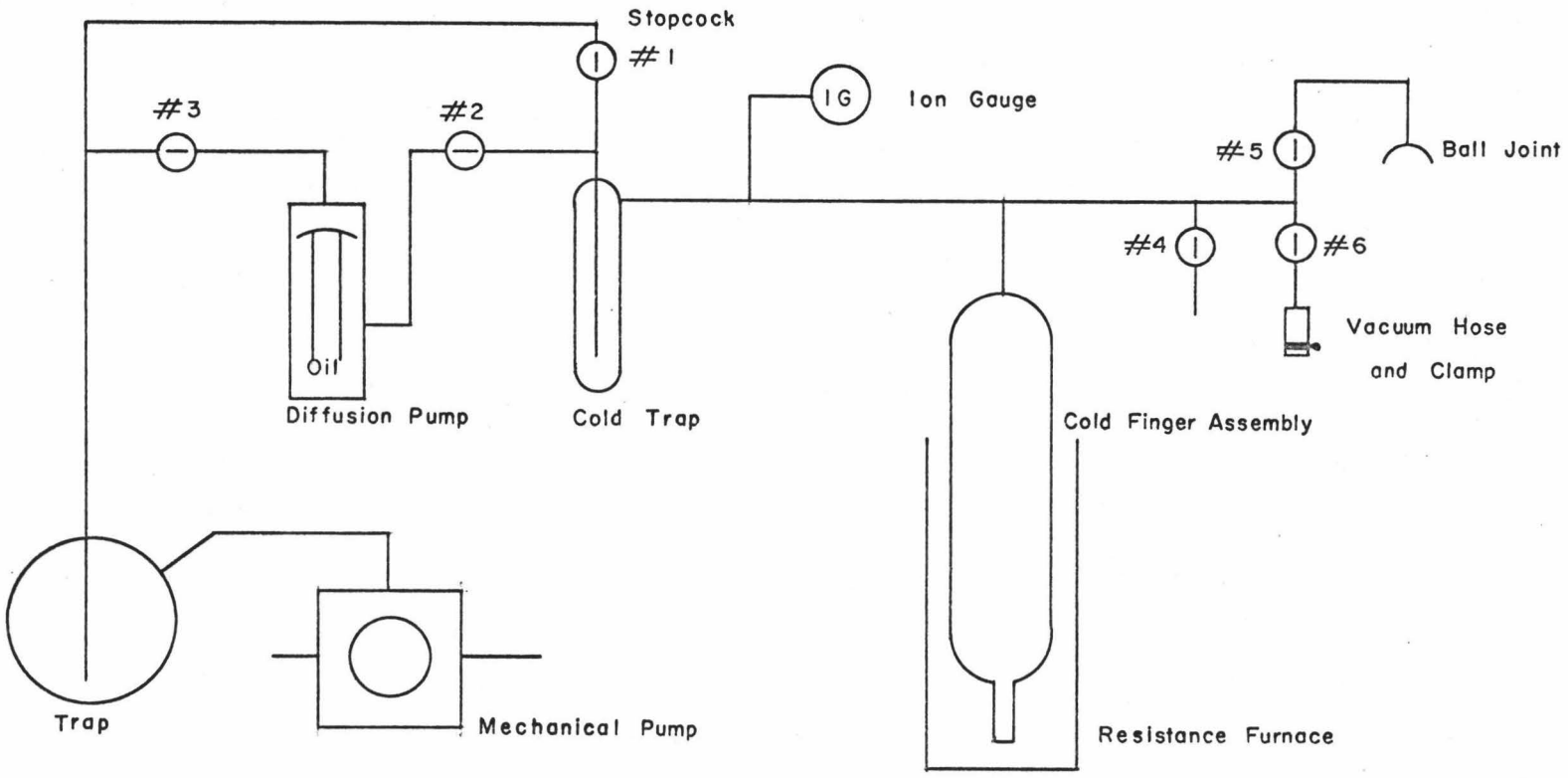

Figure 6: Cold Finger Vacuum Deposition System

the cold finger. The condensate was washed from the finger with de-ionized water, and was then quantitatively transferred into 5 milliliter volumetric flasks. After drying the cold finger, the process was repeated at a higher temperature. Samples were collected from approximately 200° to 1100°C in 40°C increments. Temperature measurements were made with an external calibrated chromel-alumel thermocouple.

The solutions in the volumetric flasks were allowed to equilibrate at ambient temperature for one hour and then filled to the volume mark. These samples were stored in sealed polyethylene vials until they could be analyzed for sodium and potassium by atomic absorption.

Usually condensates from six temperature increments could be collected per day. The rock sample was stored overnight, under vacuum, at ambient temperature with a dry ice-acetone bath on the cold trap. The water flow was off during this period.

3. Cleansing of Sample Chamber and Containers

In some cases, the technique was used to collect sodium and potassium volatiles of less than 1 microgram per temperature increment. This necessitated extremely clean conditions to keep the blanks low. The reaction tube, quartz crucible, cold finger, and volumetric flasks were cleaned with a hot 80% concentrated sulfuric acid-20% concentrated nitric acid solution for one hour, followed by five rinses of tap water and five rinses of de-ionized water. The volumetric flasks were stored

filled with de-ionized water, while the other glass components were dried. The de-ionized water in the flasks was run as a blank determination.

The polyethylene vials were soaked in a 50% nitric acid solution for four hours, rinsed five times with tap water and five times with de-ionized water. They were air dried in a filtered air hood and were sealed until use.

4. Sample Analysis for Alkali

Lewis (102) ran the liquid samples directly on a Perkin-Elmer 303 Atomic Absorption unit with recorder. The solutions were run alternately with mixed sodium-potassium standards and the concentrations were read from the standard curves. The estimated error was calculated on the basis of reading the standard curves to ± 0.1 milliliters of standard.

Portions of the solid samples were fun for total sodium and potassium content by a standard addition method. When there was sufficient sample, four 100 to 150 milligram portions were decomposed according to Bernas's method (103), except that the sample was moistened with water rather than aqua regia.

Contrary to Bernas's results, the slope of the absorbance versus potassium concentration curve was seriously depressed by the hydrofluoric-boric acid solution, so the solutions were not run directly on the atomic absorption unit. Instead, pairs of solutions were prepared by diluting the $HF-H_3BO_3$ solutions, 5/50 and 5/50 plus 0.20 µg.K/ml., with 9 meq./l. of lithium added to each to enhance the absorptivity of the potassium.

For each set of samples, the following controls were run: blank HF-H_3BO_3, HF-H_3BO_3 plus 0.20 μg.K/ml., HF-H_3BO_3 plus 0.80 μg.K/ml., and HF-H_3BO_3 plus 1.00 μg.K/ml. The same treatment was followed for standard addition of sodium. The sodium and potassium contents were read from standard curves.

For small samples less than 50 milligrams, all the sample was dissolved in one solution. Duplicate sets of dilutions were made-two with standard addition and two without-to minimize any error due to absorption from glassware and from handling.

5. Treatment of Data

The vacuum deposition technique yielded the amount of sodium and potassium volatilized from a sample at a known temperature. Where the mass spectrometer had the ability to identify the chemical compositions of the volatilized alkalis, this technique gave only the total amount of alkali released. The simplicity and amount of information acquired made vacuum deposition a valuable tool for volatilization studies. The technique described above should be applicable to any soluble volatile component.

Plots of the rate of alkali release versus temperature revealed the temperatures at which different release mechanisms were operative. Further, the plots gave comparisons of the rate of release of sodium and potassium, as well as differences between degraded and undegraded terrestrial samples, and surface and non-surface lunar rocks.

The amount of alkali loss and the total alkali content of the sample were used to calculate the fractional release, F, from the sample. From the diffusion relationships (Equations I-3 through I-8), the energy required to release sodium and potassium from a sample by its various transport mechanisms was calculated.

C. X-Ray Emission Electron Microprobe

1. Sample Preparation

The quality of electron microprobe analysis is very dependent on the proper sample polishing and coating techniques. The requirements of a polished surface for electron microprobe analysis include: a flat polished surface, minimum relief between the different mineral phases, minerals free of artifacts produced in polishing stages, malleable minerals free of flowage, and a polished surface free of scratches.

The entire surface of the polished section should be as flat as possible to insure that the correct X-ray take-off angle in the microprobe is maintained for any point on the surface. Since analysis was to be performed across mineral boundaries, the relief between hard and soft minerals had to be kept minimal. Other experiments had to be run after the non-destructive microprobe work, so contamination of the lunar samples had to be avoided as much as possible.

Mineralogical samples must be coated with graphite to provide a conducting sample for the electron beam. Improper coating could cause electron beam wandering and non-uniform

coating could mask certain regions of the sample, leading to erroneous results.

Taylor's techniques (93) were modified to prepare rock, thin section, and grain specimens for microprobe analysis. A high vacuum evaporation technique (86,102) was used to coat the samples.

a. Rocks

The size and friability of the samples necessitated foregoing grinding of the samples. Lunar samples were handled with surgical gloves at all times. Using a quartz optical flat coated with Buehler Automet lapping oil and AB Metadi 6 μ diamond polishing compound, the surface of interest was rough polished. Final polishing was with 1/4 μ diamond polishing compound. After polishing, the samples were boiled in five 10 milliliter portions of methanol to remove all polishing compound residues and foreign materials.

The rock was securely mounted in an aluminum holder with aluminum foil so that the polished surface was flush with the holder top. The holders were constructed from 1 inch aluminum rod, the diameter of the microprobe sample chamber mount. They were made 3/4 of an inch thick with the center core machined out to form a cup 1/2 inch in diameter and 1/2 inch deep.

b. Thin Section

One lunar sample that was previously run as a rock specimen on the microprobe was prepared in thin section for petrographic examination and further probe work. The polished

surface initially used for probe studies was cleaned of graphite by polishing with the 6 μ diamond compound and rinsing with methanol. With a diamond tipped scribe, a microscope slide was cut into a 1 inch circle. The clean polished surface of the sample was glued to the slide with Lakeside 70 thermoplastic.

Using a carbide steel jeweler's saw, the lunar rock was cut off at a thickness of approximately 2.4 millimeters. With a new chrome-steel file, the sample was ground to 0.8 millimeters. Polishing with 6 μ and 1/4 μ diamond compound brought the sample down to about 50 microns where it would transmit light. Following photographic mapping and petrographic analysis, the thin section was coated for microprobe study.

c. Grain Mounts

Individual grains as small as 6 microns can be prepared for microprobe analysis by mounting them in Bakelite. Since the dyes in colored Bakelite volatilize under the electron beam and cause pressure build-up in the microprobe vacuum system, pure amber Bakelite must be used. A 1 inch die with furnace attachment and a Carver hydraulic laboratory press were used to prepare Bakelite discs.

1 1/2 inches of coarse Bakelite powder was put in the die, preheated to 150°C for 15 minutes, and pressed at 10,000 p.s.i. for 15 minutes at 150°C. A circular cup was machined into the surface of the disc. It was important that the cup be as flat and smooth as possible and that it was parallel with the base

of the disc. The depression was about 3 millimeters deep with a diameter of 10 millimeters. After the disc was machined, it was cleaned in acetone to insure removal of any oil.

One to five grains were placed in the depression and covered with < 150 mesh amber Bakelite. Scratches on the base of the Bakelite disc were used to identify the different particles in the mount. The mount was replaced in the die and covered with another 1/2 inch of coarse Bakelite. The material was preheated and pressed in the same manner as above. The result was a plug containing the grains sandwiched in the center of the Bakelite.

The Bakelite plug was ground down to just above the grains on a 240 grit carborundum wheel. Polishing was continued with 6 μ and 1/4 μ diamond compound until all the grains were exposed and about one half their original diameter. Final polishing was done on a water soaked felt lap with 0.03 μ alumina powder.

d. Graphite Coating

The rocks, thin section, and grain mounts were coated using a Kinney (Model KSE-2) high vacuum evaporator unit. The ends of 1/8 inch high purity spectrographic graphite rods were ground down to a 0.040 inch diameter about 3/16 inches long. Two of these rods were put on the evaporator filament leads so that they were touching each other under pressure. The polished specimens were placed about 1 1/2 inches below the rods with a polished brass slug as control. A bell jar was placed over the

evaporator unit and the system was purged with dry nitrogen and pumped to a pressure in the 10^{-6} torr range.

Gradually the power was applied to the graphite rods allowing them to degas at red heat. After degassing, power was increased until just below the sputtering point of graphite and a carbon coat was laid down on the samples until the brass control turned purple. All the samples coated in this manner gave a uniform and ample conducting surface of microprobe analysis.

2. Instrument Description (95)

Analyses were done on a Materials Analysis Company (MAC Model 400S) combined microprobe analyzer and scanning electron microscope. This model featured a high effective X-ray take-off angle which offered low x-ray absorption, and thus allowed the analysis of fairly rough specimens. The large depth of focus of the scanned electron images further enhanced the capability of examining rough specimens.

The electron-optical column was comprised of a triode electron gun, double condenser lens, and objective lens. A column airlock was provided in order that specimens could be changed without disturbing column vacuum thereby permitting the electron beam to be left on. A refracting light microscope variable to a magnification of 640x, with a resolution of 0.5 microns, facilitated visual viewing of the sample.

The X-ray units were Johansson spectrometers with the X-ray emission, the curved crystals, and the proportional

counters mounted on a Rowland circle radius of 5.61 inches. The crystals viewed the specimens at a constant effective X-ray take-off angle of 38.5°, which allowed analysis to be performed over a 2θ angular range of 20° to 145°. With the crystals shown in Figure 7 (105), namely LiF, PET, ADP, KAP, LOD, and mica, all elements in the Periodic Table down to boron were analyzable. Figure 8 (105) shows the wavelength dependence of gas absorption for the three instrument proportion counters.

Instrument electronics allowed signals of selected monochromatic X-radiation, specimen current, reflected electron, secondary electron, electron induced conductivity, and cathodoluminescence to be displayed on an oscilloscope, recorded, or read on a meter. Signal outputs could also be printed out on a teletype. Area, line, or point electron beam scans were possible at rapid and slow speeds. The electron beam had manual or automatic programmed-stepping across a specimen or the specimen could be moved under a stationary electron beam. Area scans could be displayed at magnifications from 100 to 10,000 x with an electron beam resolution of about 700 Å.

3. Operation Parameters

With considerable aid from Legrone (106), instrument parameters were developed to run potassium, sodium, and silicon on the coated geologic samples. The electron beam was operated at 20 KV (earlier work at 15 KV) and a sample current of 0.1400 microamps was maintained for all analyses.

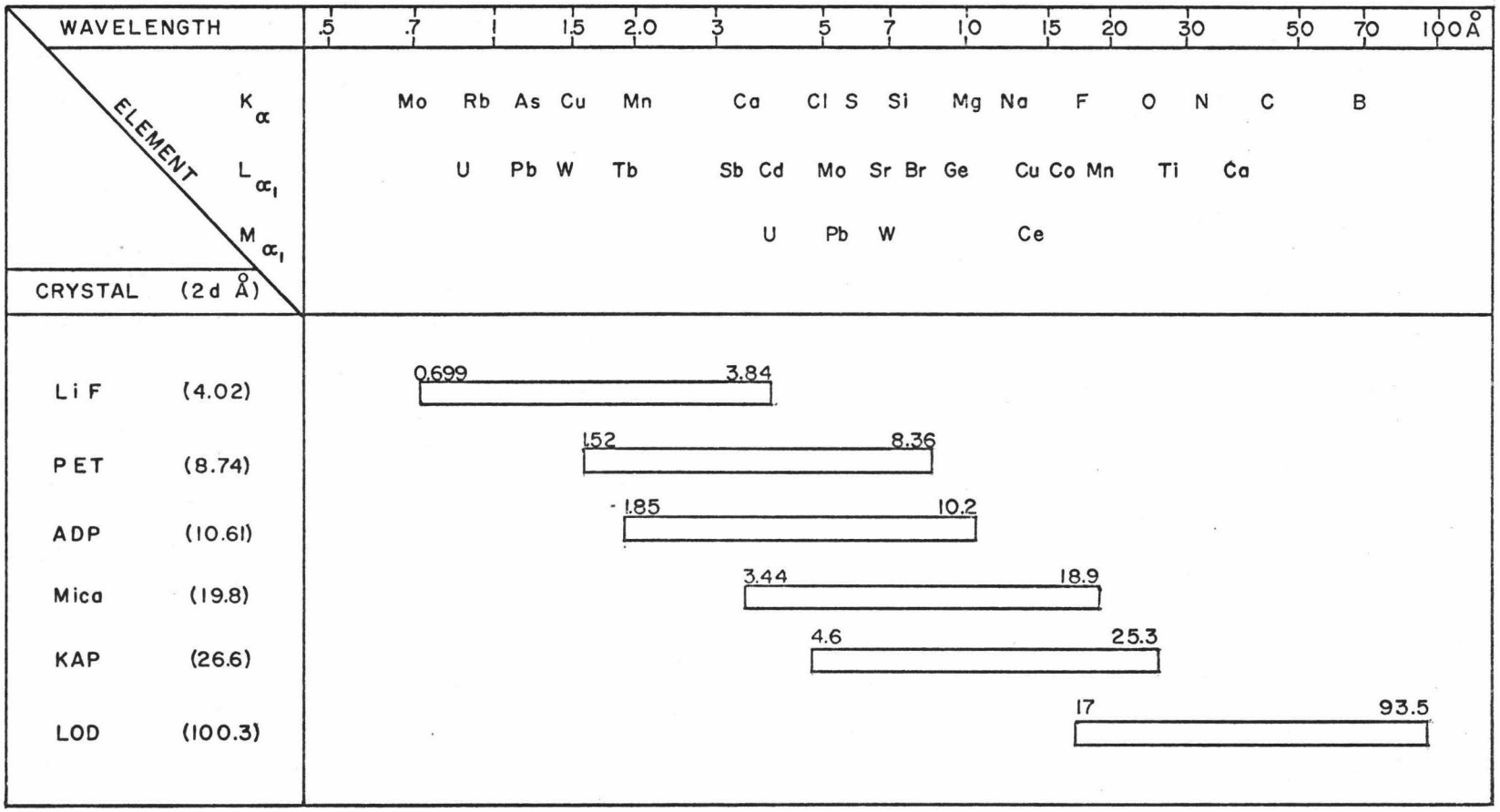

Figure 7: Spectrometer Wavelength Coverage

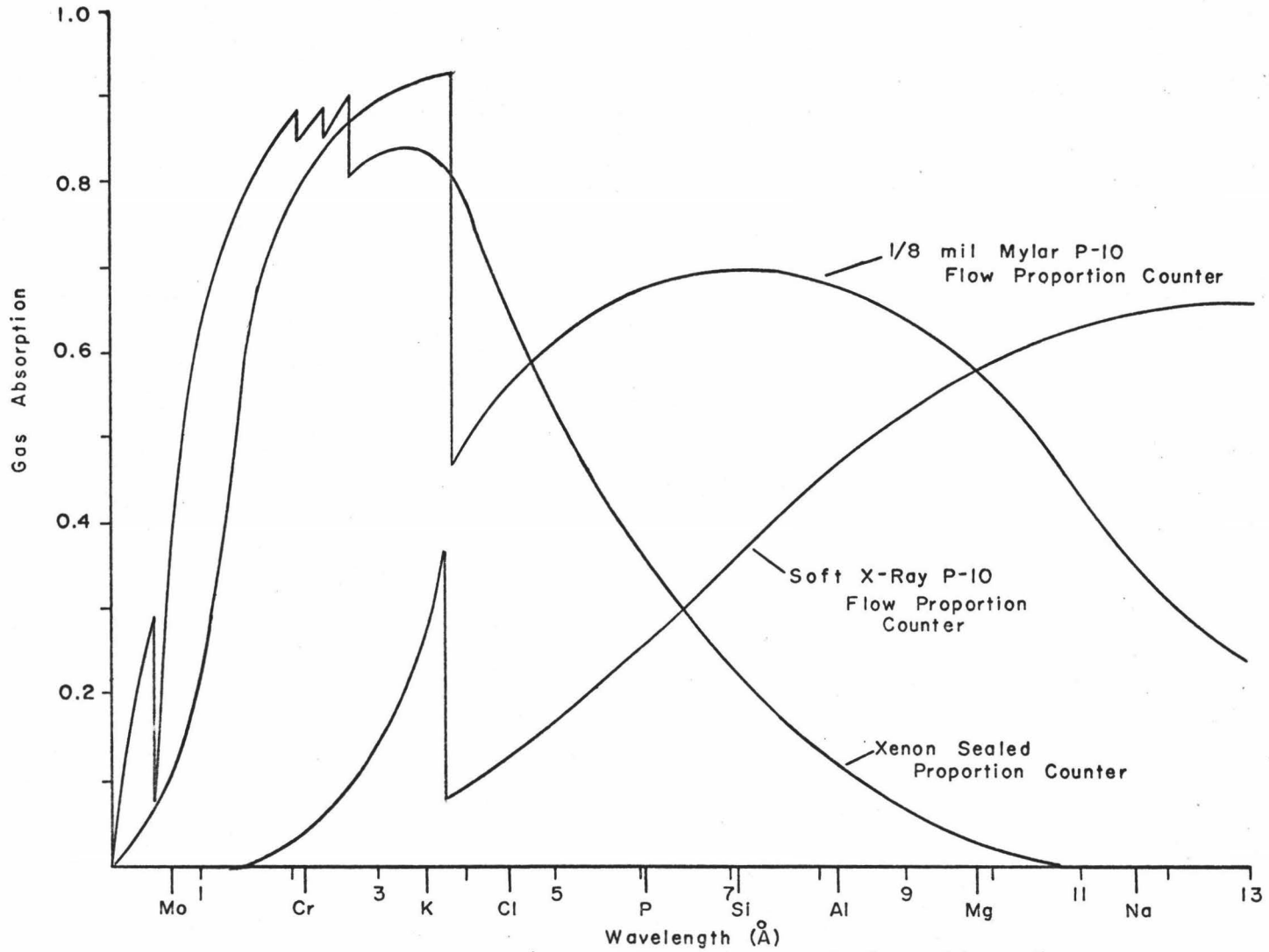

Figure 8: Wavelength Dependence of Gas Absorption

Potassium was detected with the lithium fluoride crystal and the xenon-sealed proportional counter using the 3.742 Å K_α line. The potassium was tuned in using graphite coated potassium bromide as a standard material. Using a KAP crystal and the ultra-thin P-10 gas flow proportional counter, the 11.9 Å K_α line of sodium was tuned in using a sample of chemically pure sodium metasilicate (Na_2SiO_3). The same standard was used for setting the electronics for the 7.1261 Å line of silicon with the P-10 flow proportional counter and a KAP crystal. Later work on the analysis of silicon necessitated switching to the mica crystal because the KAP crystal cracked during use. However, since mica had nearly the same characteristic wavelength as KAP, performance was not affected too much.

4. Qualitative Microprobe Comparisons

Initial samples were analyzed for potassium and sodium in an effort to learn about the distribution of these elements in the samples. Polaroid pictures of electron backscatter images were obtained from the oscilloscope to reveal the sample topography. The spectrometer ratemeters were connected to the oscilloscope for photographs of the distribution of sodium and potassium. 2 minute free-sweep multiple scans were photographed to insure ample intensity from the low alkali content of the samples. A calibration grid was photographed in the electron backscatter mode to estimate the size of the areas being scanned. All pictures were taken of sample areas enlarged 200 times.

Similar scans were obtained on the prepared thin section, but prior to the microprobe work the section was mapped photographically in an effort to uncover the types of minerals present and to provide a map for microprobe scanning. Using a Zeiss microscope with a built-in 35 mm. camera, photographs of the thin section were taken. Kodachrome II Daylight Film was used with the automatic shutter of the camera controlling the exposure times of each photograph. Complete sets of pictures were taken of the surface edge of the thin section at magnifications of 78.75 x and 200 x. Each picture taken at 200 x was duplicated using polarized light transmitted through the thin section. A standard scale with 10 and 100 micron markings was photographed at 78.75 x and 200 x to estimate crystal size.

Later samples were analyzed for potassium and silicon to reveal any correlation between the crystalline (and glassy) silicates and the alkali distribution. The silicon area scans were photographed for a 2 minute multiple scan exposure and the potassium for a 4 minute scan at a sample magnification of 200 x. Secondary electron scans of the sampled areas were also photographed to provide a picture of sample topography.

5. Statistical Microprobe Comparisons

With the use of a stationary electron beam and the X-ray ratemeters, statistical data for the distribution of sodium and potassium was acquired. The bean was moved manually from the original surface edges of samples to internal regions. At

uniformly spaced points, detector counts for sodium and potassium were recorded for 10 second periods. The first few periods were ignored to allow for stabilization of the X-radiation and then four sets of counts were made. From these points, a mean and a standard deviation were determined and plots were made of the average counts sodium and potassium versus distance from the surface edge.

Comparison of different areas of alkali distribution were made by the application of the "t-test" (107,108). The "t-test" is a statistical method to compare averages of the same types of data determined by different methods or for different regions or lots of a sample. If the resultant t-value for the data exceeds the value from a t-table, then the data is significantly different to the confidence level used. In this case, a comparison was made of the average counts of the data for potassium (and sodium) in the surface edge regions and the internal regions of the samples. The equations used were:

$$t = \frac{\bar{x} - \bar{y}}{\sigma_z} \sqrt{\frac{n\,m}{n + m}} \quad \text{and} \qquad \text{(II-2)}$$

$$\sigma_z = \sqrt{\frac{(n-1)\sigma_x^2 + (m-1)\sigma_y^2}{n + m - 2}} \quad ; \qquad \text{(II-3)}$$

where $\bar{x}$ was the average counts for potassium (or sodium) in the surface regions, σ_x was the standard deviation for $\bar{x}$, n was the number of determinations for $\bar{x}$, $\bar{y}$ was the average counts potassium (or sodium) in the internal regions, σ_y was the

standard deviation for $\bar{y}$, m was the number of determinations for $\bar{y}$, and σ_z was the weighed root-mean-square standard deviation for σ_x and σ_y.

D. Supplementary Work

1. Laboratory Degradation Studies

Terrestrial basalts were degraded by potassium or sodium to provide samples for mass spectrometry, vacuum deposition, and electron microprobe analysis as well as for some preliminary studied of the erosion phenomena. The terrestrial samples had well-known chemical and geologic compositions and were chosen for their expected similarity to lunar maria materials.

Reagent grade potassium and sodium, stored under mineral oil, were the source of alkali vapor. A procedure was developed to remove organic contamination from the alkali metals and to retard their oxidation. A 1 centimeter cube of alkali metal was scraped clean of oxides, placed in the tube shown in Figure 9A, and rinsed with hexane. Using the ball-joint attachment of stopcock #5 on the vacuum deposition system (Figure 6), the tube was quickly evacuated to remove the volatile hexane. Gentle heating melted the alkali metal, allowing it to flow into the smaller tube. This tube was cut off and the samples of alkali metal were stored in a desiccator until needed.

A 2 to 3 gram terrestrial basalt was placed in the bottom of a 13 x 100 millimeter test tube, which was pinched to hold

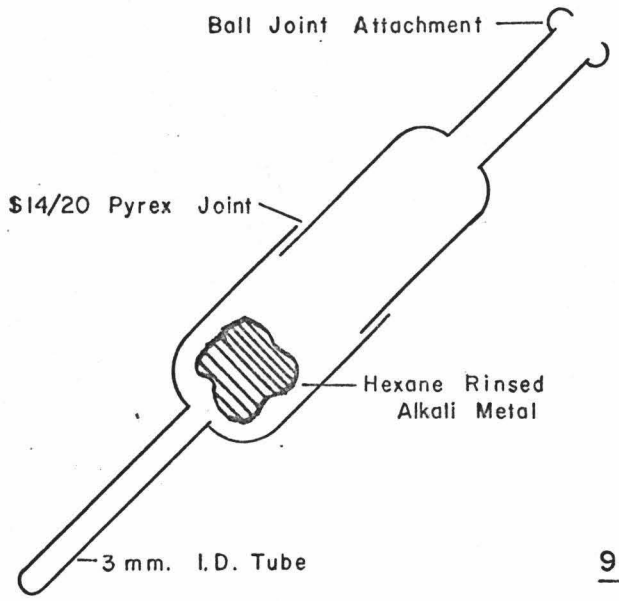

9 A:

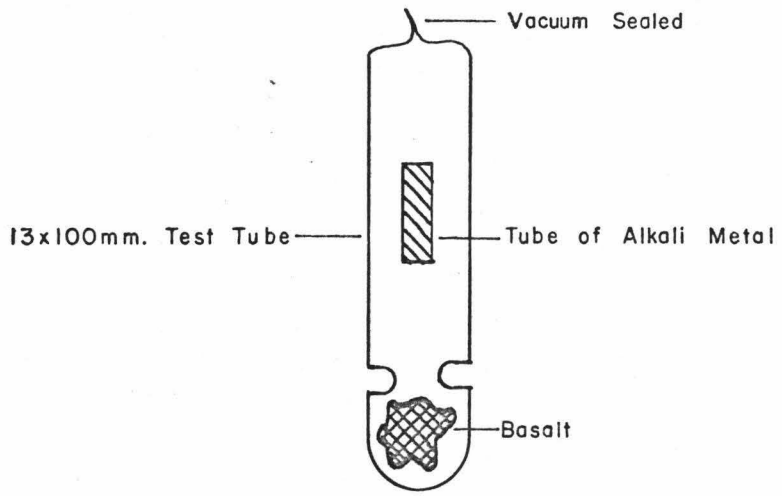

9 B:

Figure 9: Alkali Degradation Equipment

the sample in place. After discarding the oxidized open end, a 1 centimeter tube length of the alkali metal was cut off and placed in the reaction tube shown in Figure 9B. This tube was evacuated to at least 10^{-4} torr and sealed under vacuum by attaching it to stopcock #6 of the vacuum deposition apparatus (Figure 6). During the degradation temperature cycle, the tube was inverted in order that only alkali vapor came into contact with the basalt.

Samples were degraded at two different reaction conditions. Some of the reaction tubes were exposed to a one lunar day temperature cycle shown in Table II. The second group was run at 250°C for times up to two weeks. Samples were heated by placing the reaction tubes in a dibutyl-phthlate heat bath. All samples were periodically observed for physical changes. At the end of the reaction cycle, samples were removed from the reaction tubes, washed with methanol and water, and pH readings of the rinses were taken. Samples were flushed with water until the rinses were neutral to pH hydride paper. The degraded sample products were analyzed for sodium and potassium content by the atomic absorption technique discussed earlier.

2. Mass Spectrometric Gas Analysis

Possible reaction gases formed by different components of the reaction tubes were run on a Hitachi-Perkin-Elmer (Model RMU-6E) mass spectrometer. The reaction tube samples were outfitted with break-seal attachments for these gas studies. Samples of sodium, potassium, sodium and basalt, potassium and

TABLE II. SIMULATED LUNAR DAY TEMPERATURE CYCLE

Terrestrial Day	°C	°K
1	0	273
2	23	296
3	57	330
4	77	350
5	92	365
6	107	380
7	127	400
8	127	400
9	127	400
10	127	400
11	117	390
12	97	370
13	67	340
14	27	300

The high temperature step-wise heating of rocks and isotope analysis of the rare gases released was undertaken by Reynolds and his colleagues (66), all with mass spectrometers.

2. Volatilization from Minerals

Wedepohl (67) used the differential volatility of elements in emission spectrography to improve measurements and levels of detection. Fletcher (68) has employed a volatilization procedure for the analysis of synthetic mixtures for lithium and of feldspars for sodium. Using a distillation process, Edwards and Urey (69) determined the amount of alkali metal in meteorites. The method was based on the volatilization of chlorides from silicates in an induction-heated crucible within a water-cooled jacket. In this way, the chlorides which would normally react with a heated furnace were quantitatively recovered as a volatile product in a form suitable for measurement by flame-spectrophotometry without further chemical processing.

The consistency of recovery of sodium and potassium from silicates initially containing less than 1 percent and 0.1 percent respectively was ± 3 percent. In addition to the alkalis, the method was applicable to a number of other metals. Spectrographic evidence revealed that gallium, zinc, lead, and silver were concentrated in the volatile portion and were absent in the residual solid. The authors suggested that tungsten, cadmium and other metals with volatile chlorides could be analyzed by mixing sodium carbonate and calcium

basalt, and an empty reaction tube, were run through a 250°C temperature cycle for two weeks. These tubes were attached to the mass spectrometer and spectra of the residual gases were taken.

3. X-Ray Diffraction Comparisons

A Norelco diffraction unit was used to obtain diffraction patterns of degraded and unreacted samples. A copper X-ray tube at 35 KV and 20 ma. was used as the source and a 20 range from 10° to 90° was recorded. Peak heights of basalts and degraded basalts were compared for differences in the diffraction pattern. Samples were prepared by grinding them to 400 mesh and smearing the powder on a balsam coated area of a glass slide.

4. Microscopic Observations

Besides the microprobe work and the photomicrographic mapping of the lunar thin section, additional microscopic work was necessary. Upon receiving the lunar samples from NASA, they were examined for their physical characteristics. Unclassified lunar fines were separated and classified according to type. These grains were used for the microprobe work and some chemical analyses of their alkali content. Following the microprobe work on the Bakelite grain mounts, the samples were cleansed of graphite, mounted on a glass slide and prepared in thin section for petrographic identification. The thin section procedure, discussed earlier, was used.

5. Emission Spectrometric Studies

Hale (109) agreed to analyze various fractions of the lunar rocks by standard methods of emission spectroscopy (110). Surface, internal, and the residual samples remaining after heating to 1100°C in the mass spectrometer Knudsen cell were run to observe any differences in composition. This work was designed to reveal what volatile components other than the alkalis may be present.

A few of the vacuum deposition sets of liquid samples remaining after sodium-potassium analysis were combined into liquors which were dried in a platinum evaporating dish under a heat lamp. The residues were redissolved into 5 milliliter volumes with water and dried into spectrographic graphite electrodes at 110°C. These electrodes were burned on the spectrograph to identify any soluble non-alkalic volatiles being removed from the lunar samples and condensed on the cold finger during the deposition studies.

E. Sample Description

1. Lunar Samples (111)

a. #12002

Fragment #12002, 140 weighing 0.77 grams and fragment #12002, 144 weighing 0.48 grams were received. Rock #12002 originally weighed 1529.5 grams and was picked up by Astronaut Conrad in the vicinity of the Lunar Landing Module during his first extravehicular activity on the lunar surface. This sample was described as a fine to medium-grained

holocrystalline basalt with a gross composition of 50% pyroxene, 30% plagioclase, 15% oliving, and 3-4% ilmenite.

During fragmenting, this rock was not classified according to the fragments being surface or internal pieces. However, from the physical appearance of the fragments and the presence of a micrometeorite impact crater on one, conclusions were drawn that a surface and an internal fragment were received. Fragment #12002, 140 contained a fairly large-sized vug with well-defined grayish crystals, which were probably plagioclase. A triangular face of this fragment had the small glass-lined impact pit mentioned above which was raised above the surface and surrounded by a "whitish halo." This face was an original surface which had been exposed to the lunar environment. Fragment #12002, 144 contained no vugs and all faces of the rock were obviously freshly broken, because of the clear mineral components and the lack of dust adhering to any face. This sample was considered an internal section of the lunar rock which was isolated from direct interaction with the lunar surface environment.

b. #12022

Fragment #12022, 47, weighing 0.92 grams, was an internal piece of a rock that originally weighed 1864.3 grams. This sample was removed from a large mound on the lunar maria about 150 meters northwest of the Lunar Module and almost 100 meters north of Head Crater. The sample was described as an olivine dolerite and modal analysis revealed a mineral composition of 29.3% olivine, 26.8% clino-pyroxene, 22.7% plagioclase, and

21.2% opaque minerals. A differentiation of opaque minerals yielded 9.1% ilmenite, 2.0% spinel, 0.5% native iron, 0.2% troilite, and 88.2% transparents.

c. #12052

Sample #12052, 34 weighed 0.82 grams and sample #12052, 64 weighed 1.07 grams. These samples were surface pieces from a 1866.0 gram rock removed from the western rim of Head Crater. The approximate mineralogy of this olivine basalt was 40% reddish-brown pyroxene, 30% feldspar, 15% olivine and 15% ilmenite. The surface faces have a number of glass-lined pits, frequently raised above the surface, with the glass varying from olive green to a dark brown color. #12052, 34 had a very fine-grained texture, while #12052, 64 was a coarse-grained section of the same rock.

d. Lunar Fines

0.23 grams of lunar fines, #12070, 164, were received from the contingency sample which contained 1102.0 grams of unclassified material. The sample, the less than 1 millimeter fines, had the appearance of wet sand. Particles in the range of 0.1 to 1.0 millimeters comprised approximately 25% of the sample. These particles were a combination of breccias, basaltic fragments, anorthositic glasses, and glossy black fragments and spherules. Mineral types of the less than 0.1 millimeter fines were indistinguishable.

e. General Comments

All the samples were picked up by Astronauts Conrad and

Bean during the two extravehicular walks on the Apollo 12 mission. These samples were from the maria region, known as the Ocean of Storms, with landing coordinates of latitude 2.45°S, longitude 23.34°W.

Samples were received after decontamination, preliminary examination, and cutting at the Manned Spacecraft Center's Lunar Receiving Laboratory in Houston, Texas. The positions of fragments from samples #12022 and #12052 were well known. Prior to cutting, models of the rocks were made and cut in the same manner as the rocks and each fragment was identified as either a surface or an internal piece.

Appendixes A through F contain a flow chart of the individual experiments run on each lunar sample. The flow charts provide a code designation for the different experimental fragments of the lunar samples.

2. Terrestrial Basalts

HK-123, HK-124, and HK-121 were used for the degradation studies. These samples were well-known Hawaiian volcanics for which considerable chemical and mineralogical studies have been done. HK-123 was classified as a tholeiitic pahoehoe and was collected from the mouth of Makua Cave, Waianae Range, Oahu. HK-124 was an alkali-olivine basalt collected at the Pacific Rock Company's quarry 0.5 miles west of Puu Kapolei, Waianae Range, Oahu and HK-121 was a rhyodacite collected on Mauna Kuwale, Waianae Range, Oahu (112).

3. Anhydrous Boric Acid

The boron oxide, used as a mass spectrometric standard for vapor pressure calculations, was made by the dehydration of chemically pure boric acid. The boric acid was first dehydrated in a platinum crucible at 400°C for several hours and then heated at 900°C for one hour at 10^{-6} torr (100).

III. RESULTS AND DISCUSSION

A. Terrestrial Samples

1. Presentation of Data

Terrestrial samples were used to develop the experimental techniques, to determine the vapor forms of alkali release, to try and uncover the mechanism of alkali attack, and to form a basis of comparison for the various lunar samples. The preliminary degradation studies were used to provide degraded samples for study, to substantiate earlier findings by Naughton, et al. (37), and to observe any gross physical or chemical changes during degradation. Samples exposed to alkali vapor under simulated lunar diurnal surface conditions underwent considerable degradation and were very similar in appearance to lunar surface materials. After showing that lunar surface temperatures could cause significant attack, provided alkali vapor was present, most degraded samples were prepared at 250°C to speed the process of preparation.

Earlier, Winborne (33) suggested that the mechanism of comminution of basalts under lunar conditions might be the volumetric expansion of alkali metals in going from a solid to a liquid phase. Sodium undergoes a 2.5% increase in volume during melting, while potassium undergoes a 2.41% increase. Under conditions of partial restraint, the molten metal can exert forces more than significant to cause fracture of rocks. For example, cases have been reported of rupturing of piping and tanks during the melting of sodium due to volumetric

expansion effects when melting did not begin at the surface of the sodium. Under lunar conditions ranging from 127° to -127°C, sodium and potassium would pass through their melting points of 97.5° and 62.3°C during each lunar day. While molten or gaseous, alkalis could diffuse into the grain boundaries and interstices of basalts. After solidifying during the lunar night, if heated unevenly or with a thermal gradient such that melting did not proceed away from the free surface, the molten sodium or potassium could exert large forces due to restrained expansion. This mechanism would be very similar to the thermal fracturing effects due to the presence of water that Ryan (16) discussed.

The samples prepared for degradation study were heated only once and then cooled, but yet significant basalt comminution occurred. This seemed to rule out a comminution by bursting as the alkali degradation mechanism, but over many heating cycles it could have some effect. Though laboratory methods hastened the degradation process by using large concentrations of alkali, studies indicate that lunar surface materials have been exposed to the surface environment for 10^7 years or more (25). Provided that alkali vapors, or other volatiles, were released at some period into the lunar atmosphere, this would be sufficient time for regolith materials to undergo chemical attack.

During exposure of basalts to alkali vapor for a one lunar day cycle, many physical changes occurred. Sample comminution by potassium occurred much more rapidly than by sodium vapor.

For the same exposure times and temperatures, potassium attack was at least twice as rapid as sodium attack. Since there was no evidence of any attack with the reaction tubes, interaction was limited to the basalts and alkali metal. Only the alkali vapors were allowed to come in contact with the basalts.

After exposure to alkali vapor, the remaining fragments of basalt were darker than the original sample and some were partially coated with a white crystalline material even after rinsing with methanol and water. All the degraded samples were deeply pitted and the sharp angular edges of the original basalt were rounded. Certain surfaces showed evidence of flaking and cracking. In the coarser samples (HK-121), large surface feldspar crystals were much more prominent than they were in the original sample. A pumice sample that was vacuum-melted prior to degradation was very uniform, quite dense and hard. The sample was almost completely degraded by both sodium and potassium vapor.

The degradation powders ranged in size from approximately 0.075 to 0.8 millimeters. The more degradation in the samples the smaller the sample size. After wishing and drying, these powders were darker than the original basalts, had the appearance of wet sand, and were quite cohesive. They adhered to most surfaces they came in contact with and would cling to materials even at very steep angles.

Some startling similarities between these findings and selenographic observations were apparent. Loss of crater

clarity (rim rounding), deep pitting and rounding of surface rocks, and darkness of the lunar fines (#12070, 164) were a few of the similarities. A major observation of the Apollo 11 and 12 crews was the cohesive nature of the lunar fines. Particle size comparisons of the degraded powders and the lunar fines were similar (6,7).

Copious amounts of gas (probably hydrogen) were given off on treatment of the degraded samples and powders with methanol and water. Basicity of the rinses was in a direct proportion with the amount of sample degradation. Room temperature mass spectra backgrounds of the gases in reaction tubes containing only sodium, potassium, basalt, basalt and sodium, or basalt and potassium were run. The tubes containing both alkali metal and basalt had pressures greater than atmospheric pressure even though before degradation they were sealed at 10^{-5} torr. The mass spectra of the residual gases revealed nothing other than the normal permanent atmospheric gases plus some hydrogen. However, hydrogen was detected in the tubes containing only alkali which could be the source of hydrogen, from hydrides. Reaction tubes containing only basalt were still under vacuum with only the permanent gases (oxygen, nitrogen, argon, carbon dioxide) present.

Chemical analyses of the reacted basalts and degradation powders showed considerably more alkali concentration in the powders than in the basalts. Table III compares the alkali concentrations of the degraded products, powders and rock, to

TABLE III. ALKALI CONCENTRATION OF DEGRADATED SAMPLES

Sample	Powder	Rock	Original Rock
	(%Na - Na Degraded for 1 Week at 250°C)		
HK-123	3.97	3.48	1.81-2.09
HK-121	10.9	7.27	3.13-3.31
HK-124	5.42	6.05	2.60-2.89
Vac. Pumice	7.55	3.69	1.29-1.52
	(%K - K Degraded for 1 Week at 250°C)		
HK-123	1.57	0.68	0.53-0.44
HK-121	3.98	3.52	3.28-3.58
HK-124	3.23	1.08	1.09-1.20
Vac. Pumice	4.27	2.28	0.33-0.38
	(%K - K Degraded for a 1 Lunar Day Temperature Cycle)		
HK-124	2.78	1.11	1.09-1.20

that of the original rock for various samples degraded by potassium and sodium. The analysis of the products was carried out by atomic absorption using the standard method (102). The original rock analyses were done by two independent laboratories (112). Table IV shows the alkali concentrations of different samples of HK-123 exposed to potassium vapor at 250°C for 8 days. Analyses for some are given for the mixed degraded products and in other cases for the powder separated from the reacted rock.

Since these analyses indicated an increase in the alkali content of the rocks during comminution, layers of the basaltic fragments were filed off and analyzed for alkalic content to see how deep the penetration was. Table V gives the results of the analyses. Fractions a,b,c, and d were the surface layers and a_1, a_2, a_3 were subsequent layers in from filed face a. The layers filed off were approximately 2 millimeters thick and yielded about 10-20 milligrams of material for analysis. These analyses revealed no measurable increased concentration of lakali in the surface layers. Part of the problem with the filing method was the heterogeneous nature of the basaltic samples. Removal of layers of multi-mineral composition could account for the erratic alkali concentrations. It is significant to note (Table IV) that the powder fractions of the products all were between 4 and 6 percent potassium.

Table VI gives an indication of the accuracy and precision of the Lewis' method (102) for analysis of alkali in volcanic materials. Four samples of each basalt were analyzed, averaged

TABLE IV. ALKALI CONCENTRATIONS OF HK-123 EXPOSED TO POTASSIUM VAPOR AT 250°C FOR 8 DAYS

Sample	Description	%K	%Na
A	Mixed Powder and Reacted Basalt	1.286-1.298	1.699-1.642
B	Mixed Powder and Reacted Basalt	1.259-1.220	1.290-1.325
C	Mixed Powder and Reacted Basalt	1.240	1.31
D	Reacted Basalt	0.548	1.97
E	Degradation Powder	6.51	1.71
F	Unreacted Original Basalt	0.53-0.44	1.81-2.09

TABLE V. LAYER FILINGS OF BASALTS EXPOSED TO POTASSIUM AT 250°C FOR 44 HOURS

HK-123	%K	%Na	Layer Description
1b	.426	2.73	Surface
1c	.452	2.57	Surface
1d	.370	1.96	Surface
1a	.512	1.83	Surface
$1a_1$	.596	5.27	Layer in from a
$1a_2$	.492	3.24	Layer in from a_1
$1a_3$	.400	2.30	Layer in from a_2
3b	.523	1.87	Surface
3c	.569	2.02	Surface
3d	.446	1.88	Surface
3a	.520	2.02	Surface
$3a_1$	.509	3.11	Layer in from a
$3a_2$	.511	1.51	Layer in from a_1
$3a_3$	.493	2.90	Layer in from a_2
4a	1.250	6.98	Surface
$4a_1$	.540	1.74	Internal
5a	1.421	5.49	Surface
$5a_1$	.665	1.33	Internal
HK-124			
6b	1.043	2.49	Surface
6c	1.030	3.27	Surface
6d	1.009	2.11	Surface
6a	1.518	5.42	Surface
$6a_1$	1.158	4.18	Layer in from a
$6a_2$	1.211	3.62	Layer in from a_1
$6a_3$	1.480	7.78	Layer in from a_2

TABLE VI. COMPARISON OF HIG A.A. ANALYSIS OF ALKALIS VERSUS DENVER ROCK ANALYSIS LABORATORY AND JAPAN ANALYTICAL CHEMISTRY RESEARCH INSTITUTE

Sample	HIG	DRA	JACR
	%K		
HK-123	0.413±0.061	0.45	0.441
HK-121	3.38 ±0.21	3.28	3.58
HK-124	1.161±0.107	1.09	1.20
	%Na		
HK-123	1.82 ±0.02	1.80	2.09
HK-121	4.46 ±0.44	3.63	3.31
HK-124	2.96 ±0.30	2.60	2.87

together, and the standard deviation was calculated. These results are compared to separate analyses by the Denver Rock Analysis Laboratory and the Japan Analytical Chemistry Research Institute. Considering that these were multicomponent materials, the agreement is quite good.

Table VII compares the X-ray diffraction data of the degraded powders to the unreacted sample. The vacuum pumice was degraded with sodium and the HK-123 was exposed to potassium vapor. Though powder smears of small samples gave high X-ray backgrounds, the relative peak intensities were compared. Comparative spectra revealed no significant differences in the composition of degraded and unreacted samples. This supported the earlier observations of Naughton, et al. (37), and the deductions from microscopic examination, that the powders were comminuted basalts with no significant chemical or mineralogical alteration during degradation, other than an alkali increase in the degraded products.

Electron microprobe scans were made of the degraded powders by the grain mount technique, of polished basalts exposed to potassium vapor, and of polished unreacted basalts. Photographs were taken in the electron backscatter mode to obtain the distribution of potassium and silicon. Figures 10 and 11 are typical examples of the electron microprobe scans of the degraded powder fractions. The top of each plate shows the electron backscatter picture of the grain and the bottom represents the distribution of potassium. The photographs cover an area of approximately 300 x 280 microns. The

TABLE VII. X-RAY DIFFRACTION COMPARISONS OF RELATIVE PEAK INTENSITIES BETWEEN DEGRADED POWDERS AND UNREACTED BASALTS

2θ	Powder	Rock	2θ	Powder	Rock
			(Vacuum Pumice)		
22.2	21	18	42.7	24	24
27.8	14	15	44.7	24	25
27.9	17	16	44.9	30	24
28.0	16	18	52.7	14	16
28.1	13	17	55.1	15	14
30.1	64	56	55.3	15	13
30.7	26	32	60.1	16	20
30.9	30	31	61.3	13	18
35.3	27	22	61.6	19	18
35.6	28	23	61.7	24	20
36.2	24	23	66.3	17	22
42.4	18	21	66.6	19	21
42.5	28	23			
			(HK-123)		
22.4	18	17	30.3	29	24
24.2	16	18	30.9	13	14
24.8	16	14	35.5	14	13
28.2	15	18	36.2	18	16
28.4	36	38			

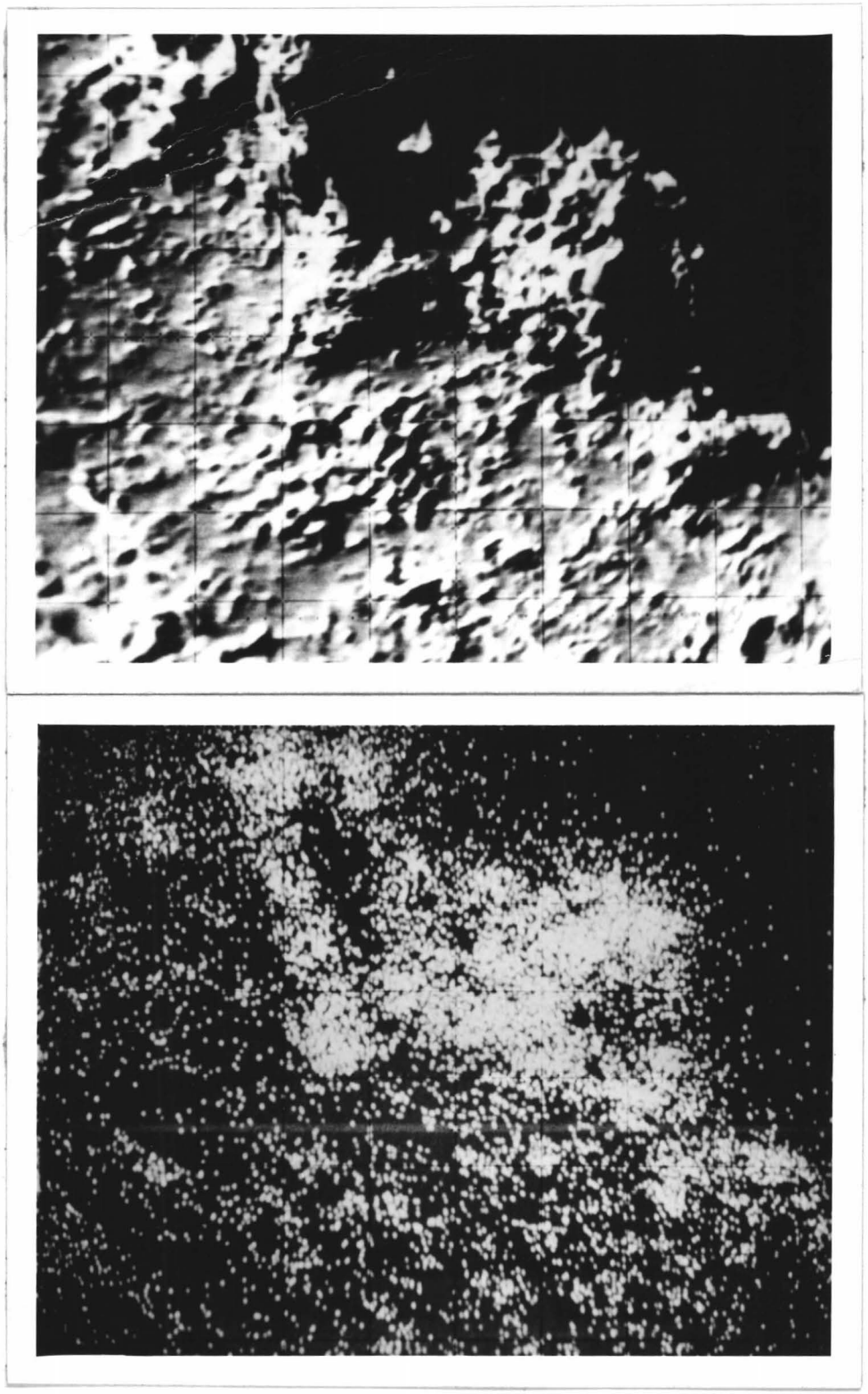

FIGURE 10. ELECTRON BACKSCATTER PHOTOGRAPH OF A K-DEGRADED HK-123 GRAIN AND ITS POTASSIUM DISTRIBUTION

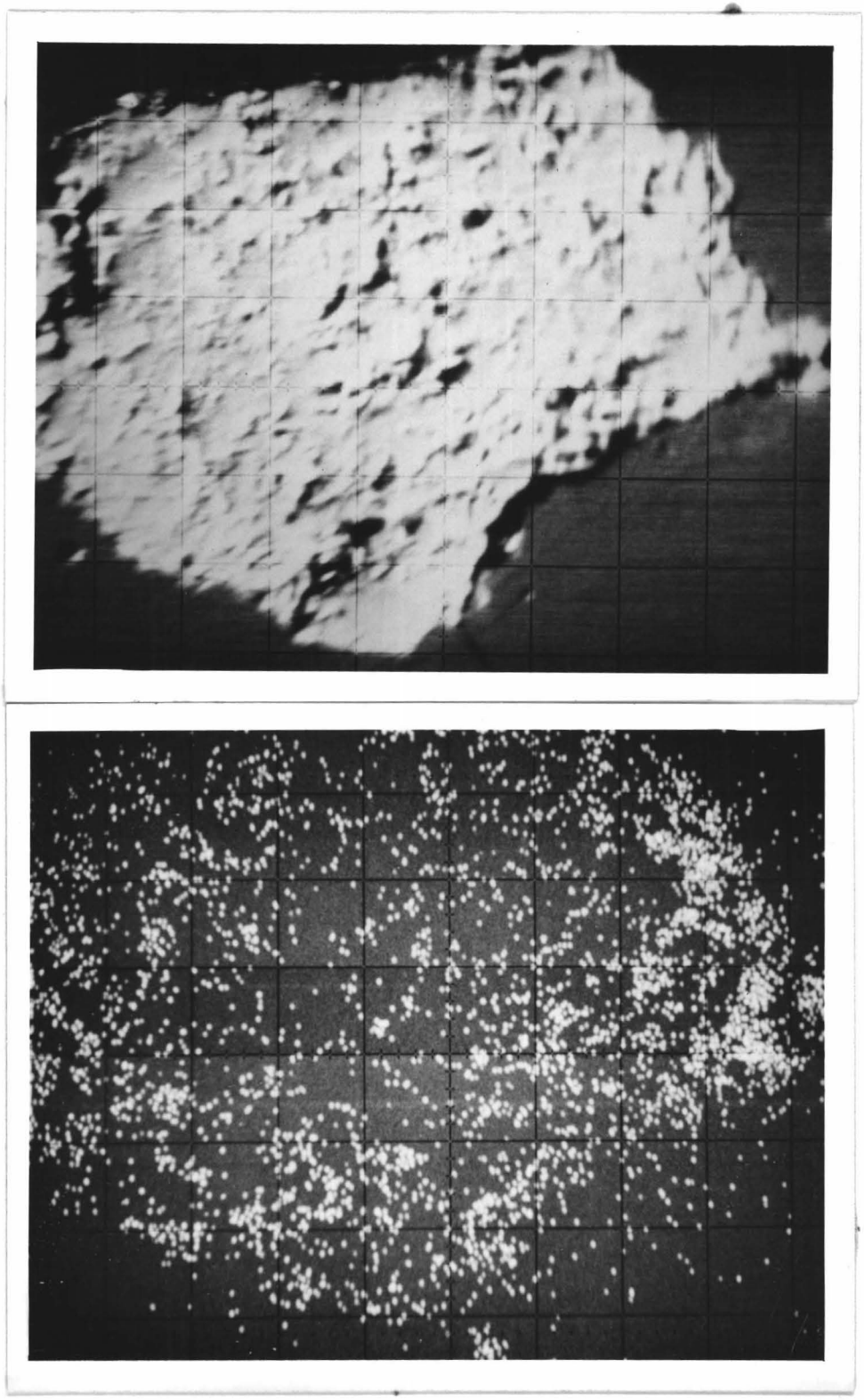

FIGURE 11. ELECTRON BACKSCATTER PHOTOGRAPH OF A K-DEGRADED HK-123 GRAIN AND ITS POTASSIUM DISTRIBUTION

individual grains showed either a very heavy potassium concentration along various edges (Figure 10) or a slight, uniform surface edge increase in potassium (Figure 11). These grains were washed thoroughly to remove any adhering metallic or soluble potassium after degradation, so that this edge build-up of potassium was tightly bound in the silicate of the grains.

The top of Figure 12 is the distribution of potassium in a basalt after exposure to potassium vapor and the bottom photograph is the unreacted basalt. This plate was typical of all the photographs that compared the unreacted with the degraded basalts, and showed that there was no difference between them, detectable by this means. Though it appears in Figure 12 that there were different overall concentrations of potassium, this was not the case. Normally, the intensity of white dots can be used to quantitatively compare amounts of one element, but these samples were run at different electron beam conditions making direct intercomparison impossible. The degraded basalt was run at an electron beam voltage of 15 KV, while the unreacted basalt was run at 20 KV. Differences of the alkali distribution in the rocks, however, would be evident.

As indicated previously, chemical analysis had shown that the degraded basaltic fragments had slightly higher potassium content than the unreacted basalts, but the microprobe scans did not show a selective concentration of potassium in any specific area in the samples examined. Apparently the potassium

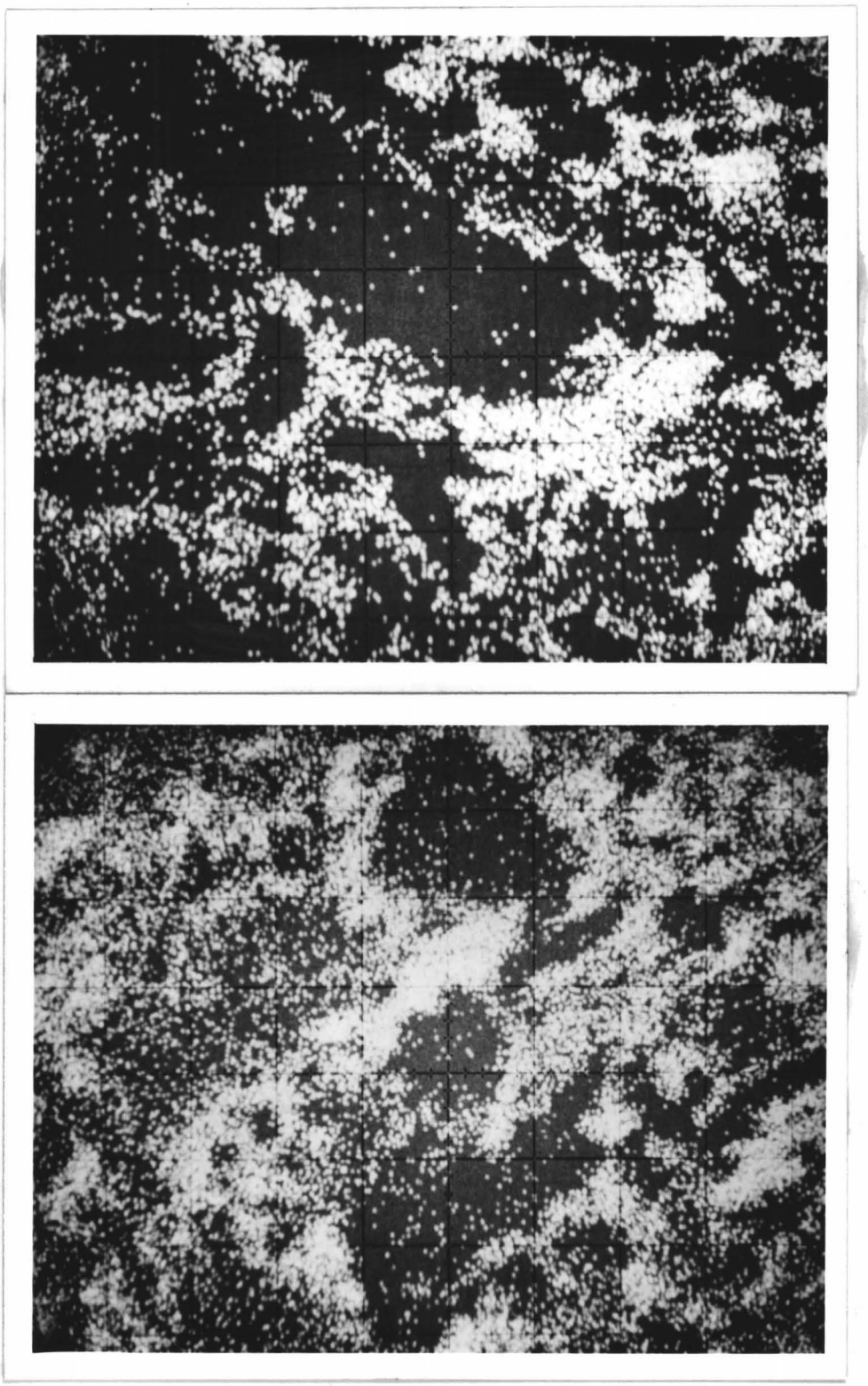

FIGURE 12. ELECTRON MICROPROBE POTASSIUM SCANS OF K-DEGRADED BASALT (TOP) AND UNREACTED BASALT (BOTTOM)

build-up was in regions where potassium was already located in the original sample. Other scans of comminuted basalts showed no significant edge or surface crack concentrations of alkali, but most of the powder fraction particles examined did have a definitely higher content of potassium.

The technique of vacuum deposition onto a cold finger yielded the amount of alkali removed from a sample at a known temperature. In addition to alkali collection, this technique could be used to determine any water soluble volatiles that might be collected on the cold finger. A few atomic absorption analyses revealed the presence of trace amounts of iron, calcium, and chlorine in the water rinses of samples evaporated above 850°C. The alkalis collected at the high temperature runs were clearly visible on the cold finger. Usually the finger was coated with a purplish-silver gray coating, which oxidized to a white material when the system was opened to the atmosphere. This white material was very soluble and was easily washed from the cold finger. At about 1000°C, near the liquidus point of most of the samples, the cold finger usually contained a yellowish-brown coating, along with the alkali coat, which was only slightly soluble in water. These were the samples that contained traces of iron and chlorine, which may be due to direct particle transfer from the sample to the cold finger rather than volatilization.

Figures 13 and 14 are typical plots of the loss of potassium and sodium from potassium-degraded and unreacted HK-123. For

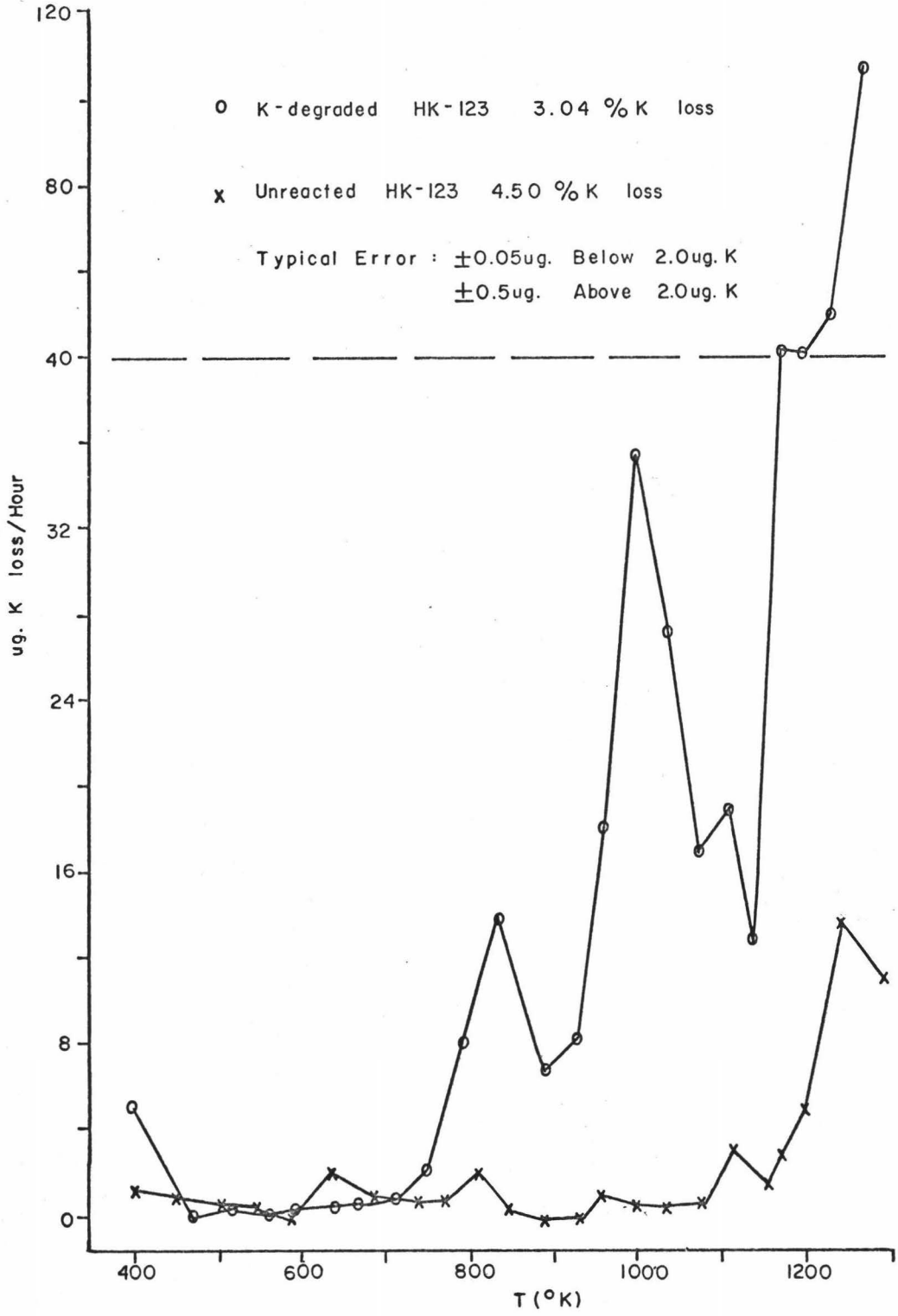

Figure 13: Potassium Loss versus Temperature

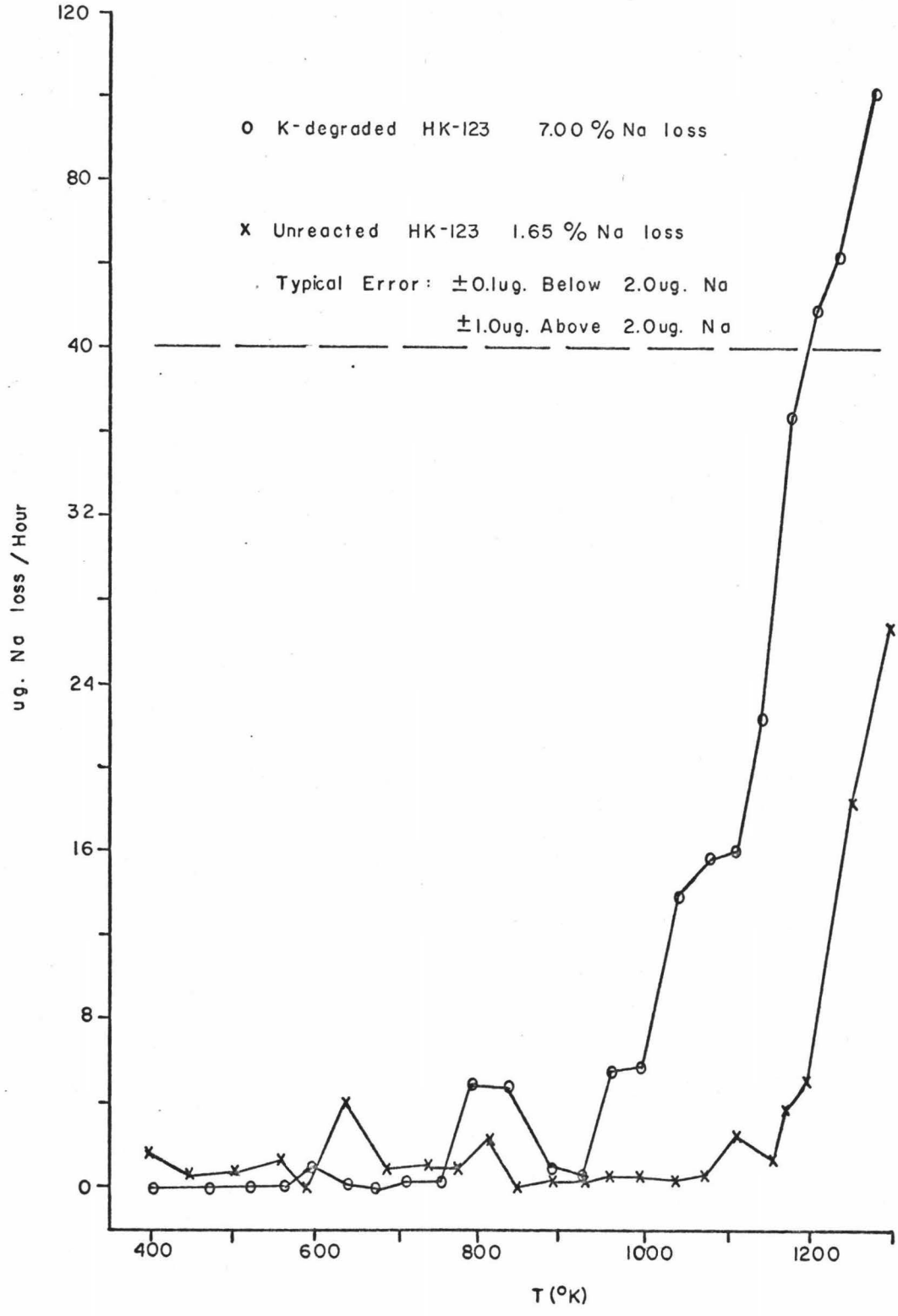

Figure 14: Sodium Loss versus Temperature

the unreacted samples, the sodium and potassium release were very similar. This was not surprising since both alkalis are found in the same basic minerals and they could be expected to undergo similar release mechanisms. The higher percentage loss of potassium reflects a higher dissociation vapor pressure of its compounds (37).

The vaporization experiments with the potassium-degraded sample yielded considerable information. With increasing temperature there appeared to be three processes occurring, which were probably surface, high diffusivity path, and volumic removal of the alkalis. Some reaction between the potassium and the basalt must have occurred, since these samples melt at a lower temperature and release their volumic components at lower temperatures. Most of the potassium release from a potassium-degraded sample occurs in the middle region at about 1000°K. The sodium peak at the same temperature region increased also. Surprisingly, there was a large increase in the percentage of sodium loss in a potassium-degraded sample and most of this loss occurred in the volumic (lattice) component.

Table VIII gives the total amount and percentage of alkali lost from potassium-degraded and unreacted basalts. Also given is the ratio of the percent potassium to percent sodium loss. The error limits are the weighted standard deviations for all the individual samples of the components collected at each temperature. The last three samples presented in this table are from the large cold finger prototype which contained 2.50

TABLE VIII. TOTAL AMOUNT ALKALIS LOST FROM K-DEGRADED AND UNREACTED BASALTS

Temperature Sample Heated to in °K	µg. K loss	% K loss	µg. Na loss	% Na loss	%K loss / %Na loss
		(K-degraded HK-123)			
1223	446±.50	2.74	138±.80	3.23	.848
1273	416±.50	3.04	345±1.0	7.00	.433
1178	179±.11	7.06	328±1.1	12.3	.575
1243	192±.15	6.20	331±.35	10.12	.612
1073	122±.11	4.10	135±.22	4.30	.953
1273	201±.15	6.22	460±.31	11.02	.564
		(Unreacted HK-123)			
1223	31.3±.50	2.79	40.7±1.0	0.90	3.10
1303	50.6±.50	4.50	75.3±0.8	1.65	2.73
1263	27.0±.50	2.40	76.9±1.0	1.69	1.42
1193	61.5±.10	5.46	63.0±.33	1.39	3.94
1173	115.±.50	10.2	227.±.80	5.00	2.04
1283	45.2±.11	4.02	110.±1.1	2.22	1.81
1273	428.±2.3	3.80	1080±6.3	2.17	1.75
		(Unreacted HK-121)			
1273	547.±3.4	0.71	901.±6.3	1.24	.57
		(Unreacted HK-124)			
1258	507.±3.1	1.84	912.±6.5	1.34	1.37

grams of basalt, while all the other samples are from the small cold finger design using 250 milligrams of basalt. The degraded samples all had percentage loss ratios less than 1, while the unreacted HK-123 ratios were greater than 1, reflecting the high relative rate of release of sodium in a potassium-degraded sample, as mentioned above.

Figures 15 and 16 are typical plots of the log D/a^2 (diffusion coefficient divided by the square of particle size) versus the reciprocal of temperature for potassium and sodium loss from degraded and unreacted HK-123. Using the Arrhenius equation (I-8), the energy of release of alkali from a basalt can be calculated from the slopes of these plots. Energy values are presented for the three temperature regions where different release mechanisms seem to occur. The greater rate of potassium release corresponded to the lower energy values. Volumic (lattice) diffusion energies for degraded samples appeares to be lower than unreacted basalt energies. Higher log D/a^2 values for degraded samples coincided with the larger fractional loss of alkali. Tables IX, X, and XI present the energy of release for potassium and sodium from the three temperature regions where alkali release occurred in degraded and unreacted samples.

For ideal diffusion, the square of fractional release, F^2, is proportional to time at a fixed temperature (Equation I-5). Therefore a plot of F^2 versus time should be a straight line. If losses in previous heating cycles occurred comparable to the amount of alkali released at a particular temperature, then the

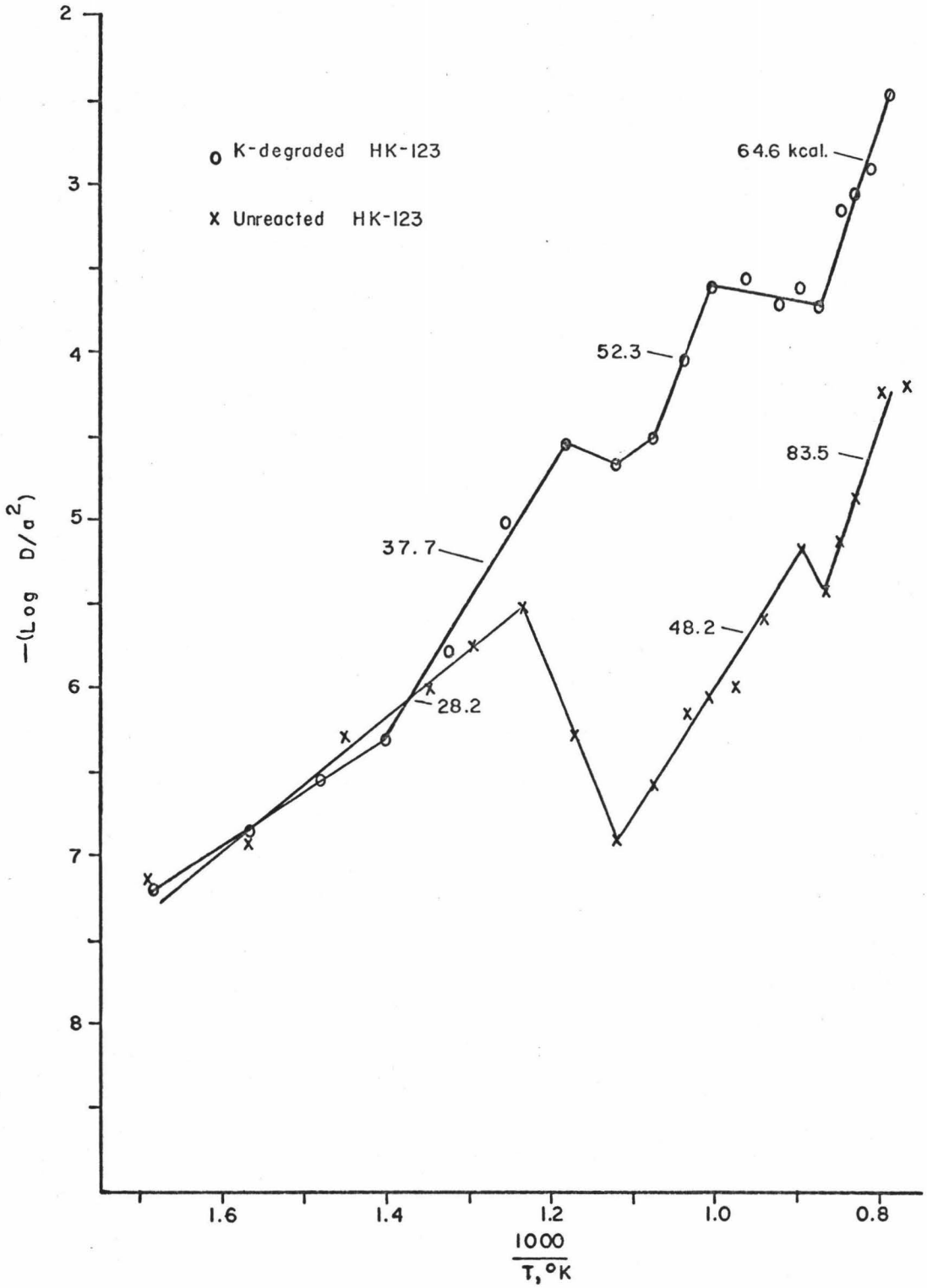

Figure 15: Log D/a^2 versus 1000/ T, °K for Potassium Loss

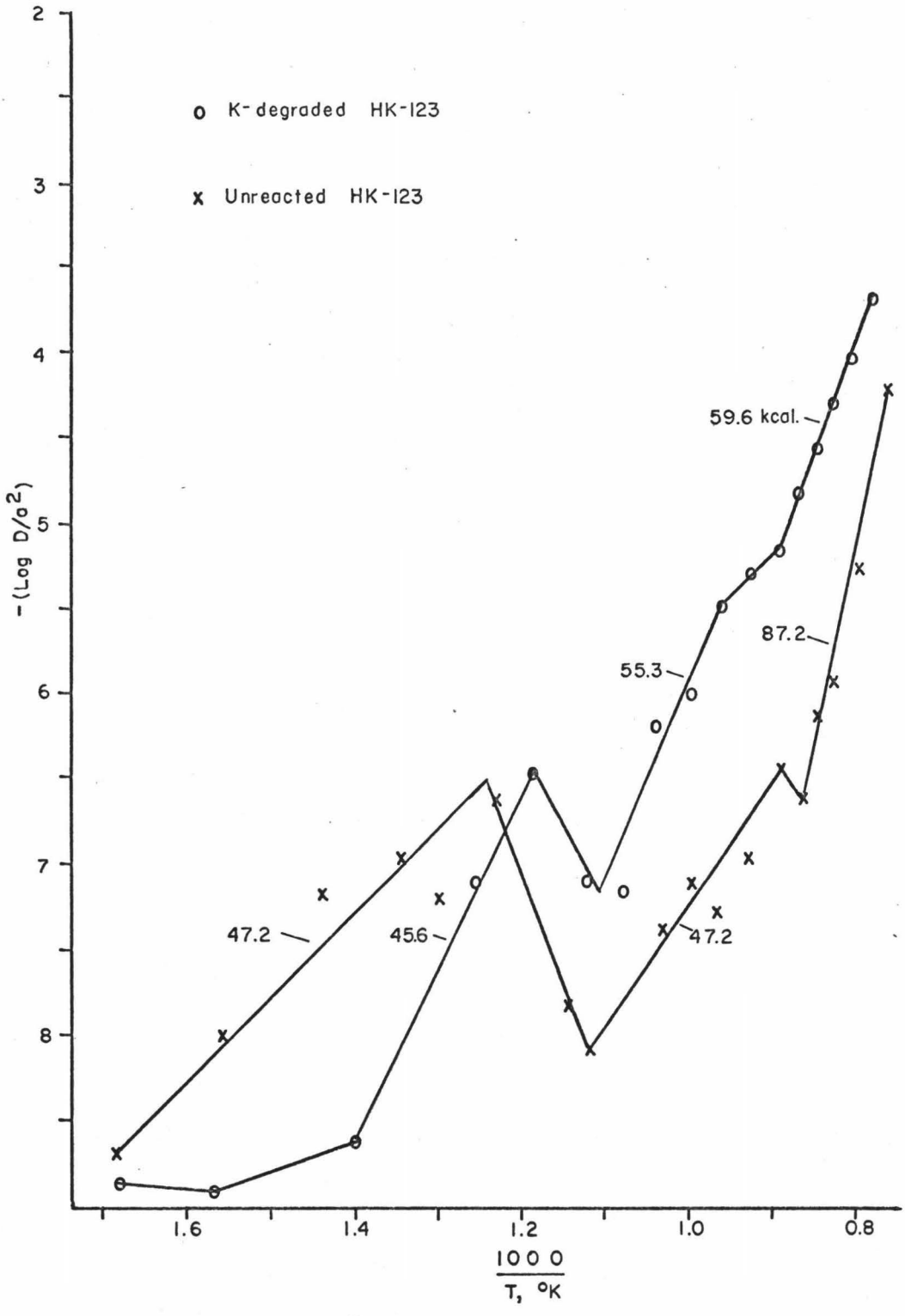

Figure 16: Log D/a^2 versus 1000/T, °K for Sodium Loss

TABLE IX. HIGH TEMPERATURE RELEASE REGION
(LATTICE OR VOLUMIC DIFFUSION)

Temperature at which K Starts to be Released, °K	Energy of K Release in kcal.	Temperature at which Na Starts to be Released, °K	Energy of Na Release in kcal.
		(K-degraded HK-123)	
1150	69.3	1115	58.4
1080	64.6	1110	59.6
1060	31.1	1060	52.7
990	15.1	990	33.1
1120	13.1	1120	51.7
		(Unreacted HK-123)	
1120	83.5	1120	87.2
1160	84.1	1160	81.6
1160	137.4	1160	119.3
1080	57.4	1080	62.3
1080	44.2	1080	32.8
1130	62.8	1130	68.3
1080	93.0	1030	75.3
		(Unreacted HK-121)	
960	44.1	1130	54.3
		(Unreacted HK-124)	
1160	86.4	1130	121.9

TABLE X. INTERMEDIATE TEMPERATURE RELEASE REGION
(HIGH DIFFUSIVITY PATHS)

Temperature Range of K Release, °K	Energy of K Release in kcal.	Temperature Range of Na Release, °K	Energy of Na Release in kcal.
		(K-degraded HK-123)	
970-1150	38.5	930-1115	35.8
890-1080	52.3	925-1110	55.3
980-1060	68.7	960-1060	61.5
930-1060	10.4	930-1060	8.0
880-990	19.4	880-990	33.6
860-1120	18.0	870-1120	26.1
		(Unreacted HK-123)	
930-1120	28.2	900-1120	47.2
930-1160	36.0	860-1160	29.4
950-1160	83.4	910-1160	31.9
860-1080	33.5	860-1080	33.7
890-1080	31.0	890-1080	24.0
930-1040	55.5	930-1040	54.4
--	--	900-1030	34.4
		(Unreacted HK-121)	
--	--	860-1130	34.7
		(Unreacted HK-124)	
930-1130	33.0	930-1160	29.2

TABLE XI. LOW TEMPERATURE RELEASE REGION
(SURFACE DIFFUSION)

Temperature Range of K Release, °K	Energy of K Release in kcal.	Temperature Range of Na Release, °K	Energy of Na Release in kcal.
	(K-degraded HK-123)		
720-970	33.4	780-900	24.6
710-890	37.7	750-890	45.6
720-980	26.9	660-960	22.9
770-930	40.1	760-930	24.1
730-880	24.2	820-880	60.0
700-860	40.1	700-870	33.5
	(Unreacted HK-123)		
600-900	21.6	600-900	18.6
600-900	16.4	600-900	20.9
560-750	15.7	550-900	18.7
780-860	18.0	780-860	15.5
	(Unreacted HK-121)		
560-960	8.0	560-960	12.1
	(Unreacted HK-124)		
710-930	25.9	710-960	19.1

straight line should not go through the origin. The previously lost amount should be given by the ordinate at time zero. The slope of the line may be used to calculate D/a^2. Figure 17 gives some of these plots at various temperatures. The point at the ordinate (time zero) was the square of the fractional amount of alkali released prior to heating at the temperature shown. Figure 17A and B show the increase in D/a^2 with temperature for potassium and sodium. The larger D/a^2 values for potassium reflect its higher mobility and ability to be released in greater amounts for a fixed time and temperature. Figure 17 C and D show a comparison in the volumic release region for an unreacted and a potassium-degraded sample. Though D/a^2 values did not change for potassium, they increased by an order of magnitude for sodium in going from an unreacted to a degraded sample. This coincided with the earlier observation that there was a greater volatilization of sodium from the volumic region in potassium-degraded samples.

Figures 18 and 19 are plots of relative ion intensity versus temperature for the various volatiles detected by the high temperature mass spectrometer studies. Only alkali volatiles were found in the mass region 0 to 100 a.m.u. If other volatiles were present they were below a vapor pressure of 10^{-6} torr, the limits of instrument detection. The major difference between the potassium and sodium spectra was the large amount of diatomic sodium released compared to the relatively small amount of diatomic potassium. Spectra revealed the same three temperature zones of release found in the vacuum

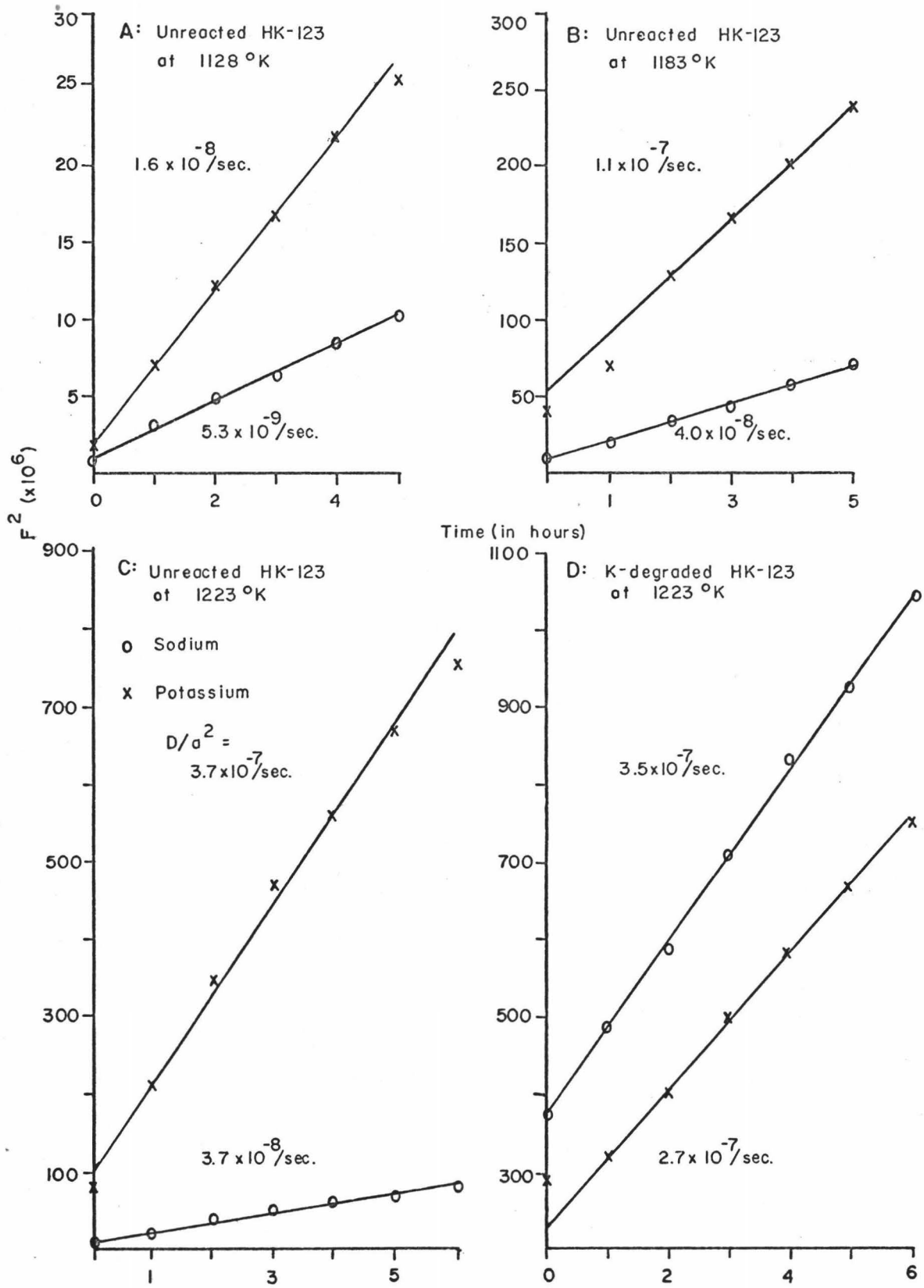

Figure 17: F^2 versus Time

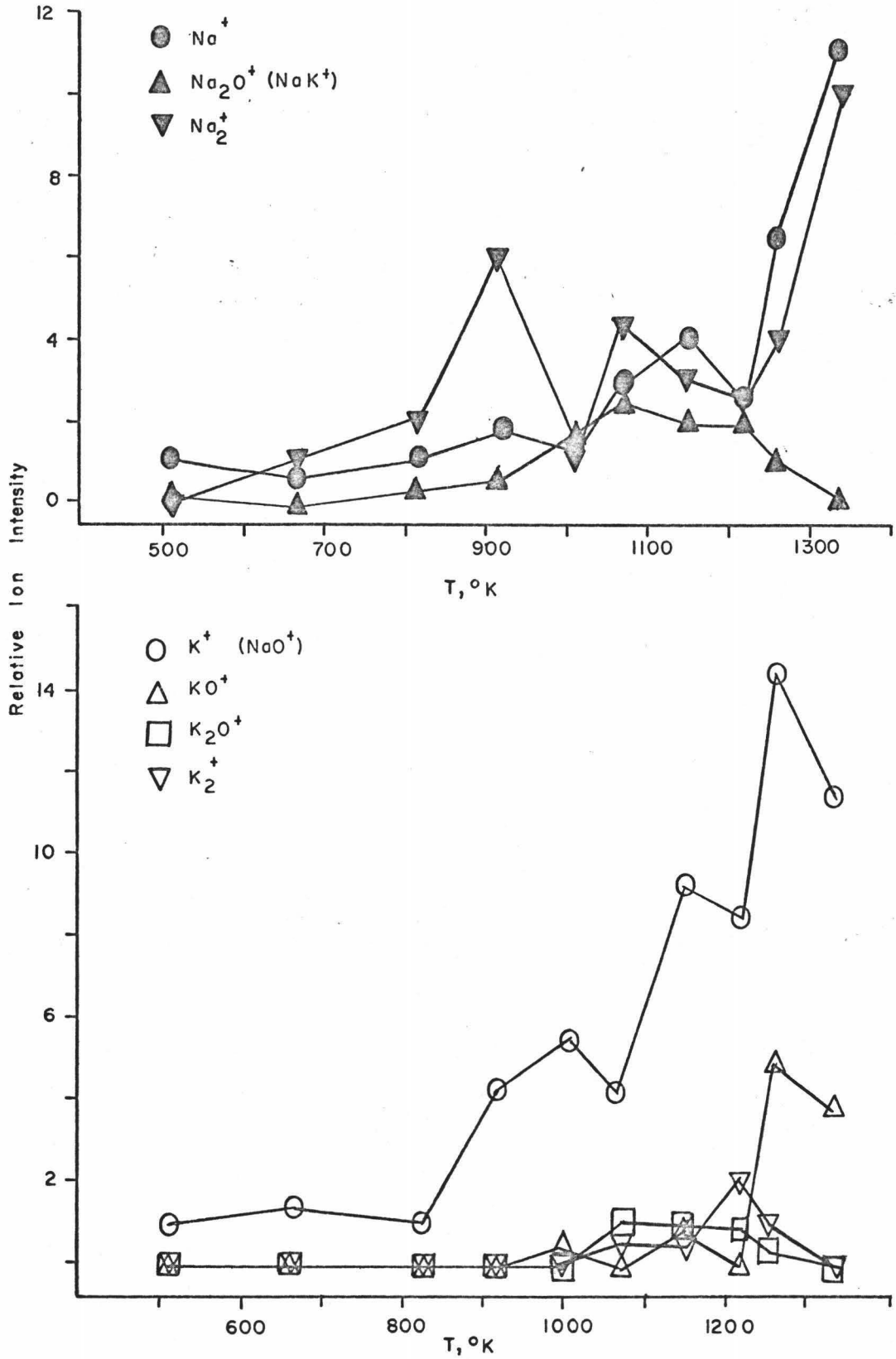

Figure 18: Alkali Vapors from Unreacted HK-123

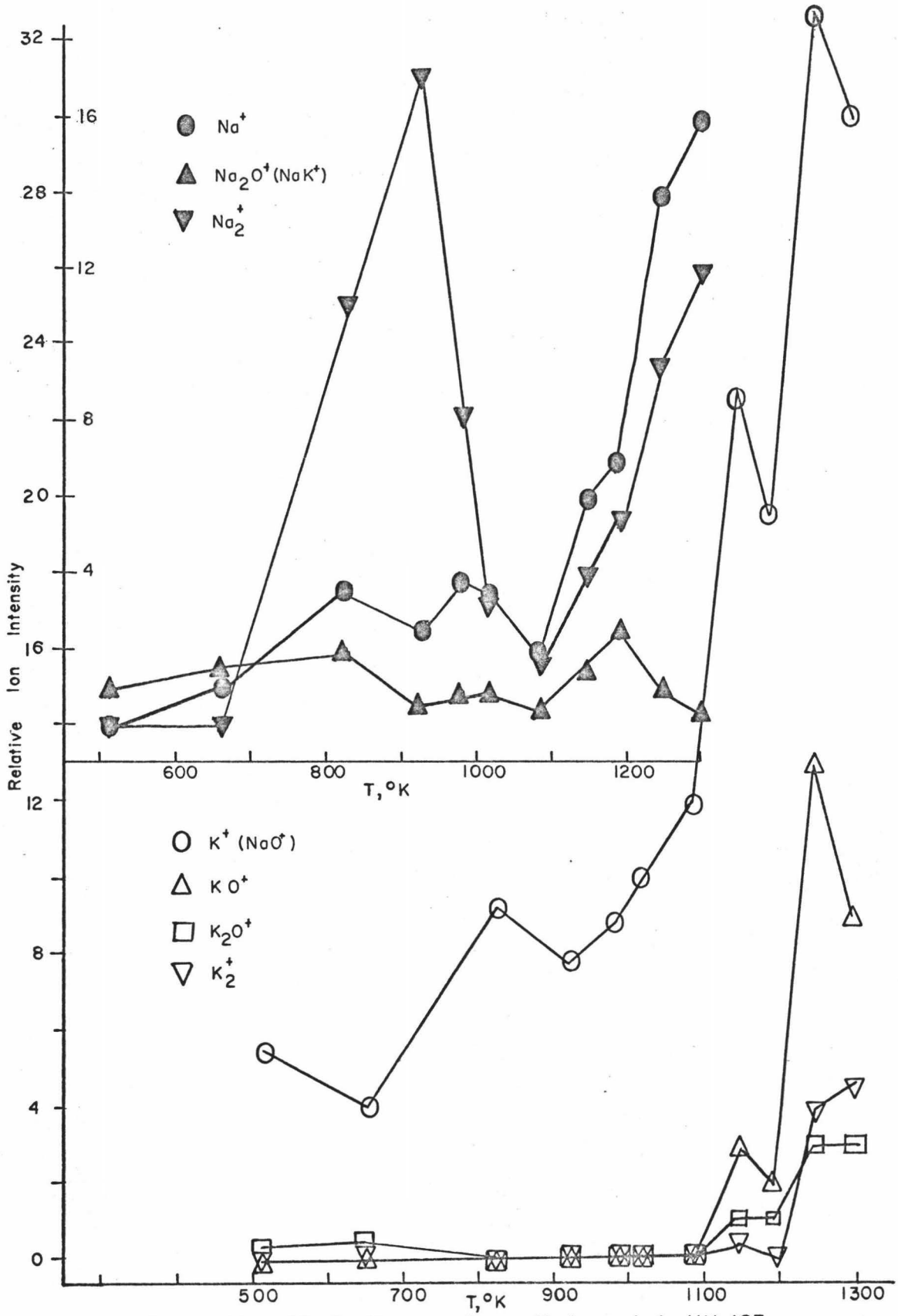

Figure 19: Alkali Vapors from K-degraded HK-123

deposition experiments. There was a surprising amount of diatomic sodium found in the low temperature release region. Below 1000°K, the major alkali volatiles were elemental potassium; and elemental, diatomic and oxidized sodium. Other than larger amounts of released alkalics, there was no indication of any difference in the volatiles between undegraded-degraded samples. Most of the potassium released in the potassium-degraded samples was elemental. Unfortunately, K^+ and NaO^+ (mass 39), and Na_2O^+ and NaK^+ (mass 62) were indistinguishable in the mass spectra, but the possibility of which vapor forms exist will be discussed in a later section. Comparison with the relative intensity of KO^+ would indicate that NaO^+ would probably not be a significant contributor to the mass 39 peak.

By using anhydrous boric acid as a standard material for calibration of the mass spectrometer, the absolute pressures of the alkali vapors were determined. Figure 20 presents the B_2O_3 curve obtained after final instrument modifications were made. This is a plot of the logarithm of the ion intensity of $B_2^{11}O_3^{16}$ times the temperature versus the reciprocal of temperature. Also, plotted in this figure is the result of the work of Inghram, et al. (113) for B_2O_3 on their mass spectrometer. Since the pressure of a species is proportional to the product of the ion intensity and temperature, the curves should be straight line differing due to the different mass spectrometer and Knudsen cell designs.

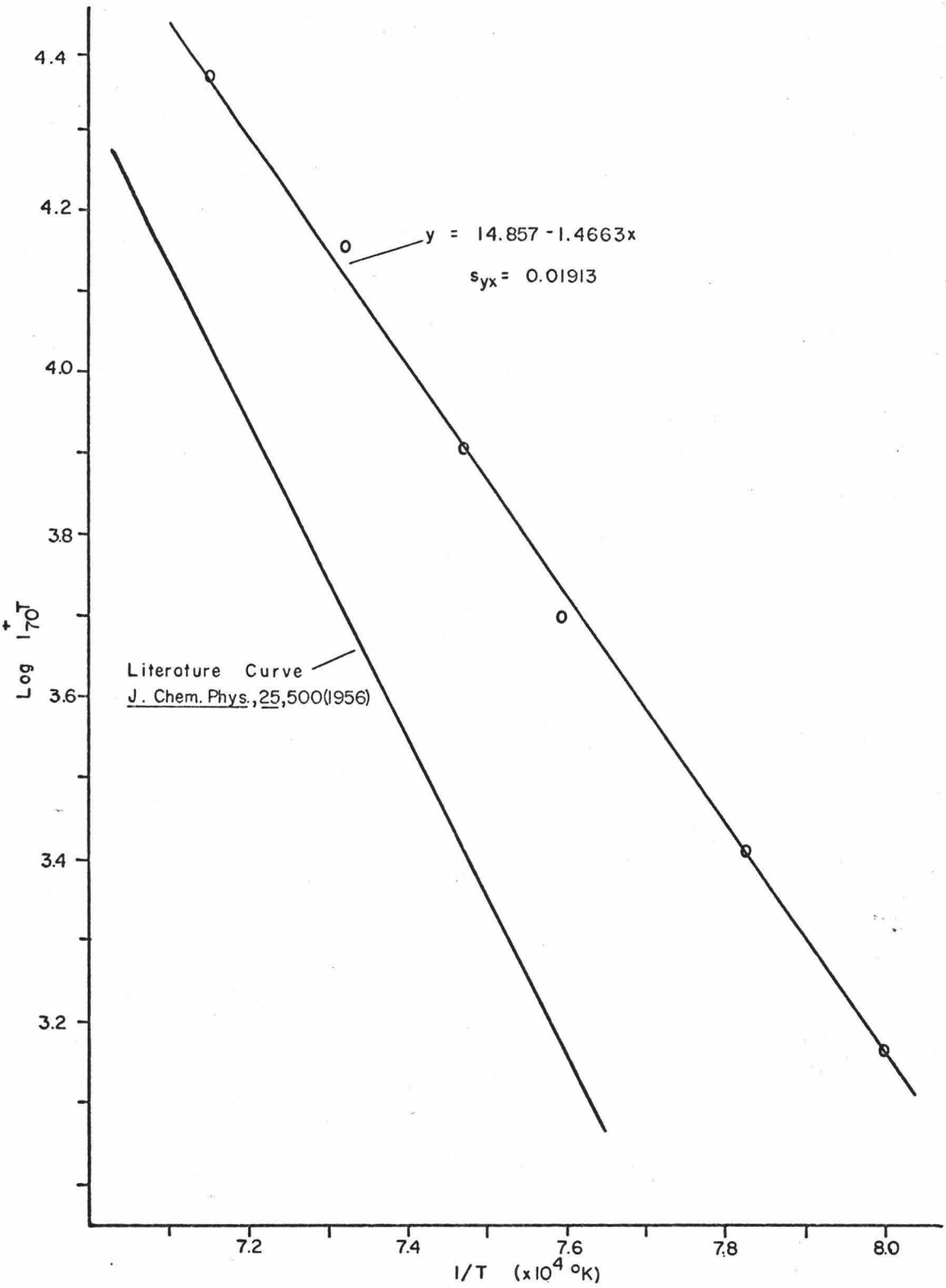

Figure 20: Log $I^{+}_{70}T$ versus 1/Temperature for $B^{11}_2 O^{16}_3$

The characteristic curve for each instrument allows accurate absolute vapor pressures to be determined independently. From the relative ionization cross sections of vapor species (59), the vapor pressure of $B_2^{11}O_3^{16}$ (Figure 4), the characteristic ion intensity of $B_2^{11}O_3^{16}$ for the mass spectrometer (Figure 20), and the ion intensities for the alkali vapors (Figures 18 and 19), the absolute pressures of the volatiles can be calculated at each temperature (Equation I-1). These pressures are shown in Table XII. These vapor pressures will be used for comparison with lunar samples in the next section and for some thermodynamic considerations in the theoretical section.

Accurate vapor pressures by the B_2O_3 standard technique could be calculated for all temperatures above 1180°K; and by extrapolating the curve in Figure 20, pressures of all species above 1050°K could be estimated. This covered the intermediate and high temperature release regions of alkali from basalts. No quantitative data could be obtained for the low temperature region, since B_2O_3 did not have a measureable vapor pressure. In the higher temperature regions, only volatiles above 1×16^{-6} torr had a significant ion intensity for pressure calculations.

2. General Discussion of Results

From the terrestrial studies, it was learned that volcanic materials release significant amounts of their alkali concentrations as volatiles. The volatile alkalis had easily measureable vapor pressures and were primarily elements, diatomics, or oxides. Rate of alkali loss versus temperature

TABLE XII. PRESSURES OF ALKALI VOLATILES

K-degraded HK-123

Ion(Mass)	Pressure (x 10^5/torr) 1088°K	1148°K	1193°K	1248°K	1298°K		Ion Cross Section
$K^+(39)$	15.7	48.9	51.5	129.	152.	--	38.8
$NaO^+(39)$	34.6	108.	114.	284.	336.	--	17.6
$KO^+(55)$	--	59.6	49.0	47.3	42.2	--	42.1
$K_2O^+(94)$	--	1.01	1.22	5.66	7.29	--	80.9
$K_2^+(78)$	--	.336	--	7.96	11.4	--	77.6
$Na^+(23)$	7.10	35.3	50.0	150.	220.	--	14.3
$Na_2O^+(62)$	.811	3.95	7.96	4.74	3.15	--	31.9
$NaK^+(62)$	.456	2.35	4.79	2.91	1.77	--	53.1
$Na_2^+(46)$	2.64	11.8	19.6	45.4	82.7	--	28.6
$B_2O_3^+(70)$	.056	.447	1.59	7.95	28.2		19.9

Unreacted HK-123

Ion(Mass)	Pressure (x 10^5/torr) 1073°K	1153°K	1223°K	1263°K	1338°K
$K^+(39)$	5.61	19.8	29.1	59.8	69.6
$NaO^+(39)$	12.3	43.6	64.2	132.	154.
$KO^+(55)$	--	1.98	--	19.0	22.3
$K_2O^+(94)$	.606	.989	1.60	7.84	--
$K_2^+(78)$	.303	.494	3.46	2.06	--
$Na^+(23)$	10.6	23.1	23.3	72.8	214.
$Na_2O^+(62)$	3.79	5.19	8.38	4.96	--
$NaK^+(62)$	2.27	3.13	5.05	3.04	--
$Na_2^+(46)$	7.58	8.65	11.6	22.4	82.2

indicated that three forms of release were occurring with maxima at 850°, 1050°, and 1250°K. These objectives of the research have been achieved as well as the development of necessary techniques. The evaluation of the terrestrial data in terms of the mechanism of alkali comminution still has to be discussed.

Before drawing conclusions from the data, the accuracy of the results should be considered. Tables VI and VIII and Figures 13 and 14 gave an indication of the limits of error on the alkali analyses of liquids and solids by the atomic absorption standard addition technique. The methods of analysis had a much lower error than errors from the inhomogeneity of the volcanic samples.

Large variations from sample to sample were very apparent in the vacuum deposition technique. However, when comparing unreacted and degraded basalts, definite trends were apparent. The calculated energies of alkali release were probably quite inaccurate. In some cases only two or three points determined the linear line used for energy calculations. There seems to be some fine structure in the vacuum deposition plots, which is probably due to the heterogeneity of the samples; i.e. different minerals may shift the three temperature release maxima. The deposition technique was quite efficient in collecting the volatiles. Figure 17 shows that heating a sample for one hour allowed sufficient time for steady state release to be established for a given temperature and that the plots of F^2 versus time for any individual sample gave

consistent results. Blank runs indicated that inhomogeneities in the basalts were the significant sources of error for alkali collection.

The uncertainty in the vapor pressures as determined from mass spectral data was probably at least 25%. The vapor pressure of B_2O_3 is well-known and so are the ionization cross sections. Figure 22 gives a straight line with a very small limit of error. Ion intensities used to calculate the volatile pressures were averages from four spectra collected over an hour at each temperature. In most cases, these relative ion intensities were within one intensity unit of each other.

Though most of the electron microprobe work was limited to the lunar samples, significant comparisons were made with and within the terrestrial samples. Once proper instrument parameters were determined, the electronic stability of the microprobe permitted consistent results on a day-to-day basis. The ease of detecting silicon and the alkalis by X-radiation gave quite accurate distribution plots of the elements. Some volatilization of sodium and potassium could be expected due to the conditions under which the analyses were conducted. The volatilization loss was a function of beam size and specimen current. However, while in the scan mode, the probe beam was constantly moving which considerably reduced localized melting and volatilization.

The terrestrial studies seem to substantiate a comminution of polycrystalline basalts into their component minerals via a

breakdown of mineral boundary forces. Other than an increase in the alkali content during degradation, the chemical analyses, X-ray diffraction, microscopic examination, and microprobe analysis indicated no significant alteration of the chemical or mineralogical nature of the degraded basalts. Some degraded grains contain this alkali increase on their surface edges, where they have apparently parted from the parent basalt.

Natural rocks exhibit a degree of fracture and porosity and seldom achieve the theoretical density of their component minerals. They contain gas vesicles, fractures, parting cracks, inclusions, grain boundaries in various degress of disorder, as well as other internal surfaces. Fisher (77), Sippel (78), and geochronologists (79,80,81,82) recognized these flaws as being sources of high diffusivity paths which can allow easier diffusion-controlled paths of entry (or release) than lattice diffusion. Diffusion along these internal surfaces should occur at temperatures and activation energies between those for surface and lattice diffusion. The vacuum deposition studies have shown that the increase in the rate of alkali release from basalts occurred at these intermediate temperature and energy levels. Sippel (78) determined activation energy ranges of 10 to 43 kilocalories for sodium self-diffusion into nine minerals at these intermediate temperature regions which compares quite well with a range of 10 to 60 kilocalories for the degraded basalts (Table X).

One can hypothesize that the observed degrading of basalts by the alkali metal took place as a result of vapor or capillary penetration by the metal along internal surfaces, followed by a subsequent reaction of the metal with the silicate boundaries which disrupted them and caused spallation into the component minerals. Not much is known about the boundary forces and the bonds which hold minerals together in heterogeneous rocks, nor is a lot of information available on the reaction of metals with silicate linkages. Eitel (114) discussed the change in viscosity of silicate melts by the introduction of various components to the magma. It has been found that potassium and sodium are network modifiers, while elements such as silicon and aluminum are network formers. The introduction of alkalis into magma gives a lowering of viscosity by disrupting the silicate linkages.

At sub-molten temperatures, disruption by alkali could occur along grain boundaries leading to comminution. The presence of alkali in these internal regions may give rise to competition for the oxygen in the Si-O-Si linkages between the alkali and the silicate. Potassium is a greater network modifier than sodium which agreed with the preliminary studies showing more effective degradation by potassium than sodium. The alkali metals have a strong tendency to oxidize, which may cause "pseudo-oxidation-reduction" reactions along boundaries causing sufficient strain to disrupt individual minerals from their parent basalt. The microprobe studies indicated surface

concentrations of potassium on degraded grains which would be expected if these reactions were occurring.

Some of the data collected contained anomalies, which must be accounted for if a mechanism is to be consistent with the results. The first question that arises is why does potassium degrade samples more effectively than sodium. The mass spectrometer data gives some enlightenment on this. At lower temperatures, a significant portion of the sodium vapor was in diatomic form while most of the potassium vapor was elemental. The size of the diatomic vapor molecules may not permit easy entry into the internal surfaces, or the stability of the dimeric sodium may not allow significant reaction along boundary regions. In their presentation of the thermodynamic and physical properties of alkalis, Garelis and Thomson (115) reported on the significant fraction and stability of diatomic sodium present due to dimerization, while not much diatomic potassium was detected.

The other anomaly that occurred was the large increase in the release of sodium from potassium-degraded samples. This was observed in Figure 14 and in Table VIII. This sodium increase keeps the percent potassium:percent sodium loss ratio below one for all the degraded HK-123 samples. Figure 17C and D showed an order of magnitude increase in the D/a^2 value of sodium for degraded basalt while the potassium value remained relatively constant. In Table IX, there was a striking difference in the lattice diffusion energies for degraded-unreacted samples.

During degradation, one might imagine an exchange of potassium for sodium in alkalic minerals or a penetration of potassium into sodium minerals causing a "softening" of the lattice leading to a larger release of sodium at higher temperatures.

Green's investigations (116) of Norwegian granites containing intruded feldspars supplied evidence that the addition of potassium converted albite ($NaAlSi_3O_8$) to microcline ($KAlSi_3O_8$) at the contact zone. This metasomatism was attributed principally to the effect of the thermal gradient that evidently existed across the contact at the time of intrusion. Orville (117) demonstrated that metasomatism involving alkali feldspars can be expected in rocks of appropriate composition at temperatures from 300° to 700°C in the presence of alkali chloride supercritical solutions if a thermal gradient was in effect. Under a thermal gradient, a non-equilibrium amount of potassium will migrate to albitic regions and replace the sodium. The sodium will diffuse in the opposite direction to replace the potassium. Orville also showed that such alkali metasomatism could be driven by differences in anorthite ($CaAl_2Si_2O_8$) content between the plagioclase of two adjacent bodies. At temperatures below 400°C the exchange reaction between feldspar and vapor phases was very slow. However, the composition of the final products showed that several percent of the alkali originally present in Orville's artificial feldspars had been exchanged for alkali in the vapor. He concluded that a second feldspar phase (too little to be detected by X-ray

powder diffraction techniques) was formed at the surface of the original feldspar without affecting the bulk of the feldspar material.

In nature, Orville found that the waters of thermal hot springs, which were at considerably lower temperatures than those used in the laboratory studies, show great enrichment in sodium relative to potassium. At wairaki, New Zealand, solutions at 250°C that contain only 3 to 10 mole percent potassium relative to total alkalis are presently replacing plagioclase by potassium feldspar. At the Upper Geyser Basin in Yellowstone Park, solutions containing only 3 mole percent potassium were actively replacing plagioclase by potassium feldspar at temperatures in the neighborhood of 200°C. From this data, it seems likely that alkali metasomatism will take place in the presence of an alkali-bearing vapor phase as a natural consequence of temperature, pressure and compositional gradients.

Alkali metasomatism could be a strong contributing factor to the degradation mechanism of basalts under lunar conditions. The large non-equilibrium concentration of potassium in the vapor phase would tend to replace the sodium in the alkalic minerals. The thermodynamics of this exchange are favorable (shown in the theoretical section of this discussion). At the low temperatures where degradation occurs (127° and 250°C), this exchange would be minor and occur at the internal surfaces where the alkali vapor has penetrated the basalt. The microprobe data showed the build-up of potassium on grains in the degraded

products.

Thus, the large amount of sodium that was released at high temperatures in the degraded basalts can be accounted for by alkali metasomatism. This sodium increase was observed in both the vacuum deposition and the mass spectrometer data. What may have happened in these cases were supplementary high temperature reactions that had nothing to do with the original comminution. During heating, the large amount of potassium that was taken up in the internal surfaces during degradation is released at approximately 475° to 675°C. This temperature range was where Orville (117) found considerable alkali metasomatism occurring. The released potassium vapor could react with the basalts causing a "softening" of the lattice and consequently the release of larger amounts of sodium at the higher temperatures.

Alkali metasomatism can account for a greater degradation by potassium than by sodium. First, though exchange of potassium in feldspars is favorable thermodynamically, the reverse process is not. Second, the larger amount of elemental potassium vapor over sodium vapor in volatiles from basalts would favor potassium exchange. Furthermore, the larger amounts of sodium minerals to potassium minerals in the basalts would favor potassium exchange in the presence of potassium-rich vapor.

In conclusion, terrestrial studies under lunar environmental conditions showed that a basalt released significant alkali vapor at subliquidus temperatures and that a primary component

of the volatiles was gaseous alkali metal. These vapors will comminute basalts at lunar day temperatures with little alteration of the original rock, probably via a boundary reaction mechanism. These results will serve as the base of comparison for investigation of lunar materials for evidence of this attack occurring on the lunar surface. References to the physical similarity of degraded basalts to the lunar regolith materials have already been made.

B. Lunar Samples

1. Presentation of Data

The consideration that comminution of lunar rocks may be caused, at least partly, by the action of volatilized alkali metals was investigated using the techniques developed for the terrestrial studies. The same general limits of error hold for the lunar samples as for the terrestrial samples. The limited amount of lunar samples available necessitated that conclusions be drawn from very few experiments. Consequently, the lack of sufficient data made comparisons of individual samples somewhat inconclusive. The different sample weights, alkali contents, and mineralogy of each lunar sample further complicated comparisons. In most cases, behavior of the lunar samples was compared to the degraded and unreacted terrestrial samples rather than to each other. The vacuum deposition, mass spectrometer, and emission spectrometer techniques were used for the volatile behavior studies. It was expected that the electron microprobe would prove to be the most effective mode of inquiry to obtain

evidence for alkali metal comminution of lunar samples. The general description of the lunar samples was discussed earlier and the sequence of lunar experiments can be found in Appendixes A to F.

Figures 21 through 26 are the rate of alkali loss versus temperature data for the rock surface, soil, and internal fragments of maria material. All the potassium data is on the same scale, with the sodium data plotted on twice the potassium scale. Table XIII compares the total amount of alkalis lost from the different types of regolith material. In general, the plots showed alkali-release-maxima at about 750°, 1050°, and 1300°K, which was very similar to that found for terrestrial rocks. The surface rocks show a larger intermediate temperature peak than the internal rocks and were similar to the potassium-degraded terrestrial basalts. The lunar soil (< 0.1 mm.) gave a slight indication of the intermediate temperature maxima. However, the perfection of crystallizations on lunar rocks (6,7), the extremely small particle size, and the large percentage of the soil that was individual crystals and brecciated material would drastically cut down on internal surfaces which were apparently responsible for the intermediate temperature maximum.

Except for #12002, 140, the surface rocks and soil have percetn potassium:sodium loss ratios less than one, while the internal samples have ratios greater than one. Again this was in agreement with the degraded-unreacted terrestrial basalt comparisons. There may be several reasons for the large loss of

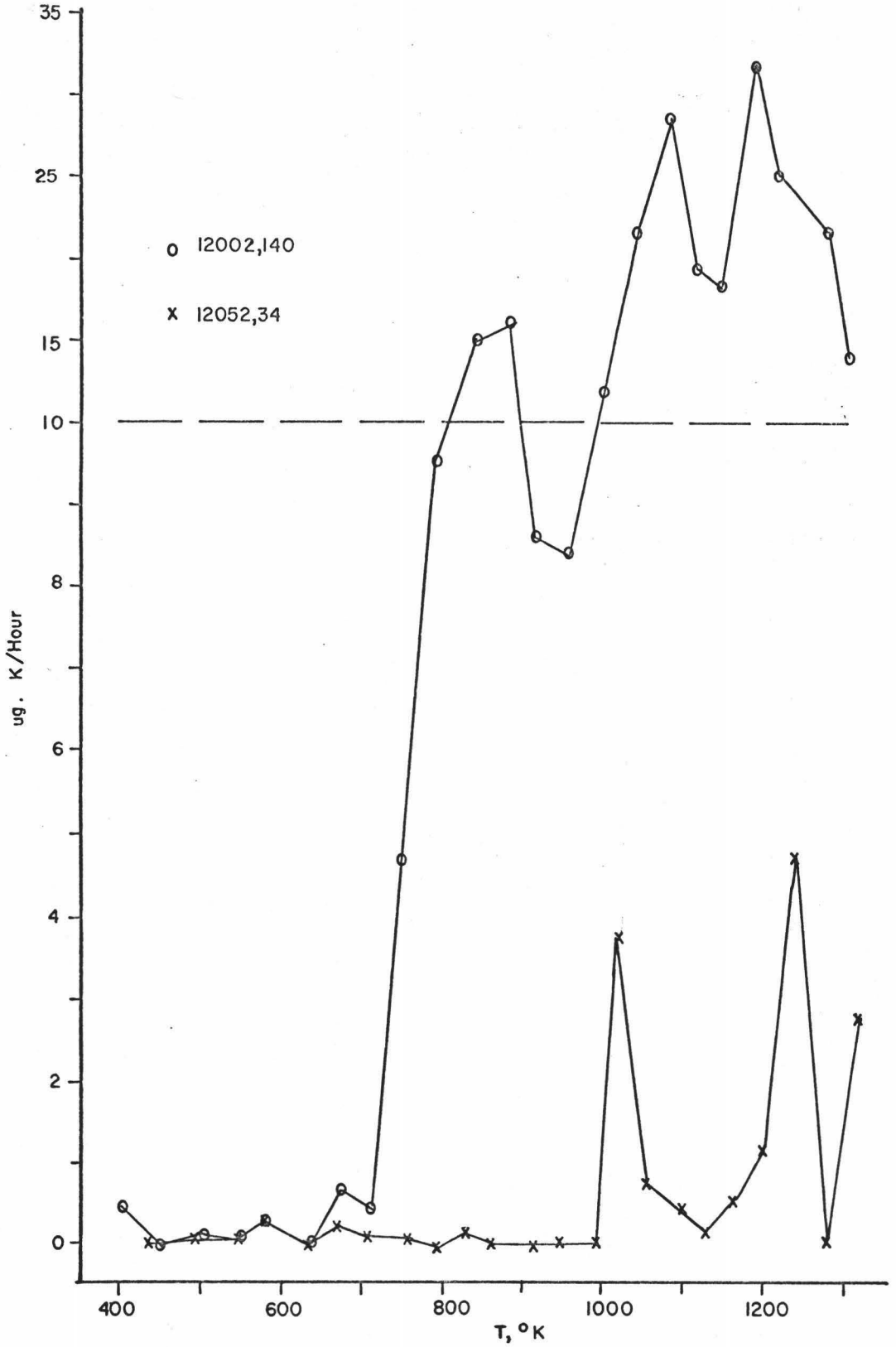

Figure 21: Potassium Loss from Lunar Surface Rocks

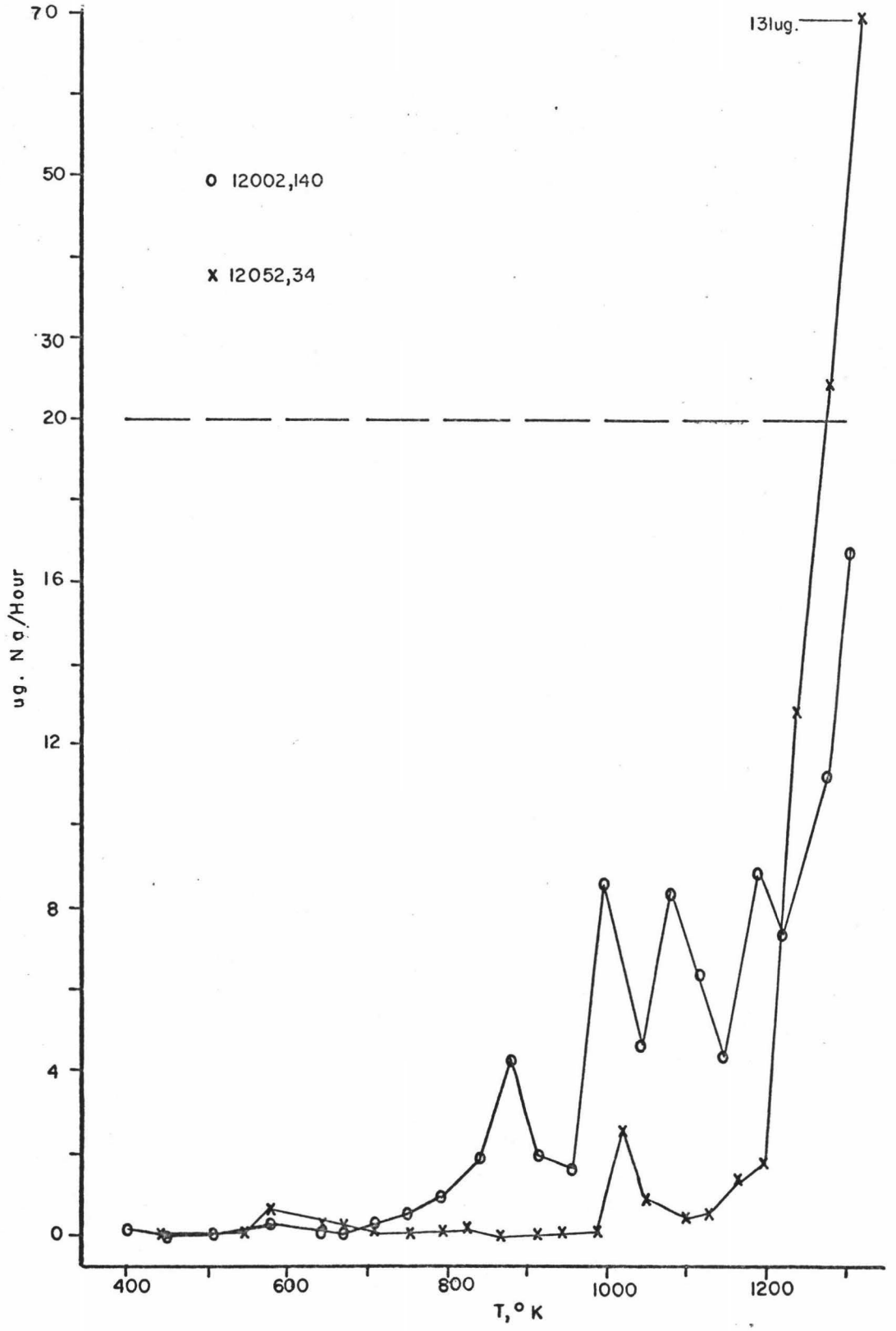

Figure 22: Sodium Loss from Lunar Surface Rocks

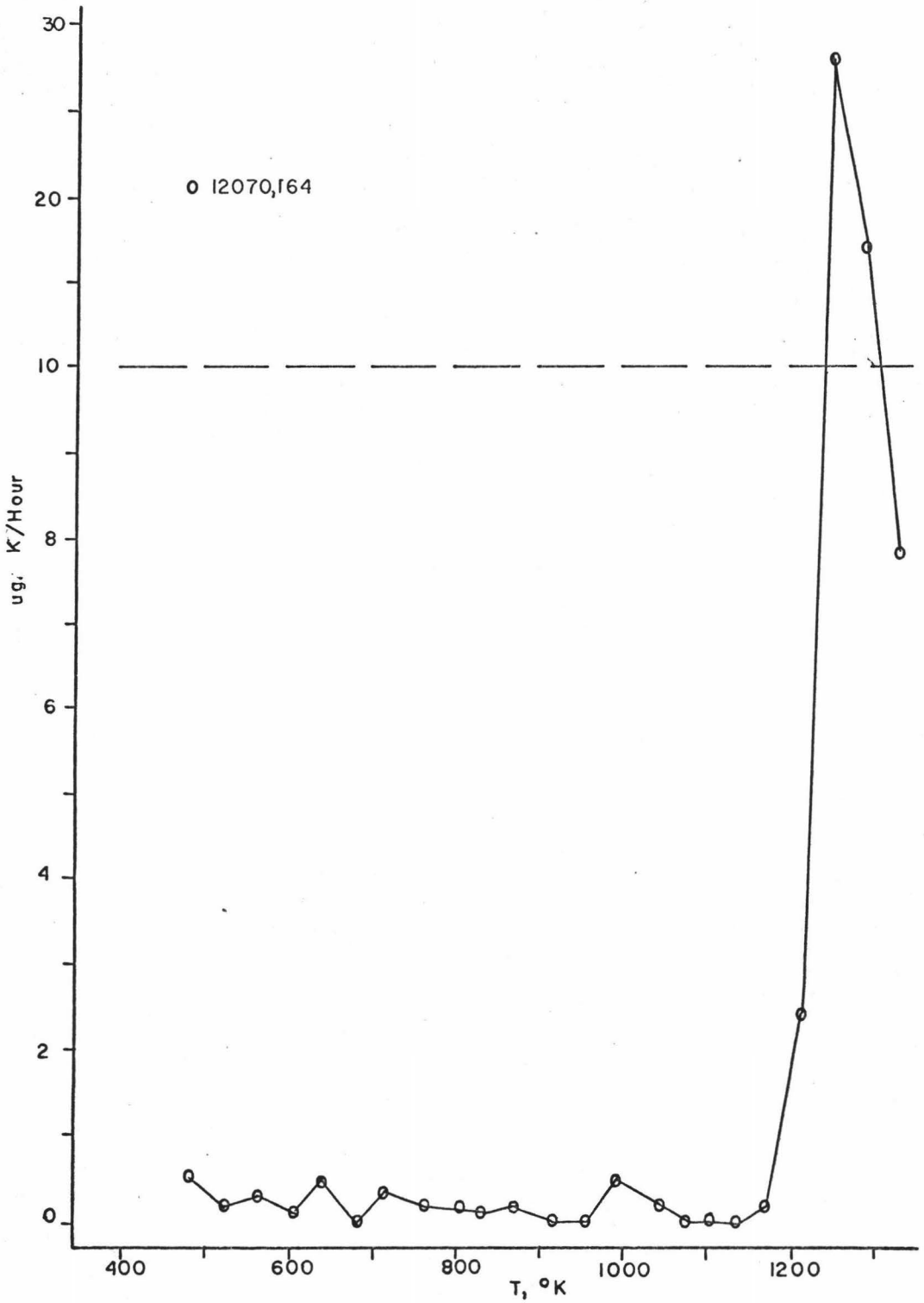

Figure 23: Potassium Loss from Lunar Soil (<0.1mm.)

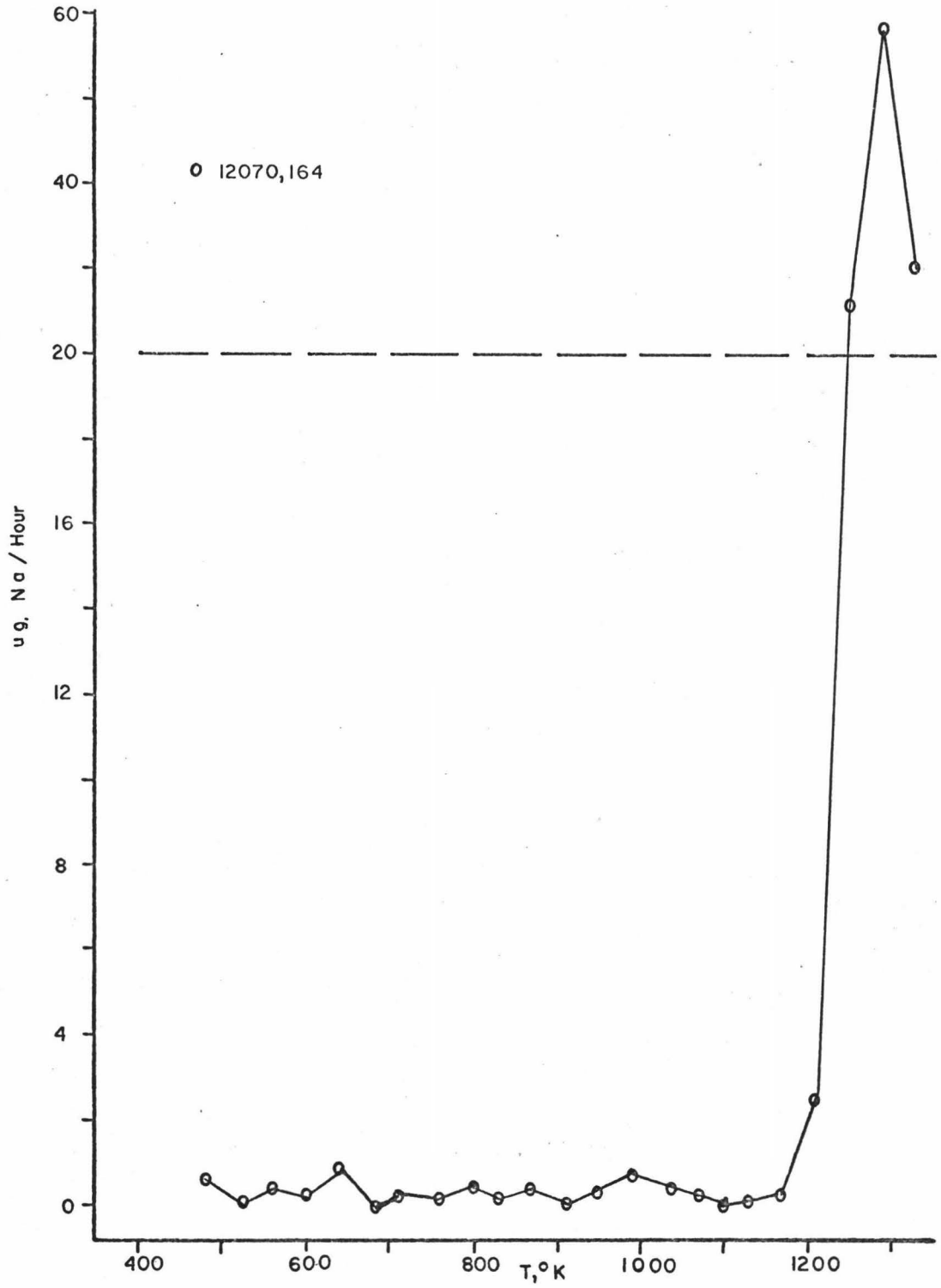

Figure 24: Sodium Loss from Lunar Soil (<0.1mm.)

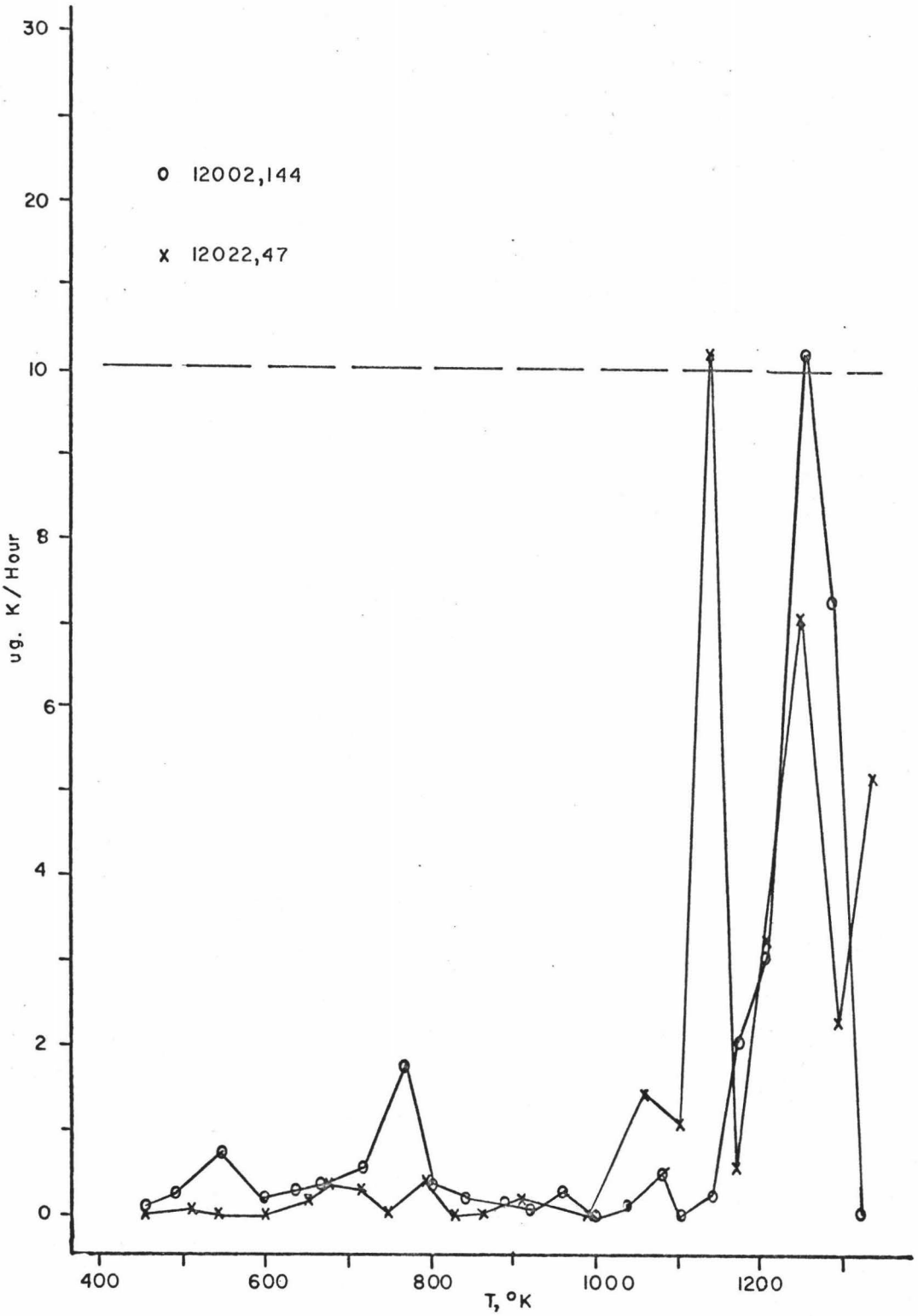

Figure 25: Potassium Loss from Lunar Internal Rocks

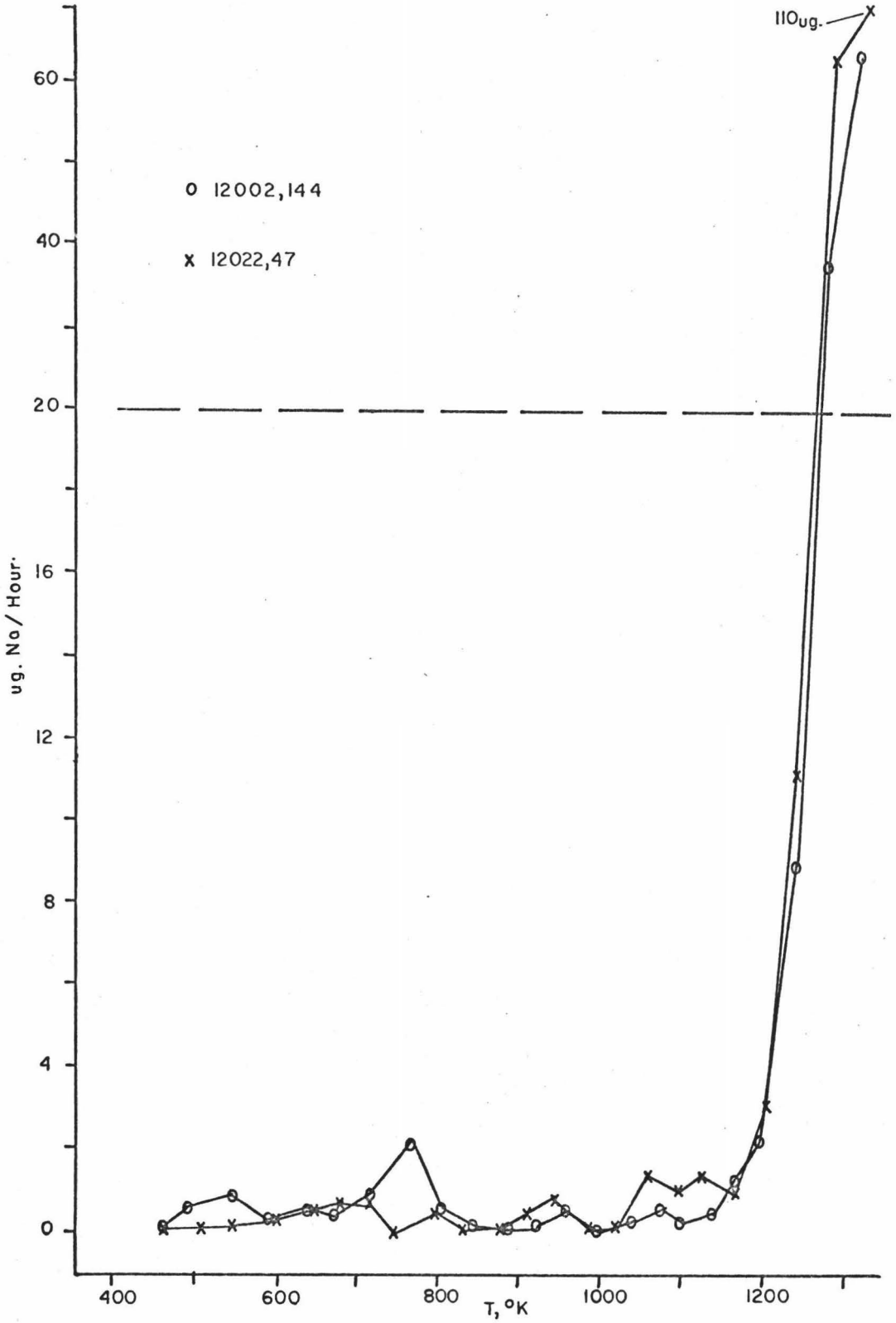

Figure 26: Sodium Loss from Lunar Internal Rocks

TABLE XIII. TOTAL AMOUNT ALKALIS LOST FROM LUNAR ROCKS

Temperature Sample Heated to in °K	µg. K loss	% K loss	µg. Na loss	% Na loss	%K loss / %Na loss
		12002,140 (Surface Rock)			
1308	261.±.24	65.7	89.1±.03	13.6	4.82
		12052,34 (Surface Rock)			
1323	15.8±.02	5.72	178.±1.1	14.7	.389
		12070,164 (Soil <.1 mm.)			
1333	58.9±.11	21.1	122.±.19	26.2	.805
		12002,144 (Internal Rock)			
1323	30.1±.02	13.7	124.±.15	8.19	1.67
		12022,47 (Internal Rock)			
1333	33.7±.02	18.0	197.±1.1	14.5	1.24

potassium in #12002, 140. This sample contained a large vug which was lined with plagioclase crystals and a fairly large glass-lined impact pit with a surrounding "white halo" (probably condensed volatiles). The thin section of this sample showed signs of shock effects on the minerals. All these factors could have contributed to a "mutation" of the lunar rock, making release of alkali from the sample easier. Another explanation for large alkali loss may be from contamination. #12002, 140 was the first rock run on the microprobe and it was mounted by its base in thermoplastic. This thermoplastic penetrated the rock and may have caused anomalous results. During heating of this rock, organic material was observed on the cold finger and the mass spectrometer showed organic contamination. The other samples were not contaminated.

Investigations indicated that the present maria materials have lost a significant portion of their volatile components (6,7,25). However, Table XIII shows that internal (or fresh) samples still release a significant portion of their alkalis at sub-molten temperatures. The lunar material releases an even greater percent of alkali than the terrestrial rocks (Table VIII). The relative amount of potassium volatilized was still higher than the sodium loss.

Prior to heating, the rock samples were a very light gray color and the soil was a dark gray color. As the samples were heated, the rocks got darker in color and the soil sample lightened a bit. When sample #12022, 47 was heated, there was

a definite odor of sulfur gases after the sample was opened to the atmosphere. At high temperatures, the cold finger had the same general appearance as when terrestrial samples were run. The tip of the cold finger was coated with a yellowish, and a silver-gray, material. The silver-gray material oxidized to a white material and was quite soluble in water. The yellow material was only slightly soluble.

Figures 27 through 30 show the plots of Log D/a^2 versus the reciprocal of temperature. Table XIV summarizes the energy data obtained from these plots. This data was not as clear-cut as data for the terrestrial samples since the alkali release regions were not clearly shown, other than for lattice diffusion at the higher temperatures. However, the basic curve shapes for surface rocks and soil and for internal rocks were similar. The only energy data which was at all accurate was the lattice diffusion values and these indicated slightly lower energies of release for the alkalis in the surface regions. Generally, the potassium values were lower than the sodium values, which accounted for a greater percent release of potassium. More data would have to be collected for the same rocks to accurately determine energy of release values.

Hale (109) used emission spectroscopy to analyze the portions of cold finger solutions remaining after alkali analyses. He found aluminum, magnesium, silicon, calcium, iron, platinum, and copper in addition to the alkalis. In sample #12022, 47, he found the same elements plus some titanium and

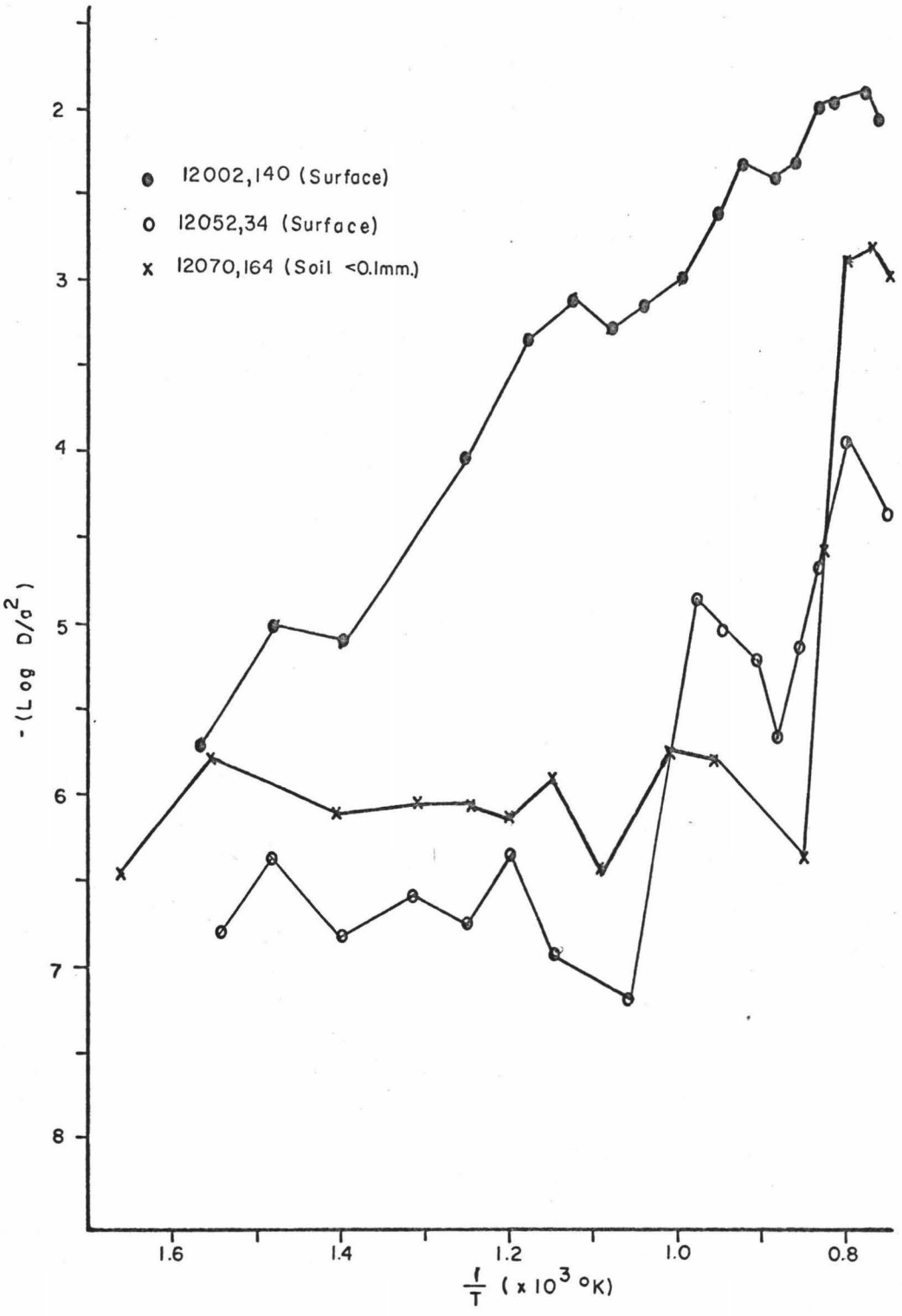

Figure 27: Log D/a^2 vs. 1/T for Potassium Loss

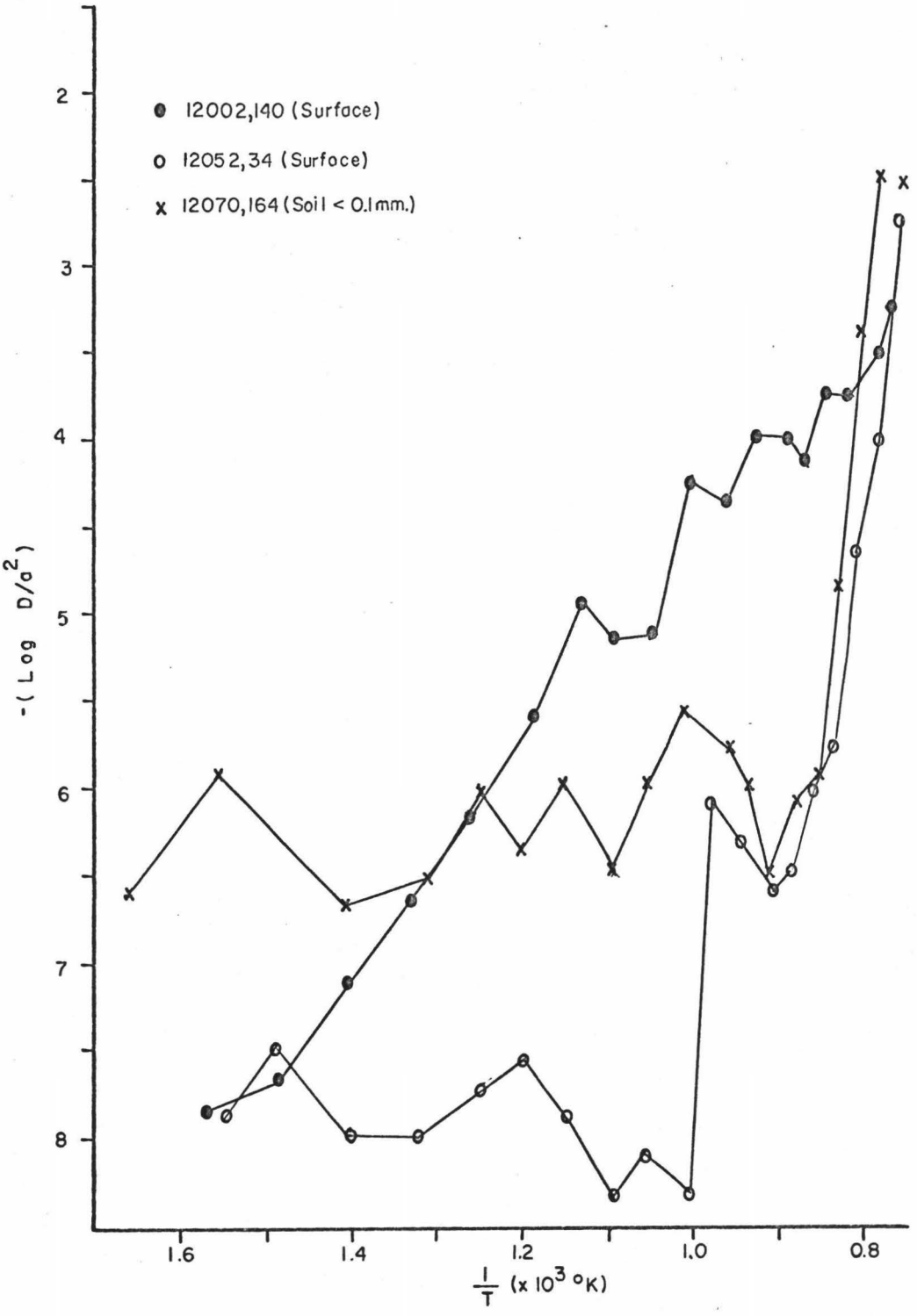

Figure 28: Log D/a^2 vs. $1/T$ for Sodium Loss

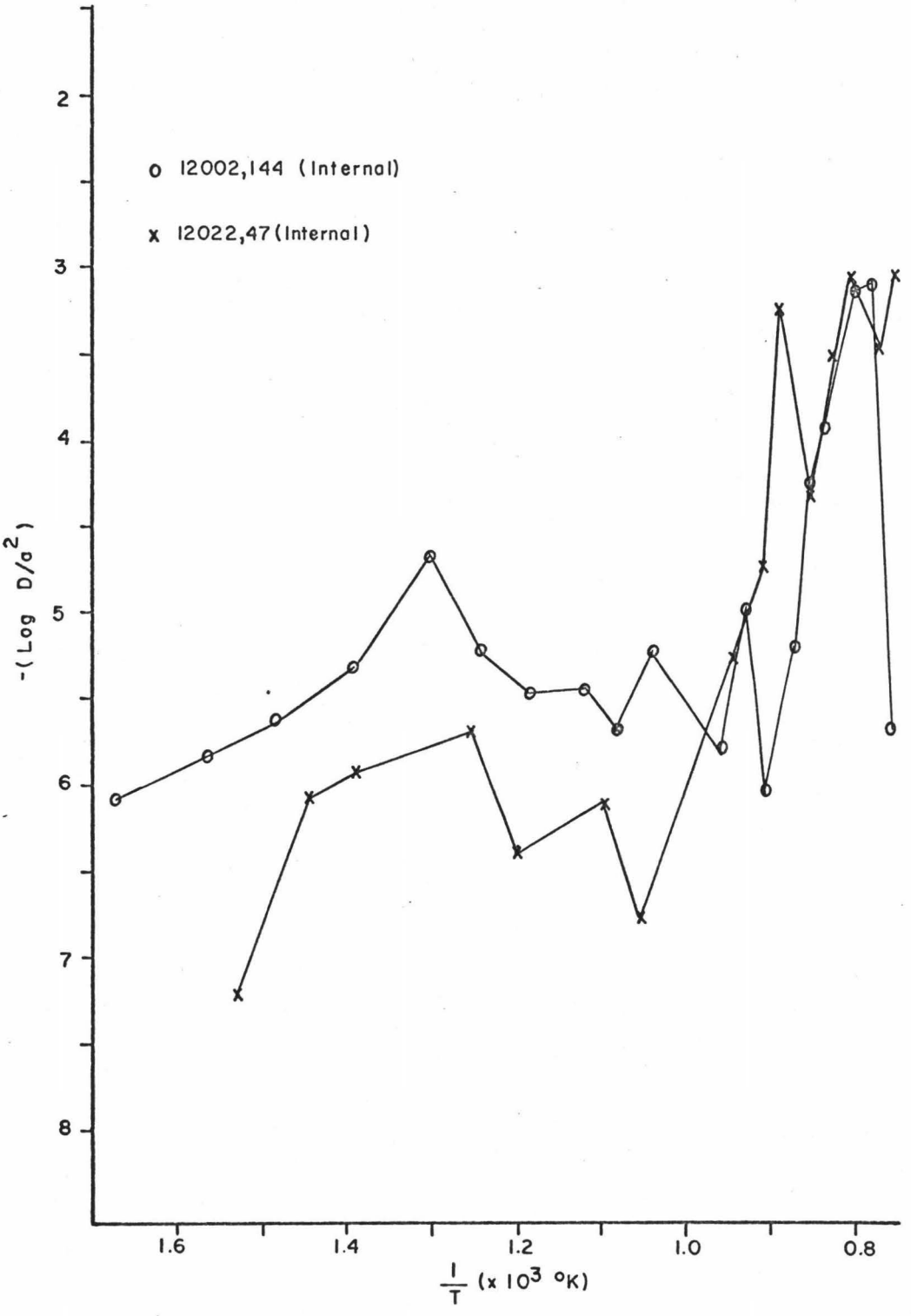

Figure 29: Log D/a^2 vs. 1/T for Potassium Loss

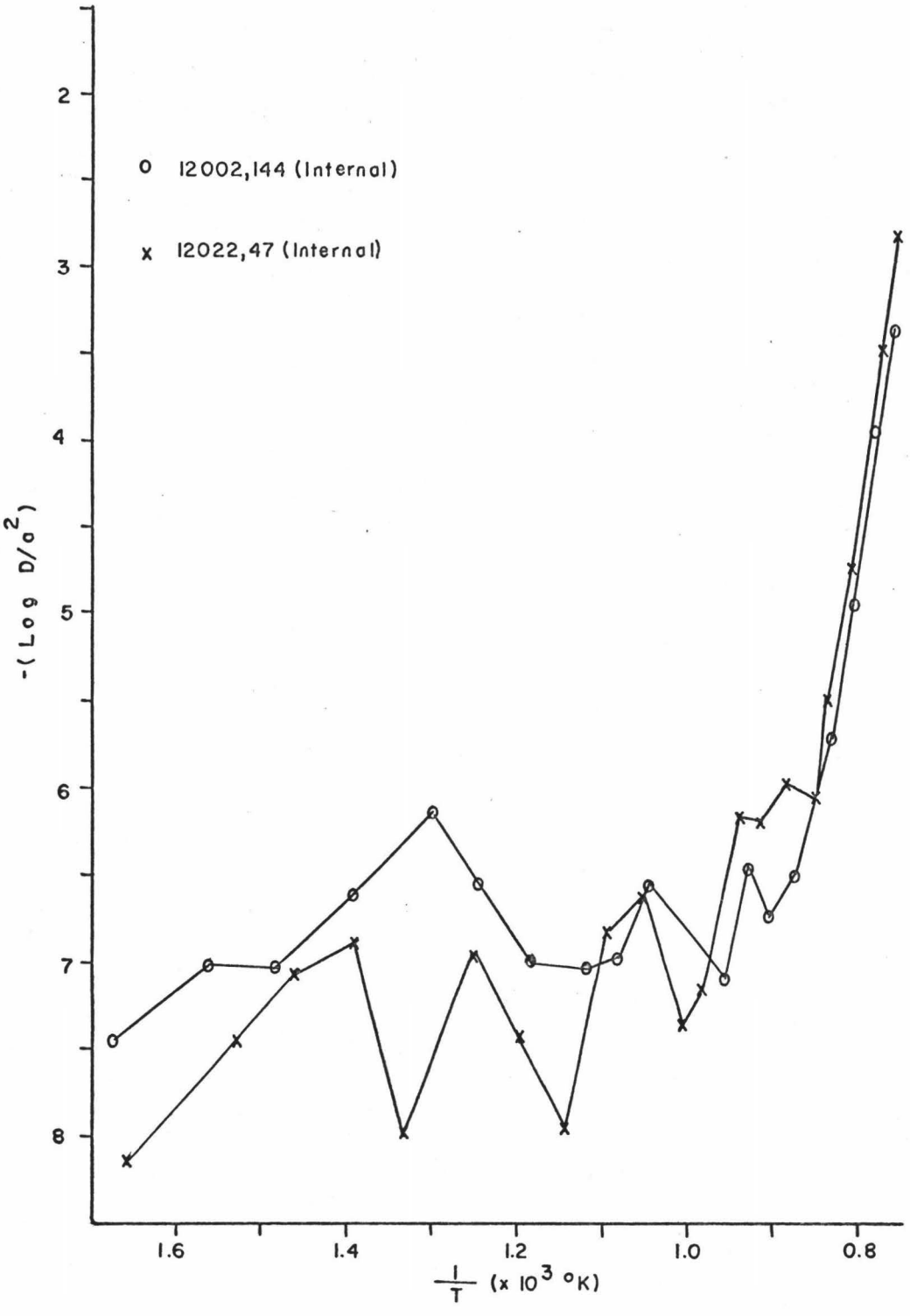

Figure 30: Log D/a^2 vs. 1/T for Sodium Loss

TABLE XIV. ENERGY OF ALKALI RELEASE IN LUNAR SAMPLES

Sample	Range of K Release in °K	Energy of K Release in kcal.	Range of Na Release in °K	Energy of Na Release in kcal.
	(High Temperature Region)			
12002,140	1150-1310	58.4	1150-1310	86.2
12052,34	1130-1325	99.6	1130-1325	150.
12070,164	1130-1335	112.	1130-1335	125.
12002,144	1100-1325	126.	1140-1325	127.
12022,47	1100-1330	110.	1170-1330	143.
	(Intermediate Temperature Region)			
12002,140	960-1150	39.6	960-1150	42.7
12052,34	1000-1130	42.8	990-1100	45.7
12070,164	950-1070	35.8	910-1100	46.9
12002,144	1020-1100	36.3	1000-1100	38.2
12022,47	1020-1100	46.3	1000-1100	35.3
	(Low Temperature Region)			
12002,140	640-960	33.9	700-960	35.3
12052,34	640-870	26.7	640-870	26.7
12070,164	670-920	32.0	670-920	35.2
12002,144	600-840	33.3	600-840	21.5
12022,47	600-840	32.7	600-840	25.1

silver. The presence of these elements was reported on the basis of three or more analytical lines found. The platinum was probably from the platinum evaporating dishes used to dry the deposition liquors. Copper and silver were present in the lunar rocks in trace amounts and the other elements were major components of the rocks. Most of these elements are not usually considered to be volatile elements (with the exception, possibly, of silver). Their presence may be due to atomic sputtering near the melting point of the samples. Analysis of the solid samples of rock, revealed the same general composition of elements as the Apollo 11 samples (25), except that Hale found some evidence of boron, which was not detected with emission spectrometry by earlier investigators.

Figures 31 through 33 are the plots of the relative ion intensities of alkali versus temperature for the alkali volatiles detected using the high-temperature mass spectrometer. Figure 34 shows the pattern of SO_2^+ and SO^+ released in sample #12022, 47. This was the sample in which the odor of sulfur gases was detected during the deposition runs. These two gases were the only volatiles other than the alkalis detected in the mass range from 0 to 100 a.m.u. Reid, et al. (118) reported the presence of troilite (FeS) in sample #12022. Smales, et al. (63) placed an upper limit of 500 ppm sulfur in the Apollo 11 samples. The sulfur dioxide probably arose from the decomposition of troilite with the sulfur monoxide being the fragment arising from the ionization of sulfur dioxide. There were three different temperature zones of sulfur gas release which corresponded to

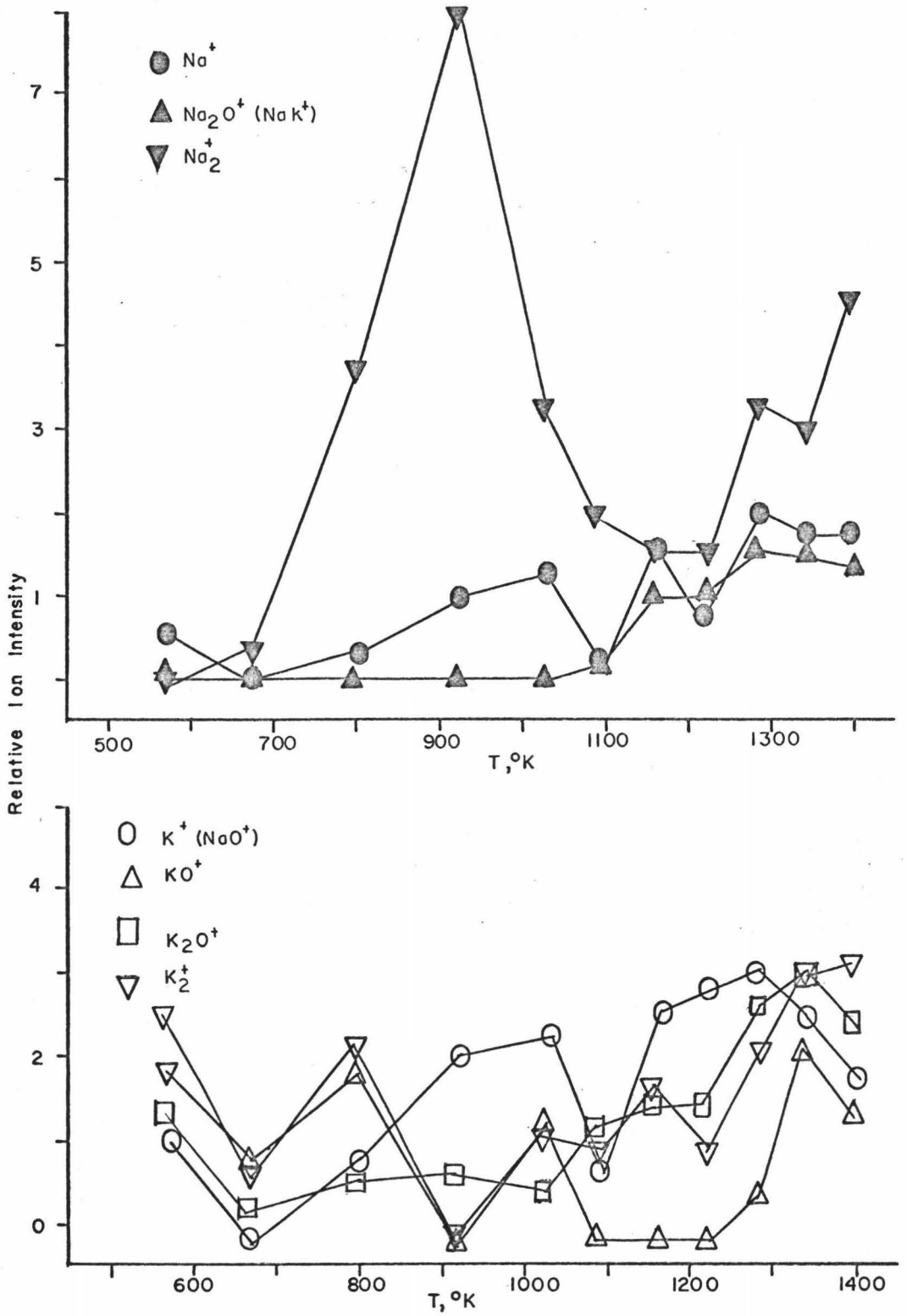

Figure 31: Alkali Vapors from Lunar Rock # 12002,140

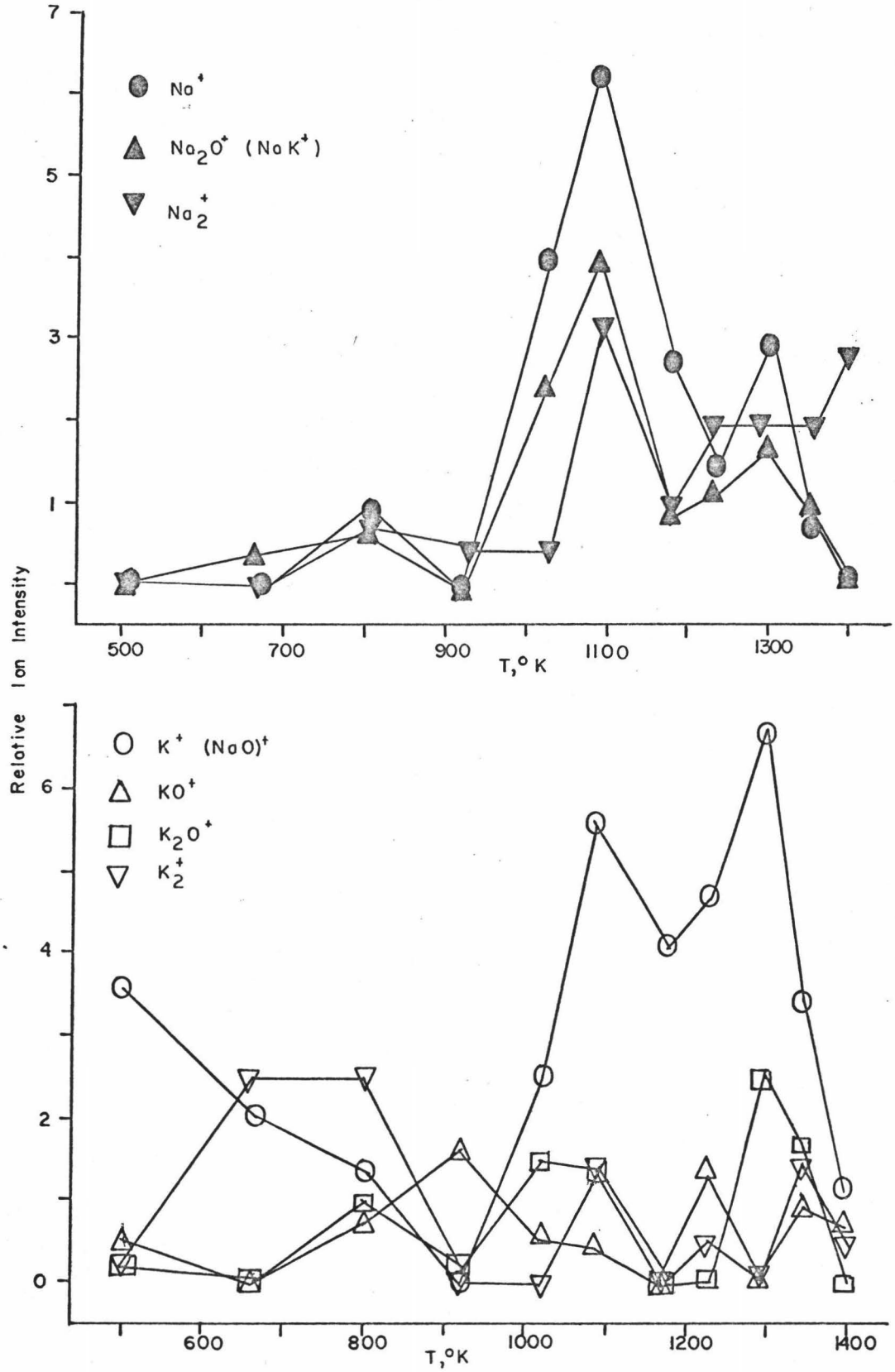

Figure 32: Alkali Vapors from Lunar Rock #12002,144

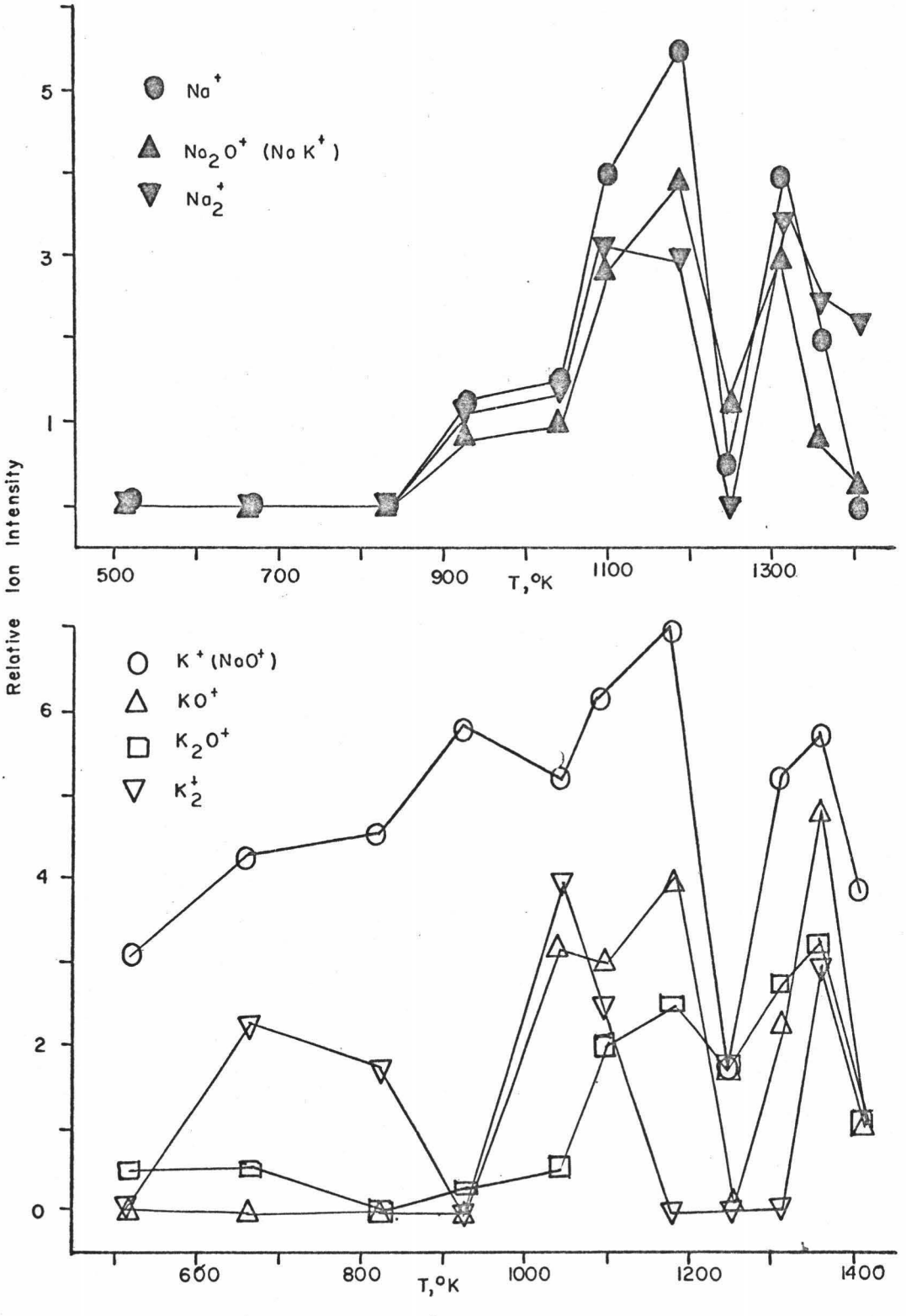

Figure 33: Alkali Vapors from Lunar Rock # 12022,47

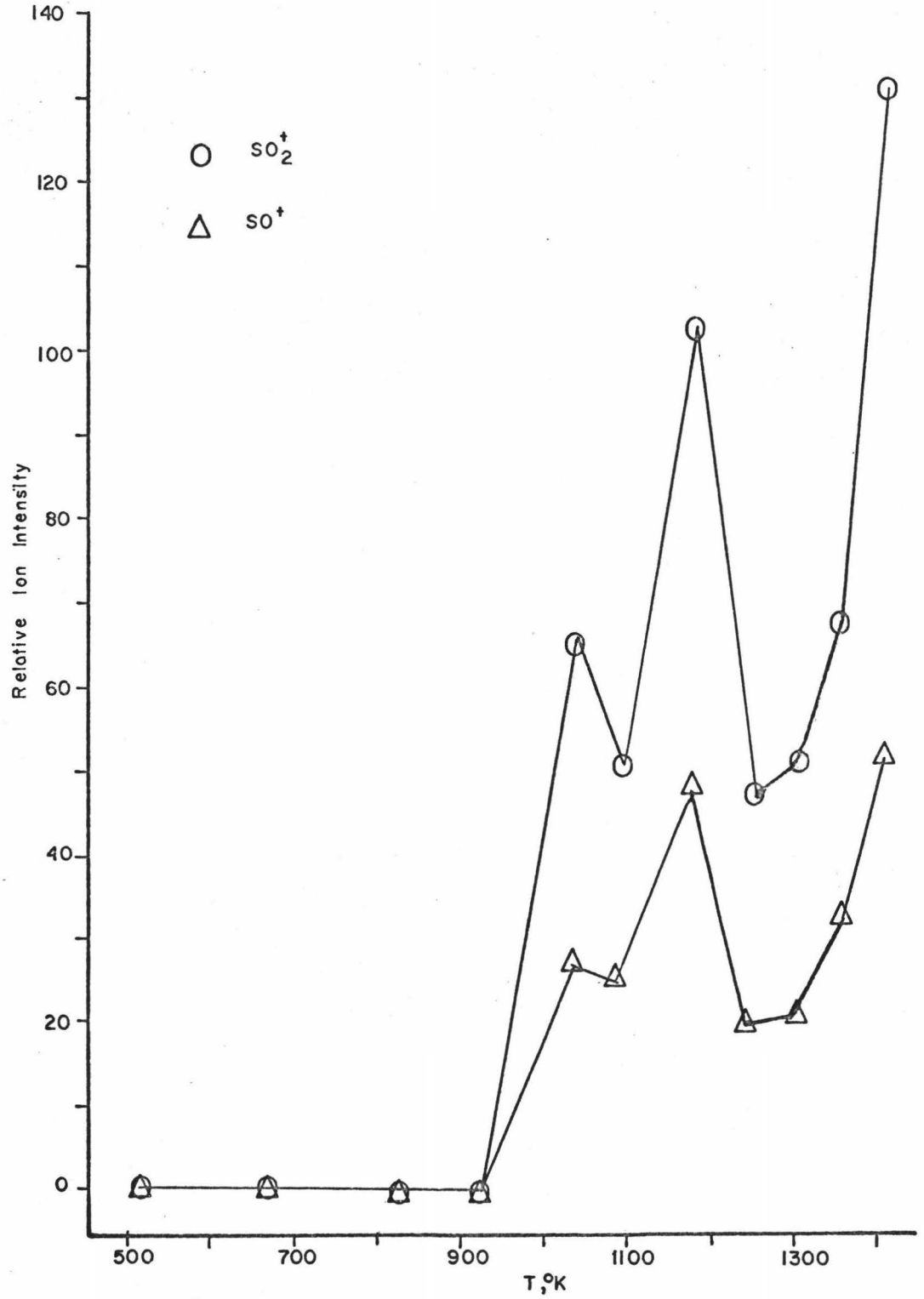

Figure 34: Sulfur Vapors from Lunar Rock # 12022,47

the same phenomena for alkali release. The temperature maxima were higher since troilite decomposes at higher temperatures.

The vapor pressures of the alkali volatiles are shown in Tables XV and XVI. These pressures will be used to discuss behavior of volatiles in the lunar environment in the theoretical section of this work. The major difference between these results and those for the terrestrial samples was the larger amount of non-elemental potassium vapor released in the low temperature range. Again, the release of alkalis was very similar to the total release found in the vacuum deposition studies. The potassium metal showed a higher relative vapor pressure than the sodium metal. At lower temperatures, there was very little sodium released compared to the amount of potassium vapors.

Table XVII summarizes the amount of potassium and sodium present in the samples of lunar material used in various experiments. The vapor deposition analyses were made by totaling the amount of alkali in the residue after heating plus the amount of alkali collected on the cold finger. The values in parentheses are separate analyses of the different fractions of the same sample. The lunar fine sample received from NASA contained only the particulates less than 1 millimeter in diameter. About 17 weight percent of the lunar fines were particles between 0.1 to 1.0 millimeters in size. The basaltic fragments were separated from the other coarse particles (breccias, anorthositic glass, glassy beads, and crystallites).

TABLE XV. PRESSURES OF ALKALI VOLATILES IN LUNAR ROCKS

12002,140 (Surface Rock)

Pressure (x 10^5/torr)

Ion(Mass)	1088°K	1163°K	1218°K	1283°K	1343°K	1398°K
K^+(39	1.55	7.18	11.0	16.9	19.2	17.2
NaO^+(39)	3.40	15.9	24.2	37.2	42.4	38.0
KO^+(55)	--	--	--	2.22	13.3	10.6
K_2O^+(94)	.843	1.72	2.42	6.36	9.97	9.18
K_2^+(78)	.702	2.10	1.69	5.42	10.4	12.4
Na^+(23)	.955	9.75	6.86	26.2	30.3	36.2
Na_2O^+(62)	.171	2.92	4.11	9.39	11.7	11.6
NaK^+(62)	.102	1.75	2.46	5.63	6.99	6.98
Na_2^+(46)	3.80	4.87	6.86	21.3	26.0	46.6

12002,144 (Internal Rock)

Pressure (x 10^5/torr)

Ion(Mass)	1093°K	1178°K	1233°K	1303°K	1353°K	1403°K
K^+(39)	8.11	10.9	16.2	34.8	25.9	10.0
NaO^+(39)	17.9	24.0	35.9	77.2	57.1	22.2
KO^+(55)	.670	--	4.73	--	6.83	5.55
K_2O^+(94)	1.04	--	--	6.21	6.20	--
K_2^+(78)	1.09	--	.857	--	5.54	2.01
Na^+(23)	24.6	19.8	14.0	42.2	15.0	--
Na_2O^+(62)	7.04	3.23	5.21	11.0	9.01	9.80
NaK^+(62)	4.24	1.94	3.13	6.63	5.40	5.87
Na_2^+(46)	6.42	3.06	9.30	14.0	20.1	31.1

TABLE XVI. VOLATILES IN 12022,47 (INTERNAL ROCK)

	Pressure (x 10^5/torr)					
Ion(Mass)	1093°K	1183°K	1248°K	1308°K	1358°K	1408°K
K^+(39)	8.84	19.5	6.90	27.7	40.6	32.0
NaO^+(39)	19.5	43.0	15.2	61.1	89.6	70.4
KO^+(55)	4.01	9.60	.364	11.0	31.8	8.27
K_2O^+(94)	1.39	3.12	3.30	6.97	11.0	3.93
K_2^+(78)	1.81	--	--	--	10.6	1.02
Na^+(23)	15.8	38.9	5.36	57.4	38.4	--
Na_2O^+(62)	5.12	12.3	6.00	19.3	7.73	2.49
NaK^+(62)	3.07	7.41	3.60	11.6	4.63	1.49
Na_2^+(46)	6.08	10.6	--	25.0	23.9	24.9
	(Troilite Decomposition)					
SO_2^+(64)	148.	536.	370.	549.	962.	2159.
SO^+(48)	91.2	308.	190.	281.	562.	1043.

TABLE XVII. ALKALI COMPOSITION OF LUNAR SAMPLES

Vacuum Deposition Samples

Sample	%K	%Na
12002,140(Surface Rock)	0.154	0.254
12052,34 (Surface Rock)	0.074(0.072)	0.327(0.416)
12070,164(Soil<.1mm)	0.124	0.194
12002,144(Internal Rock)	0.091	0.628
12002,47 (Internal Rock)	0.083(0.16)	0.602(0.488)

Lunar Fines #12070,164

Sample	%K	%Na
.1mm<Basalts<1.mm	0.660	1.57±0.16
.1mm<Residue-Basalts<1.mm	0.287	0.683±0.047
Soil<.1mm	0.124	0.194

Filings of Surface Rock #12052,63

Sample Description	%K	%Na
Separate Piece of Rock	0.140	0.352
Surface Layer, A	0.0990±.0064	1.531±.017
B, a Layer in from A	0.1099±.0070	1.660±.017
C, a Layer in from B	0.0879±.0059	1.211±.016

From the results of the alkali analyses, the high content of alkalis in the Apollo 12 fines, which has been generally commented upon, seems to be mainly a contribution of the basaltic fragments. The results of filing layers from a surface rock are also shown in Table XVII, which showed no significant gross alkali surface concentration detectable by this means.

These analyses were from small amounts of multi-component materials, but the range of alkali contents are in the same range of the values found by the Preliminary Examination Teams for the Apollo 11 and 12 materials (6,7). Generally, the surface materials and soil have higher potassium than the internal rocks. Most of the alkali in the soil fragments occurs in the coarse basaltic fragments, which would have been formed in some degree by potassium degradation of the parent lunar rocks, according to the theory being investigated here, and would show a high potassium content as a consequence. Tables XVIII through XXI show the quantitative data collected from the microprobe analysis of the regions of surface rock #12002, 144. These tables show average counts potassium or sodium for a stationary electron beam at various distances from the surface edge. The data at each point were averages of four 10 second period readouts on the X-ray ratemeters. Scans A through F were six arbitrarily chosen regions along a one centimeter surface edge. The other scans were for the thin section prepared from the same rock. These results represent two different slabs of the surface edge of rock #12002, 140. The reference edge

TABLE XVIII. AVERAGE COUNTS POTASSIUM IN THE FIRST SEVENTY MICRONS FROM THE SURFACE EDGE OF #12002,140

Scan #	Distance (in microns) 0	11.7	23.3 (29.2)	35.0	46.7	52.5	64.2	70.0
A	300	--	104	--	384	--	--	118
B	230	--	496	--	690	--	--	1068
C	296	--	85	--	25	--	--	9
D	242	--	413	--	373	--	--	553
E	994	--	1130	--	748	--	--	359
F	393	--	923	--	452	--	--	168
8(12)	104	44	36	30	--	22	--	26
16	46	57	47	46	--	58	--	44
18	2260	614	164	85	--	75	--	77
20	142	94	86	85	90	--	182	--
22,24	102	90	209	63	--	90	--	126
24 B	209	208	406	177	--	190	--	139
26 T	118	174	216	120	--	382	--	135
26 B	2018	1273	(609)	--	645	--	--	--
28	434	2595	108	85	--	174	--	246
30	90	96	87	115	--	278	--	390
32	169	158	134	2396	--	242	--	102

TABLE XIX. AVERAGE COUNTS POTASSIUM IN THE INTERNAL REGION OF #12002,140

Scan #	Distance (in microns)									
	87.5 (81.7)	105.	122.5 (116.7)	140.	157.5 (151.7)	175. (169.2)	192.5 (186.7)	210.	227.5	245.
A	--	430	--	117	--	--	--	63	--	--
B	--	112	--	132	--	32	--	--	--	263
C	--	10	--	3	--	--	--	58	--	--
D	--	661	--	658	--	--	--	207	--	--
E	--	108	--	80	--	775	--	--	--	1831
F	--	155	--	132	--	110	--	--	--	123
8(12)	--	26	--	18	--	17	--	21	--	--
16	39	--	88	--	40	--	80	--	44	--
18	97	--	124	--	385	--	169	--	--	--
20	(647)	--	(98)	--	(92)	--	(102)	--	--	--
22,24	125	--	216	--	86	--	1080	--	98	--
24 B	99	--	147	--	184	--	114	--	118	112
26 T	157	--	582	--	112	--	140	--	102	87
26 B	(244)	--	(488)	--	(980)	(710)	--	--	--	--
28	179	--	115	--	70	--	68	--	119	106
30	--	202	--	105	--	153	--	87	--	93

TABLE XX. AVERAGE COUNTS SODIUM IN THE FIRST SEVENTY MICRONS FROM THE SURFACE EDGE OF #12002,140

Scan #	Distance (in microns) 0	11.7	23.3 (29.2)	35.0	46.7	52.5	64.2	70.0
A	11	--	7	--	48	--	--	13
B	24	--	72	--	45	--	--	35
C	4	--	4	--	4	--	--	1
D	188	--	306	--	617	--	--	887
E	433	--	794	--	592	--	--	490
F	22	--	27	--	17	--	--	74
8(12)	238	117	188	168	--	86	--	97
16	317	488	364	334	--	373	--	411
18	204	78	100	69	--	92	--	75
20	188	104	98	110	114	--	112	--
22,24	58	82	464	106	--	73	--	81
24 B	126	119	176	129	--	236	--	120
26 T	96	140	124	82	--	134	--	67
26 B	271	652	(548)	--	375	--	--	--
28	120	113	93	127	--	326	--	195
30	81	93	117	102	--	78	--	44
32	164	265	139	231	--	719	--	103

TABLE XXI. AVERAGE COUNTS SODIUM IN THE INTERNAL REGION OF #12002,140

Scan #	Distance (in microns)									
	87.5 (81.7)	105.	122.5 (116.7)	140.	157.5 (151.7)	175. (169.2)	192.5 (186.7)	210.	227.5	245.
A	--	14	--	18	--	--	--	34	--	--
B	--	45	--	46	--	32	--	--	--	48
C	--	4	--	4	--	--	--	6	--	--
D	--	949	--	456	--	--	--	580	--	--
E	--	227	--	80	--	214	--	--	--	2595
F	--	494	--	445	--	11	--	--	--	670
8(12)	--	72	--	68	--	85	--	70	--	--
16	546	--	176	--	382	--	64	--	391	--
18	138	--	96	--	66	--	61	--	--	--
20	(104)	--	(86)	--	(106)	--	(104)	--	--	--
22,24	65	--	63	--	64	--	78	--	78	--
24 B	78	--	491	--	312	--	263	--	89	63
26 T	398	--	204	--	134	--	151	--	88	74
26 B	(342)	--	(128)	--	(179)	(117)	--	--	--	--
28	87	--	223	--	60	--	100	--	418	368
30	--	84	--	110	--	201	--	158	--	344

numbers refer to the number on the photographic map taken of the thin section prior to probe work. From this map, the location of the microprobe electron beam on the sample was possible.

Table XXII shows the results of comparing surface to internal regions of potassium and sodium by the "t-test" (Equations II-2 and II-3). The t values are those calculated from the data and the t' values are the statistical table values for n'+m' total determinations to the confidence level shown (108). Though the individual scans in from the surface edge did not indicate a clear-cut increase of potassium on the surface edge, statistically there was a definite difference between the surface edge and the internal regions of the lunar rock. By the use of the "t-test", there was a 90% or more chance that the higher potassium in the surface edge was significant, while the distribution of sodium was relatively uniform. Figures 35 and 36 summarize all the quantitative data collected by the microprobe. The figures show the variation of potassium and sodium at each point in from the surface edge. Also shown are the variations of surface regions of alkali compared to the internal regions and the standard deviations for the analyses.

Photographic electron backscatter and elemental X-ray intensity distributions for scans of over 200 locations on various regions of different samples were taken using the electron microprobe. At each location, pictures of sample topography and of alkali or silicon distribution were made.

TABLE XXII. t-TEST DATA

For Potassium

$\bar{x}$	σ_x	n	σ_z	n+m	t	n'+m'	t'	C.L.	i
348	505	88	426	158	1.88	120	1.66	90.0%	70
401	604	55	459	125	2.18	120	1.98	95.0%	35
414	587	44	433	114	2.33	60	2.30	97.5%	23.3
484	688	28	444	98	2.66	60	2.66	99.0%	11.7
479	643	17	387	87	2.47	60	2.30	97.5%	0

$\bar{y}$	σ_y	m
220	298	70

For Sodium

$\bar{x}$	σ_x	n	σ_z	n+m	t	n'+m'	t'	C.L.	i
189	189	88	267	158	0.66	120	1.29	80.0%	70
180	162	55	276	125	0.76	120	1.29	80.0%	35
179	168	44	286	114	0.70	60	1.30	80.0%	23.3
171	148	28	299	98	0.69	60	1.30	80.0%	11.7
150	116	17	310	87	0.80	60	1.30	80.0%	0

$\bar{y}$	σ_y	m
217	340	70

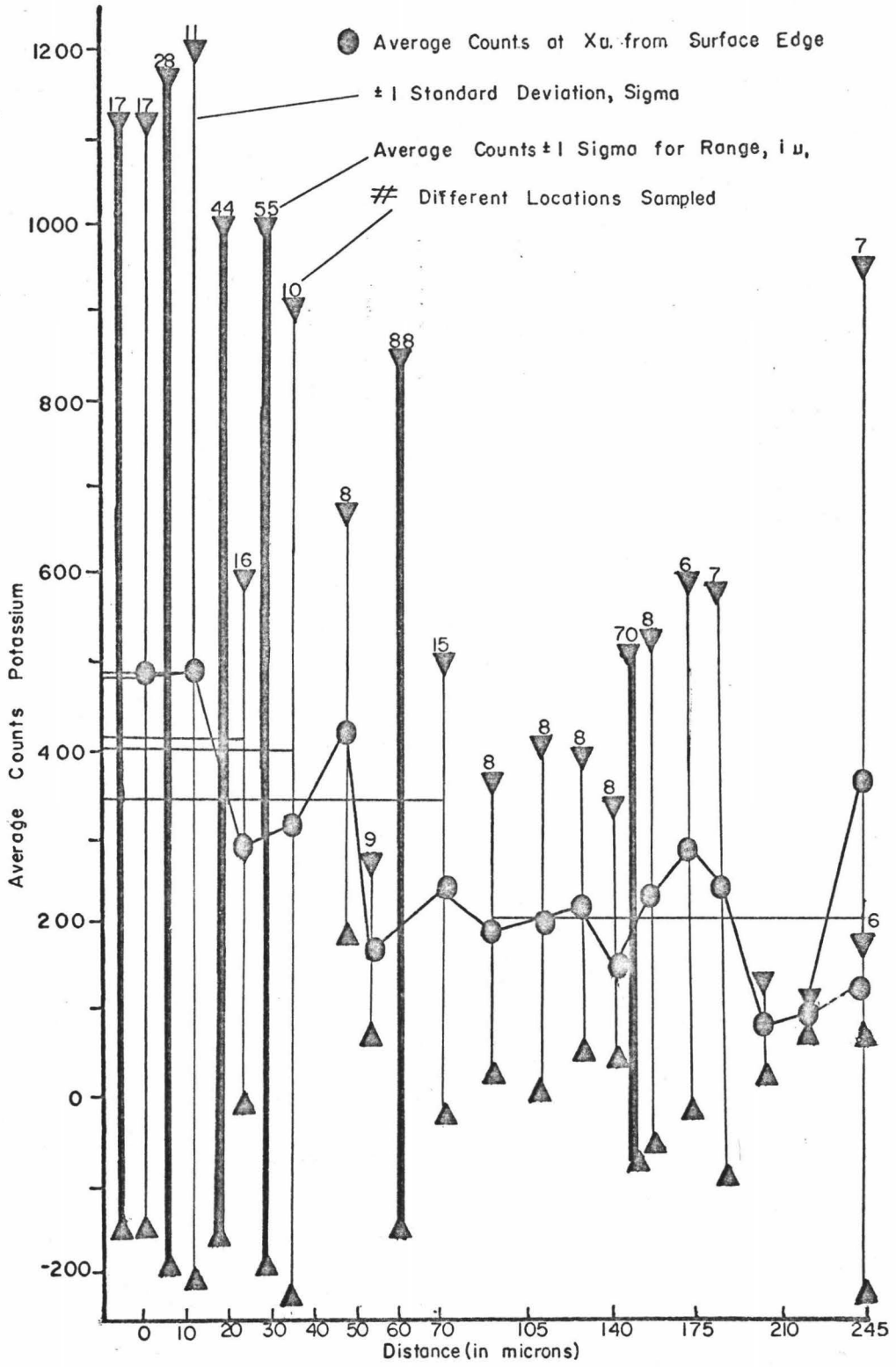

Figure 35: $\overline{\text{Counts}}$ K vs. Distance from Surface Edge

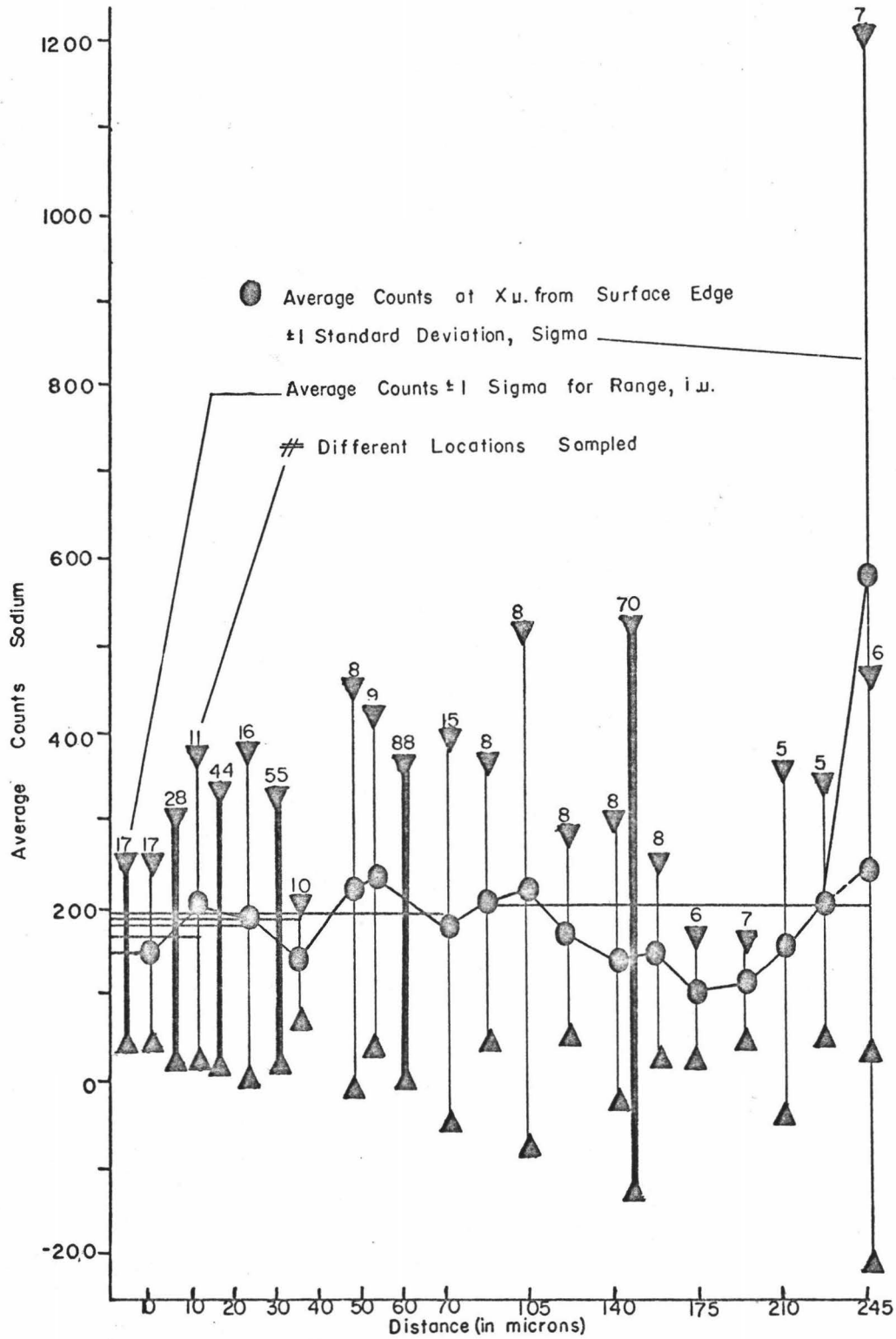

Figure 36: $\overline{\text{Counts}}$ Na vs. Distance from Surface Edge

Figures 37 through 42 are typical examples of the type of results found from the microprobe scans.

Figures 37 and 38 exemplify the surface build-up of potassium found on the lunar rock. Shown on the left hand side of the backscatter picture is the original surface edge of the lunar rock. The potassium scans reveal a definite surface concentration. Regions of scanning were arbitrarily chosen, but yet considerable areas of the surface edge had a large concentration of potassium. The sodium distribution was relatively uniform. This potassium concentration was unique to the original surface edge of the lunar rock. Freshly broken edges, sawed edges, and internal sections of the lunar rocks revealed a relatively uniform distribution of potassium and sodium. Visual, statistical and photographic observations of the surface edges showed a tendency for potassium to be concentrated in the first seventy microns from the surface edge. These concentrations were on the edges of the crystals at the grain boundaries, on surfaces of crystals along natural cracks in the sample, and along the undisturbed surface edge of the thin section.

Some investigators have suggested that this build-up may be due to a mesostasis-forming from late-stage solidification of potassium-rich glass interstitial to the polymineral structure of the rocks. If this were true, microprobe scans should reveal high silicon with high potassium. Contrary to this an anti-silicon correlation was found. Figure 39 shows an example of a surface region containing a heavy potassium concentration in

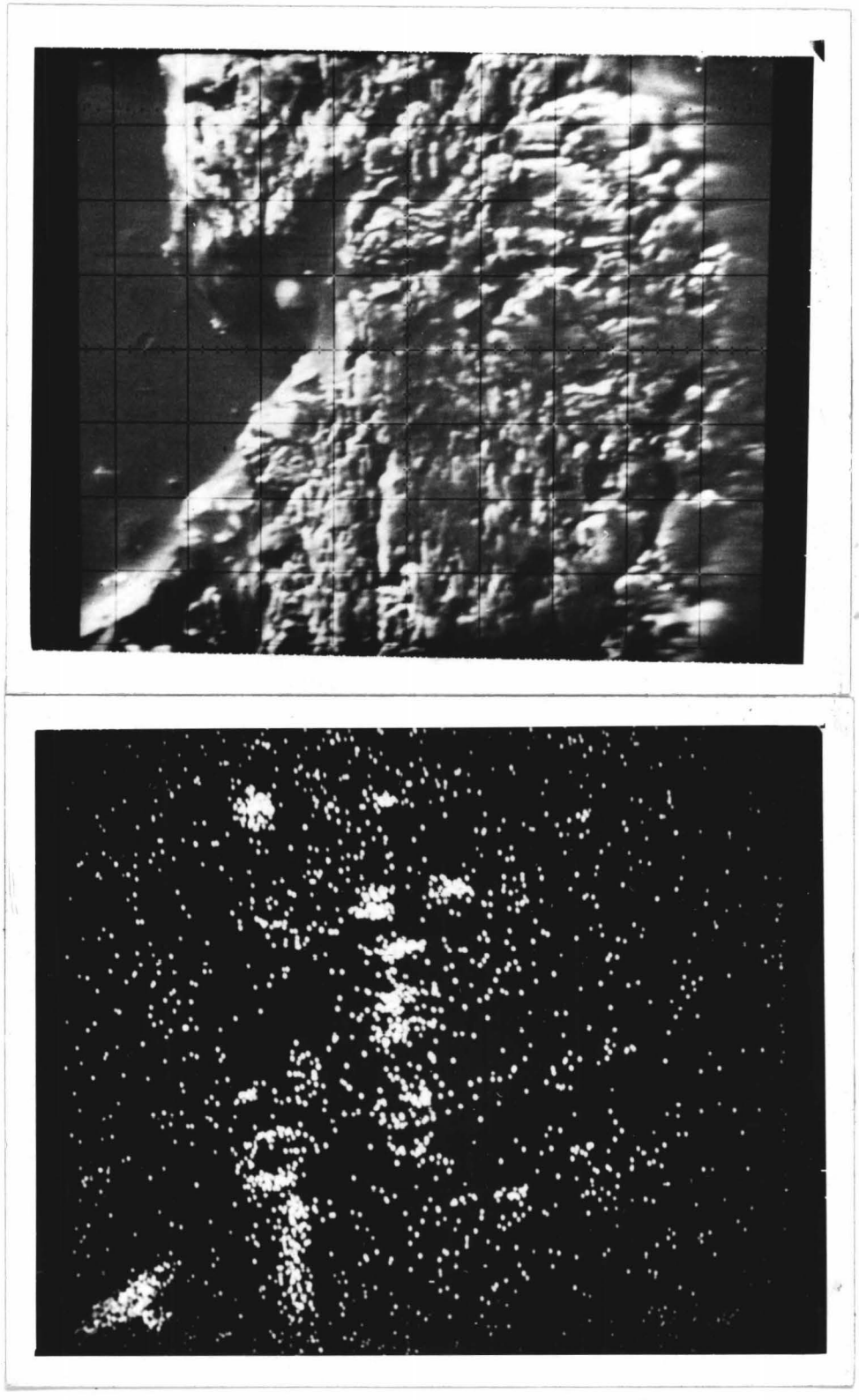

FIGURE 37. ELECTRON BACKSCATTER PHOTOGRAPH OF #12002,140 SURFACE EDGE AND ITS POTASSIUM DISTRIBUTION

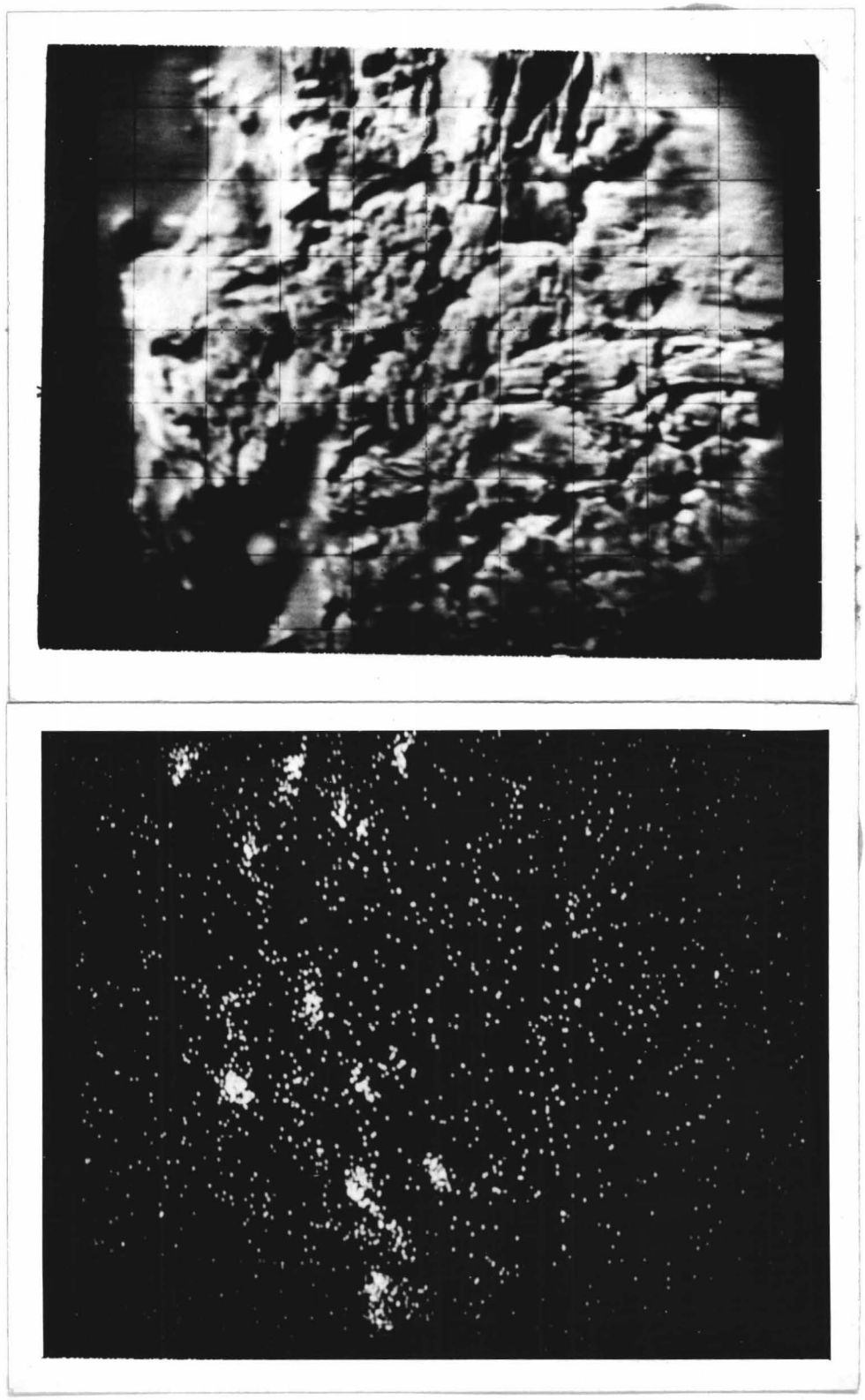

FIGURE 38. ELECTRON BACKSCATTER PHOTOGRAPH OF #12002,140 SURFACE EDGE AND ITS POTASSIUM DISTRIBUTION

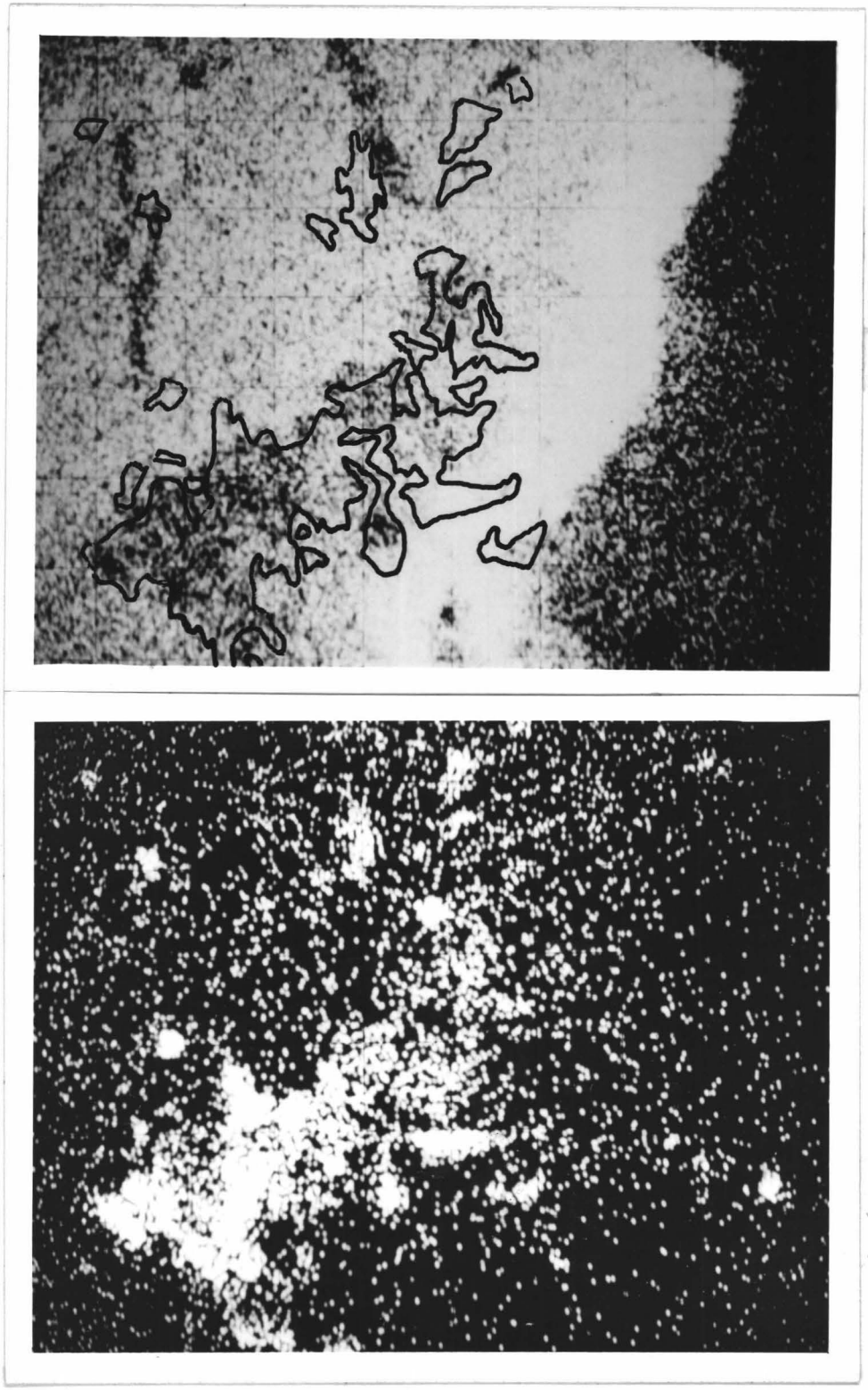

FIGURE 39. SILICON (TOP) AND POTASSIUM (BOTTOM) DISTRIBUTION OF #12052,34 SURFACE EDGE

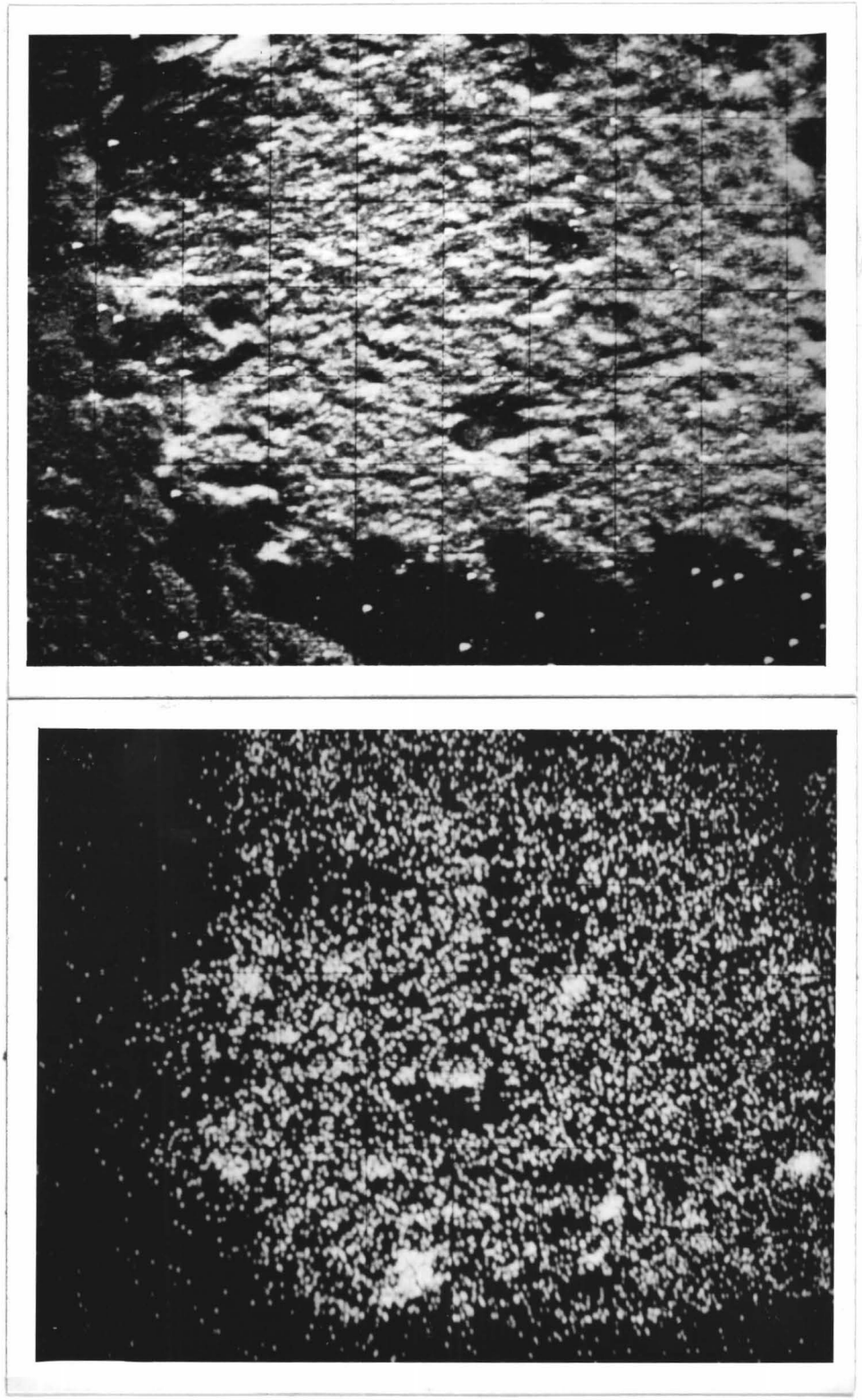

FIGURE 40. SECONDARY ELECTRON PHOTOGRAPH OF BASALT PARTICLE FROM LUNAR FINES AND ITS POTASSIUM DISTRIBUTION

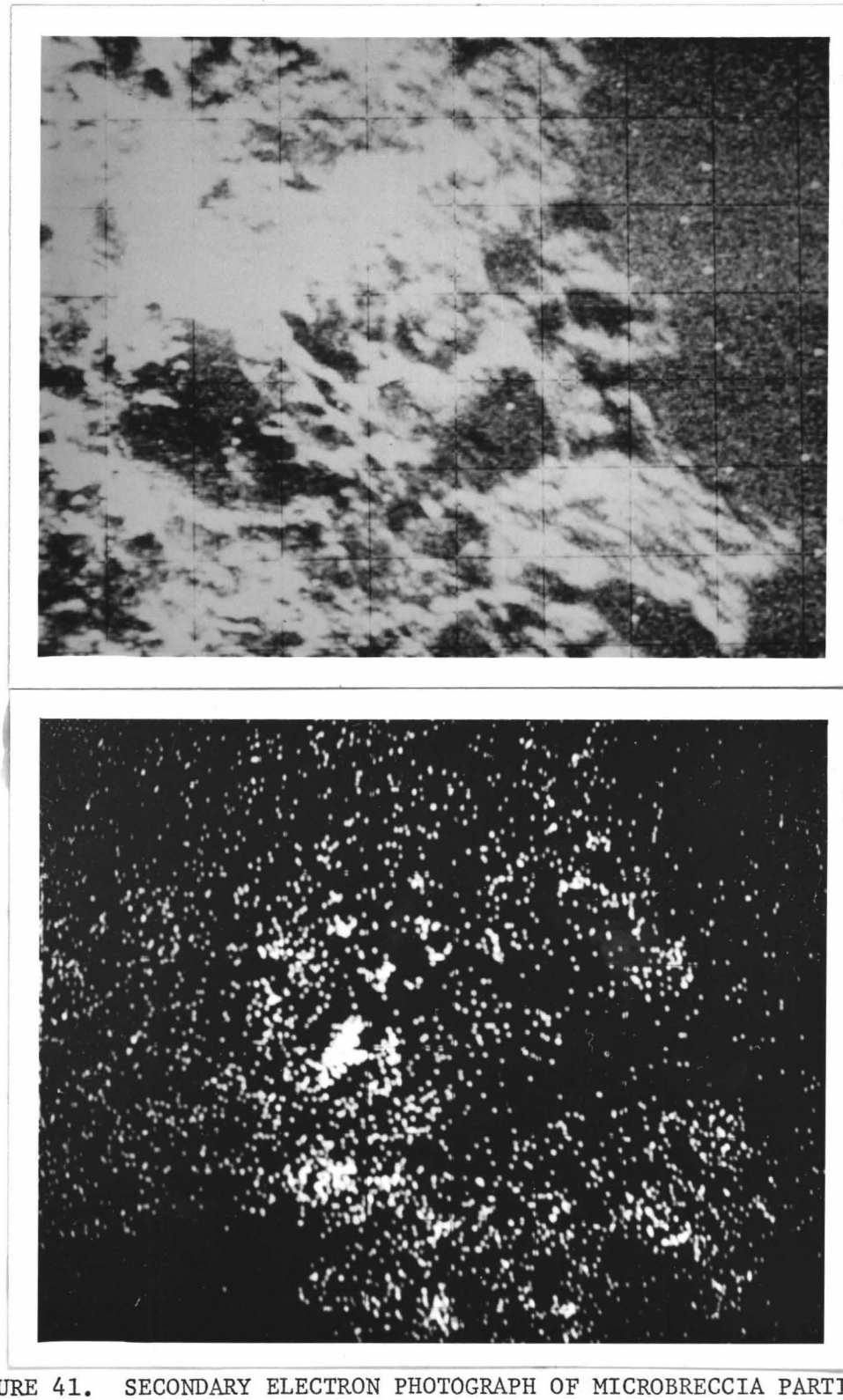

FIGURE 41. SECONDARY ELECTRON PHOTOGRAPH OF MICROBRECCIA PARTICLE FROM LUNAR FINES AND ITS POTASSIUM DISTRIBUTION

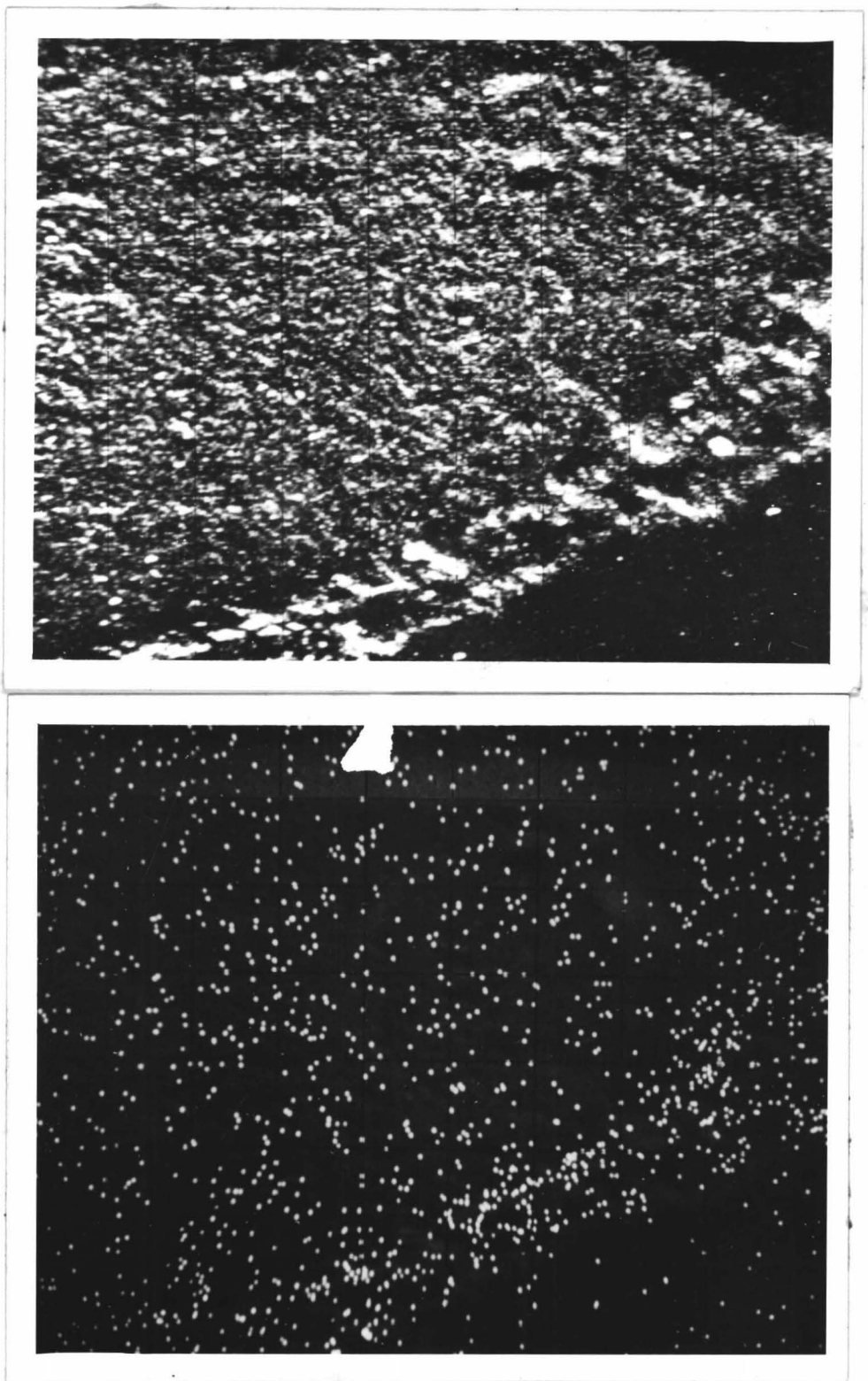

FIGURE 42. SECONDARY ELECTRON PHOTOGRAPH OF ANORTHOSITIC PARTICLE FROM LUNAR FINES AND ITS POTASSIUM DISTRIBUTION

regions where there was practically no silicon. In other cases, where there was a potassium build-up, the silicon was not any higher than other areas of the rock.

Lunar sample #12002, 140 contained an impact pit on its surface face. This impact pit was raised above the surface of the rock, glass-lined and surrounded by a "white halo" of material. Potassium and sodium scans of the crater pit showed very little alkali in the glass, but very heavy alkali in the "white halo." This was evidence on a small scale for localized melting by meteoritic impact leading to volatilization and condensation of volatile elements, which are the main processes in the hypothesis set forth here.

Figures 40, 41, and 42 are typical results from the microprobe analysis of particles in the 0.1 to 1.0 millimeter size region of the lunar soil. Figure 40 was a basaltic fragment which contained a very large concentration of potassium. Figure 41 is a microbreccia, which shows a few localized concentrations of potassium, but nowhere near the concentration found in the basaltic fragment. Microbreccias are rock fragments and powder that have been recompacted into an aggregate by pressure and/or high temperature. Figure 42 shows an anorthositic glass which was fairly common in the lunar soil and appears to be the one primary material in the soil foreign to the maria rocks. Some amounts of meteoritic material comprise the other foreign component in the lunar soil. Many individuals thought that this anorthositic component of the lunar soil might account for the high potassium content of the soils, but this

work has shown that the basaltic fragments contain the high potassium. This is in agreement with the chemical analysis of the soil in Table XVII.

An interesting observation of Figure 42 is that the lower edge of the anorthositic particle was very rough and porous. This rim contained a slightly higher potassium content which may be indicative of metasomatism by alkali vapor. The lunar soil particles generally showed evidence of a very slight potassium concentration on their edges.

Good topographic photographs of the lunar soil particles were seldom obtained due to surface irregularities, beam defocusing, and uneven carbon coatings that caused specimen overcharging in some areas. Overcharging causes large bright spots to appear in the photographs. In order to minimize large contrast differences, beam resolution must be sacrificed. These types of problems were encountered in the soil grain mounts because the porosity and friability of the particles did not permit fine polishing. Continued polishing usually led to dislodging of the lunar particles from the Bakelite mounts.

2. General Discussion of the Results

The remaining objective of this work is to answer the question does, or can, alkali metal degradation occur on the lunar surface. Investigations of the maria samples and observations about the lunar environment indicate conditions favorable for alkali degradation. Physical evidence suggestive of alkali attack was found in maria materials and has already been discussed. Some conclusions can be drawn from this work on the

Apollo 12 samples and the massive data collected during the Apollo 11 investigations.

The studies showed that significant amounts of alkali vapors could be released at sub-molten temperatures from the lunar rocks in a manner similar to the terrestrial basalts studied under a simulated lunar environment. The composition of these vapors was no different from that of the vapors found during volatilization from terrestrial basalts. There appeared to be no significant concentrations of non-alkali volatiles, at least in the case of silicon, nor is it known that these if so concentrated could cause comminution. Sample #12022, 47 (Figure 34) contained troilite, which decomposed into sulfur dioxide. These sulfur gases were released via paths which were probably similar to the transport mechanism found for alkalic removal.

Figure 43 compares some of the data for the vacuum deposition from lunar samples to that obtained from terrestrial rocks. Figure 43A shows the percent of potassium loss in a potassium-degraded HK-123 compared to a lunar surface and soil sample. Figure 43C shows the release pattern of sodium from these samples. Figures 43B and 43D are the percent of potassium and sodium loss during step-wise heating for an unreacted terrestrial and an internal lunar rock fragment. The curves are plotted on the same scale for comparative purposes.

Though less alkali was released, the lunar samples gave up a larger percentage of their alkali than the terrestrial samples. The various forms of release occurred at the same temperatures,

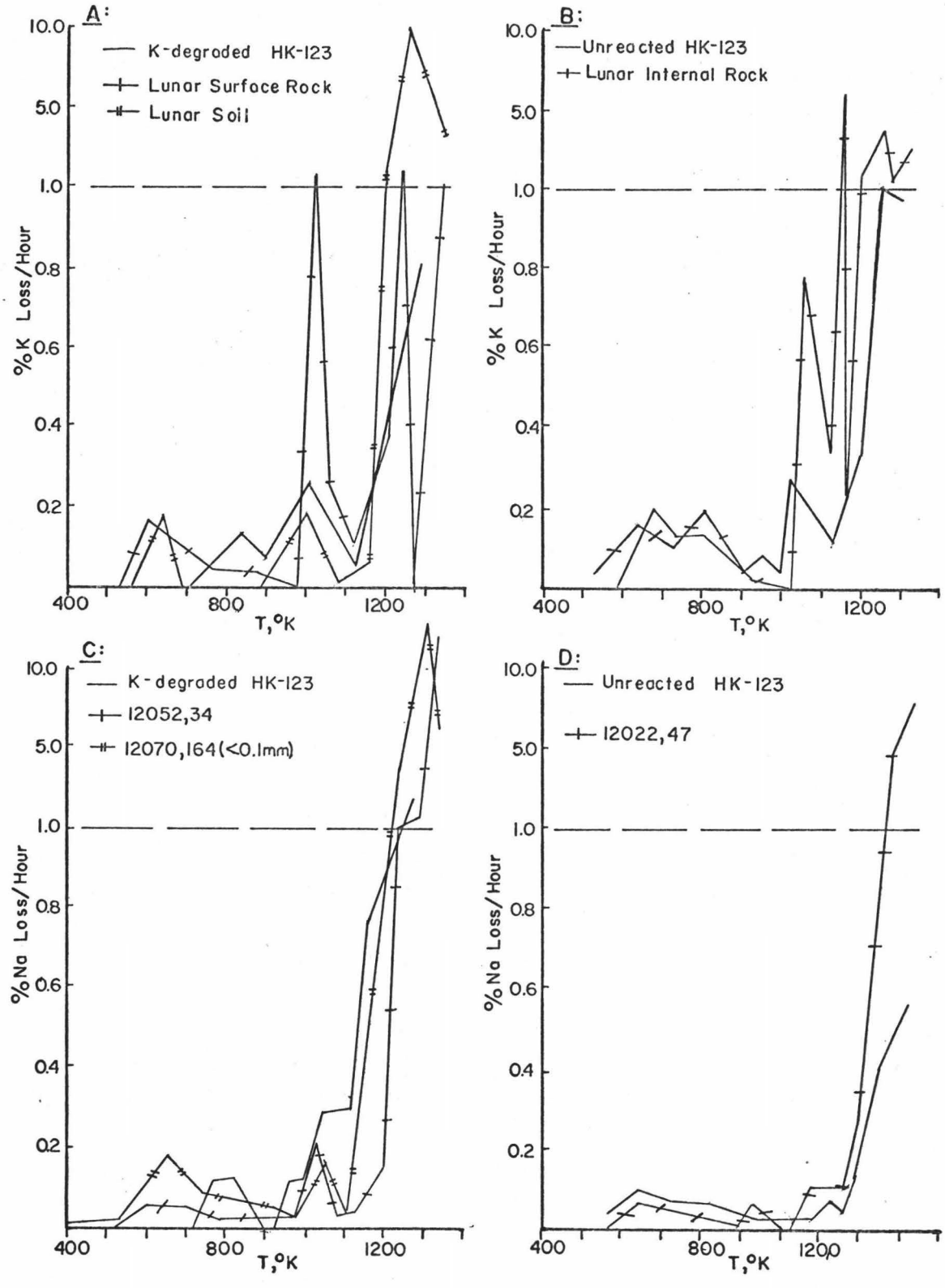

Figure 43: % Alkali Loss in Terrestrial and Lunar Samples

which was expected since the samples are similar mineralogically. The lunar surface (and to some degree the soil) sample had a significant peak in the intermediate temperature release region, while the internal sample did not have a significant peak at this temperature. The lunar internal sample and unreacted terrestrial basalt correlated very well for both the percent of alkali loss and the curve shape. The sodium release curves (Figure 43C) for potassium-degraded terrestrial basalt, lunar surface rock, and soil were also very similar. Though a lot more potassium was released in the degraded basalt (Figure 43A), the curves for percent loss were similar. An inordinate amount of potassium was released from the lunar soil sample in agreement with the larger quantity of potassium found from chemical analyses (Table XVII) and the microprobe work (Figures 37 through 42).

The statistical microprobe data (Table XXII) and the scans of lunar rocks and fines (Figures 37 and 38) revealed a concentration of potassium indigenous to original lunar surface edge regions. The potassium appeared to be associated with areas between crystals with little penetration. The anti-silicon correlation (Figure 39) for significant areas rule out the possibility that these potassium concentrations were due entirely to a mesostasis of potassium-rich glass. The high potassium content in the lunar fines was due to a disproportionately high concentration in the basaltic fragments present (Table XVII and Figures 40, 41, and 42). Scanning of an impact pit showed

alkalis present in the "white halo" (condensables from vacuum melting and volatilization) of the crater rim.

The evidence, though inconclusive, suggested that alkali metal degradation could very well be an important mechanism of erosion in the maria regolith. At the present time, no other lunar investigators are studying this phenomena. However, some supportive evidence for alkali attack can be found in the published results from the Apollo 11 samples which were collected at another maria region (Sea of Tranquillity). Apollo 12 samples are about 10^9 years younger than Apollo 11 samples, which indicates a considerable time of lunar activity causing maria formation (6,7). During these times considerable volatilization and condensation of volatiles may have occurred.

Asunmaa, Liang, and Arrhenius (119) found evidence of ablation, transport and accretion of solids, liquids and vapor on lunar rock and particle surfaces. Their microscopic studies of lunar particles showed evidence of surface melting from high velocity impacts leading to vaporization and re-ejection of the projectile materials. Solidified droplets on exposed igneous rock surfaces suggested the condensation of a liquid spray or vapor. They attribute the smooth surface features of particles to an erosion process other than meteoritic impact. Their studies of vesicles protected from weathering showed that these contained none of the vapor deposits. The vapor nucleation was associated with craters and paths of flow from impact events. These impact events would contribute to a temporary lunar atmosphere of volatiles which would recondense as vitreous and

crystalline particles, coatings, and overgrowths on surface materials.

Crozaz, et al. (120) found similar surface features on lunar particles. They feel that although impacts play a role, the dominant process for small-scale erosion was apparently not due to impact pitting. For rocks, they state that the erosion probably proceeds by removal of individual grains, with the regions around cracks and ridges being the most susceptible. The glasses, which were of considerable age, showed little evidence of erosion. On treatment with dilute acid, Hapke, et al. (121) found that the absorbed coating of fine particles dissolved away. On one grain, they found that the coating was high in magnesium and sodium. Several processes were considered to be producing a coating of the lunar particles. They were: sputtering deposition from solar wind, transient flash heating which melted only grain surfaces, redeposition of easily vaporized materials escaping from below the lunar surface, and deposition of lunar soil material vaporized by micrometeorite impacts.

Other studies substantiated some of the results of this work. Bulk analysis of lunar fines from an Apollo 11 sample revealed that potassium content was highest in the basaltic soil fragments (122). Lovering and Ware (123) reported that plagioclase minerals were zoned with up to 0.5% K_2O in their rims. McKay, et al. (124) examined the glass coating on the wall of a broken vesicle in a microbreccia and found about 5%

K_2O, which may be a condensate from impact melting. O'Hara and his colleagues (125) found that synthetic lunar-like materials heated in vacuum lost 2 to 4% potassium and sodium when held at 1200°C for 14 days. They conclude that maria materials may have been derived from alkaline basic magma with significant alkali loss during vacuum melting.

Further supportive evidence may be found when the results of the independent Apollo 12 investigations are coordinated, summarized, and made public. At the present time, evidence indicates that there were very definite processes that occurred at some stage of lunar surface history, which may have led to volatilization and redistribution of alkalis on the lunar surface. These studies have found that there are traces of surface concentrations of potassium on rocks, exposed to the lunar environment, but not on protected surfaces. The alkali release patterns of surface rocks were similar to those of alkali degraded terrestrial basalts. The basaltic soil fragments have higher potassium contents than the rocks, but appear to be simply degradation products of the lunar rocks. This would tend to substantiate a metasomatism-type comminution mechanism via internal regions of easy transport of alkali volatiles such as microcracks and grain boundaries.

The presence of only potassium may be attributed to several things. The volatilization products show most potassium to be elemental, while a lot of the sodium was diatomic. With the high concentration of potassium in the vapor phase, exchange for

sodium in the rocks would be favorable from an equilibrium standpoint. Thermodynamically, potassium vapor exchange of sodium in minerals is more favorable than the reverse process in minerals and the lunar rocks contain more sodium-bearing minerals than potassium-bearing minerals.

C. Theoretical Considerations

1. Alkali Vapor Forms

The theoretical feasibility of release of alkali from basalts should be possible by thermodynamic considerations. However, one is stymied by the lack of thermodynamic data for silicate minerals and the complicated system resulting from the many minerals in basalts. The results of this research and the observations of other investigators showed that alkalis are indeed released from basalts at elevated temperatures and decreased pressures. Hypothetically, assuming the alkalis arose from an alkali oxide somewhere in the silicate structure, some thermodynamic calculations of the equilibrium constants were made for the following reactions at 1000°K:

(1) $K_2O_{(c)} \rightarrow 2K_{(g)} + 1/2\ O_{2(g)}$ $\quad K_1 = 10^{-12}$

(2) $Na_2O_{(c)} \rightarrow 2Na_{(g)} + 1/2\ O_{(g)}$ $\quad K_2 = 10^{-17}$

(3) $K_2O_{(c)} \rightarrow K_{2(g)} + 1/2\ O_{2(g)}$ $\quad K_3 = 10^{-13}$

(4) $Na_2O_{(c)} \rightarrow Na_{2(g)} + 1/2\ O_{2(g)}$ $\quad K_4 = 10^{-16}$

(5) $2K_{(g)} \rightarrow K_{2(g)}$ $\quad K_5 = 0.48$

(6) $2Na_{(g)} \rightarrow Na_{2(g)}$ $\quad K_6 = 2.5$

The thermodynamic values of Bockris, et al. (126) and Stull and Sinke (127) were used for these calculations. These values are found in Appendix G. Other reactions of interest for which there was insufficient thermodynamic data were:

(7) $K_2O_{(c)} \rightarrow KO_{(g)} + K_{(g)}$

(8) $Na_2O_{(c)} \rightarrow NaO_{(g)} + Na_{(g)}$

(9) $K_2O_{(c)} + 1/2\ O_{2(g)} \rightarrow 2KO_{(g)}$

(10) $Na_2O_{(c)} + 1/2\ O_{2(g)} \rightarrow 2NaO_{(g)}$

(11) $K_2O_{(c)} \rightarrow K_2O_{(g)}$

(12) $Na_2O_{(c)} \rightarrow Na_2O_{(g)}$

(13) $Na_{(g)} + K_{(g)} \rightarrow NaK_{(g)}$

Using these equilibrium constants and conditions in the mass spectrometer or the lunar environment, some vapor pressures can be predicted for the elemental potassium and sodium vapors. Typical oxygen partial pressures in the mass spectrometer vacuum system were 2×10^{-6} torr and the lunar environment has an oxygen pressure of about 7.6×10^{-11} torr (25). For potassium, vapor pressures of $2.6 \times 10^{-5}(8.3 \times 10^{-8})$ torr can be expected in the mass spectrometer and $3.4 \times 10^{-4}(1.1 \times 10^{-6})$ torr in the lunar environment. The bracketed values are those values for sodium. Tables XV and XVI show pressures of about 10^{-5} torr for sodium and potassium release from the lunar rocks at approximately 1000°K. Thermodynamically, the release of potassium is much more favorable than sodium for these idealized reactions, but the lunar rocks contain more sodium than potassium (6,7) and would release larger amounts of sodium. However, it has already

been shown from the experimental results that there is a large relative release of potassium, which agrees with these thermodynamic calculations.

Looking at the other vapors found in the mass spectrometer studies, some conclusions can be made. Berkowitz, et al. (128) have shown that the vapor phase above lithium oxide contains an appreciable amount of Li_2O in addition to the constituent elements. They found some evidence of LiO, but not in the concentrations of the other vapor species. Probably most of the monoxide vapors detected in the mass spectrometer were ionic fractions of reactions in the ion source. The small amount of KO^+ detected indicates that most of the mass 39 component would be elemental potassium. Garelis and Thomson (115) reported significant diatomic sodium vapor present and no measureable diatomic potassium vapor over the alkali metals. Hicks (129) in his evaluation of the vapor pressures of alkalis and mercury, stated that potassium can be treated as an ideal monatomic gas, while the sodium vapor must be treated as a mixed component of monomer and dimer. The equilibrium constants given above show that dimeric potassium is not as favorable as dimeric sodium as a species found in the dissociation of alkali oxides at 1000°K. In fact, the dissociation of $Na_2O_{(c)}$ into dimeric sodium is more favorable than into elemental form. For the dimerization of the gaseous species, the sodium reaction is much more favorable. These considerations are in agreement with the findings from the mass spectral data of this research.

The existence of gaseous NaK is not very likely. No evidence of NaK existing in gaseous form could be found in the literature. This would require that sodium and potassium be volatilized from different minerals, or different oxides, into the gaseous state and then combined in vacuum, where large mean free paths exist.

2. Alkali Metasomatism

Earlier discussion indicated that alkali metasomatism could play an important role in alkali metal comminution. This process could occur in the lunar environment by the interaction of gaseous alkali vapor with feldspars according to the reaction:

$$NaAlSi_3O_8(\text{Albite})_{(c)} + K_{(g)} \rightarrow$$

$$KAlSi_3O_8(\text{Orthoclase})_{(c)} + Na_{(g)}$$

where the equilibrium constant, $K = Na_{(g)}/K_{(g)}$. Thermodynamic values are given in two forms. First, Clark (130) presents the silicate minerals as being formed from basic elemental oxides, while Krauskopf (131) presents feldspar values for formation from elements. These values are found in Appendix G. The calculated values of the equilibrium constants for both sets of values are shown in Table XXIII, which are the equilibrium ratios of sodium to potassium vapor at 500°, 1000°, and 1500°K for alkali metasomatism. Also found in Table XXIII is the sodium:potassium ratios for the pressures calculated from mass spectral values for the lunar and terrestrial rocks (Tables XII, XV, and XVI). Thermodynamically, potassium exchange is

TABLE XXIII. PRESSURE RATIOS OF SODIUM:POTASSIUM

(From Equilibrium Calculations)

Temperature in °K	Na:K Ratios from Clark's Values (129)	Na:K Ratios from Krauskopf's Values (130)
500	77000	120
1000	340	13
1500	43	5.5

(From Mass Spectrometer Studies

#12022,47		#12002,144		#12002,140		HK-123		Degraded HK-123	
°K	Na:K	°K	Na:K	°K	Na:K	°K	Na:K	°K	Na:K
1093	1.79	1093	3.03	1088	0.61	1073	1.89	1088	0.45
1183	1.99	1178	1.82	1163	1.36	1153	1.17	1148	0.72
1248	0.78	1233	0.86	1218	1.60	1233	0.80	1193	0.97
1308	2.07	1303	1.21	1283	1.55	1263	1.22	1248	1.16
1358	0.95	1353	0.58	1343	1.58	1338	3.07	1298	1.45
1408	0.003	1403	0.01	1398	2.10				

more favorable than sodium exchange. This is particularly true at low temperatures. Whichever equilibrium values are used, the sodium:potassium pressure ratios from the samples are all lower than the equilibrium values, because of the potassium enrichment in the vapor released from the basalts. The thermodynamic feasibility of this reaction and the presence of a potassium-rich vapor phase from the samples would strongly favor potassium vapor exchange for sodium in sodium-bearing minerals. Also, the crystallographic strain caused by this phenomena may play a part in rock disruption. The exchange would explain the greater effective rate of degradation from potassium vapor and the increased release of sodium from potassium-degraded samples.

3. The Behavior of Potassium in the Lunar Environment

Watson and his colleagues (31) discussed the general behavior of volatiles in the lunar atmosphere. Their basic assumption that the lunar atmosphere is so rarefied that molecular transport in the vapor phase can be described purely in terms of dynamical trajectories and their equations were used to present a view of the behavior of alkali vapor in the lunar atmosphere. These calculations will be made for potassium vapor, since it appears to be the most favorable vapor that could initiate comminution of lunar regolith materials. At 1000°K, the vapor pressure of potassium vapor was at least 10^{-5} torr for the lunar samples. Actually, the calculated values (Tables XV and XVI) were higher, but 10^{-5} torr will be

used for calculations as a conservative estimate of vapor distribution and behavior. Also, these pressures are for present-day materials and earlier discussion has indicated that there may have been considerably more alkali in the lunar environment during surface-forming processes.

The maximum rate of evaporation of material from a surface is given by:

$$E = p(M/2\pi RT)^{1/2} = 4.374 \times 10^{-5} p(M/T)^{1/2} \qquad \text{(III-1)}$$

where E is the maximum rate of evaporation in gm./cm^{2}sec., p is the vapor pressure in dynes/cm^2 (1 torr = 1.333 x 10^3dynes/cm^2), M is the molecular weight of the volatile, T is absolute temperature, and R is the gas constant. For potassium vapor at 10^{-5} torr and 1000°K, the maximum rate of evaporation from a basaltic surface would be 1.77 x 10^{15} molecules potassium/cm^2-sec. Assuming a 10 km. x 10 km. surface area at 1000°K for one month, the amount of potassium released into the lunar atmosphere would be about 7.6 x 10^7 moles. This gives an idea of the magnitude of volatiles released. Considerably larger areas (the marias) were probably involved in volcanic or localized melting, events on the moon. A reactive period of one month with temperatures of at least 1000°K are not unreasonable for volcanic processes (18,37).

For potassium vapor at 1000°K, the root-mean-square velocity would be:

$$V_{rms} = (3RT/M)^{1/2} = 0.798 \text{ km./sec.} \qquad \text{(III-2)}$$

This is considerably below the escape velocity from the moon (1.72 km./sec.). If one assumes, to avoid unnecessary complexity, that the reflection and emission of moles from the lunar surface can be adequately described by a cosine distribution, then the average jump time for potassium vapor at 1000°K is given by:

$$\bar{t} = 2 \times 0.86 \times W_{rms}/g = 828 \text{seconds} \qquad \text{(III-3)}$$

where g is the lunar surface acceleration of gravity, 1.67 cm./sec^2. For this velocity and average jump time, the average jump distance would be:

$$\bar{D} = 1/2\ V_{rms}\bar{t} = 330 \text{ kilometers.} \qquad \text{(III-4)}$$

Watson, et al. (31) discussed the possible escape mechanisms for molecules to leave the lunar atmosphere and escape into free space. The probability of a particle escaping on a single jump is

$$\alpha = 1 - e^{-\bar{t}/\tau} \qquad \text{(III-5)}$$

where $\bar{t}$ is the average jump time and τ is the decay time for many particle jumps. Opik and Singer (132) have formulated a mechanism for loss of heavy gas molecules (Kr, Ke) through electrostatic effects induced by photoionization resulting from solar ultraviolet radiation. If one uses their upper limit value of degree of ionization on in-flight particles to give the escape rate of electrons and accompanying ions, the τ value is approximately 10^6 seconds. Therefore:

$$\alpha_{\mu v} = 1 - e^{-828/10^6} = 8.3 \times 10^{-4} \qquad \text{(III-6)}$$

Herring and Licht (133) estimated the reduction in a lunar atmosphere due to the influx of high energy protons in the solar wind. Since protons are traveling with an assumed velocity of 10^8 cm./sec., they have an incident energy of about 5 keV. inasmuch as the energy necessary for escape of even the heavy volatiles from the lunar atmosphere is less than 5 eV, it is apparent that the energy transferred by proton-molecule impact is more than sufficient to cause escape. The molecular diameter of potassium is about 2×10^{-8} cm., hence the cross section for impact is about 4×10^{-16} cm.^{2} For a solar wind density of 10^2 particles/cm.^{3}, the decay time is equal to 2.5×10^5 seconds. This gives a probability of potassium vapor escape by high energy photons of:

$$\alpha_{h.e.p.} = 1 - e^{-828/2.5 \times 10^5} = 3.3 \times 10^{-3} \qquad \text{(III-7)}$$

Spitzer (134) has derived the equations for escape time for removal of molecules from the lunar environment by attaining a thermal velocity greater than the escape velocity. The equation of thermal escape is:

$$\tau = (6\pi)^{1/2}/3g \cdot Ve^{Y}/Y = 9.7 \times 10^4 \text{ sec.} \qquad \text{(III-8)}$$

where $Y = 3V_\infty^2/2V_{rms}^2$, V_∞ is the escape velocity (1.72 km./sec.) and V_{rms} is the root-mean-square velocity. Using these equations, one obtains an escape probability for potassium vapor at 1000°K by thermal excitation to be:

$$\alpha_{T.E.} = 1 - e^{-828/9.7x10^{44}} = 8.5 \times 10^{-3} \qquad \text{(III-9)}$$

These calculations were for potassium vapor at 1000°K, considerably below the melting temperature of basalts, but yet a large amount of vapor would be released into the atmosphere. These volatiles would be spread over vast distances (about 330 km.) and relatively few molecules will escape into space (< 1%). The average life-time for any particle to exist in the lunar atmosphere is about 10^7 seconds (135). This encompasses a period of approximately ten diurnal temperature cycles, giving ample opportunity for the alkalis to spread over the lunar surface, penetrate rocks, and initiate alkali comminution of regolith materials.

IV. SUMMARY

Mass spectrometric and vacuum deposition techniques have been developed to study the volatiles released from basalts under the conditions of a simulated lunar environment. The electron microprobe was used to investigate lunar materials for evidence of erosion by alkali vapor and to yield information on the degradation mechanism. An attempt was made to explain alkali degradation from the collected data.

Studies revealed that polycrystalline basalts will disintegrate into their component minerals with little chemical or mineralogic alteration at lunar day temperatures. These degradation products were similar in appearance to lunar regolith materials. Comminution seems to occur from penetration of alkali vapors along grain boundaries, and other internal surfaces, resulting in a breakdown of the boundary attractive forces between the various silicate structures. When basalts were heated, a potassium-rich alkali vapor phase was present. The evidence of exchange calculations on the basalt minerals indicates that low temperature alkali metasomatism might play a part in rock comminution.

The studies showed that alkali vapors were removed from regolith materials at sub-molten temperatures. The rarefied lunar atmosphere would insure widespread distribution of volatiles on the moon with little escape into free space. Observations of lunar rocks produced evidence that alkali metal degradation could very well have been an important process during maria formation. Unfortunately, the value and rarity of lunar samples prevented an extensive search for evidence of alkali metal comminution. Also,

only two isolated lunar maria have been sampled with little information about the lunar highlands or the rest of the lunar surface.

The problems of investigating lunar materials for evidence of a "primeval temporary alkali atmosphere" are sought with the same difficulties as the attempts of geochemists (136) to investigate the history of the earth's atmosphere by investigating present-day geologic samples, but magnified many times. First, considerable alterations of currently obtained lunar samples by solar wind and meteoritic impact may have occurred since the eroding events sometime during history in the course of two or three billion years. Second, the lack of a sufficient variety and number of samples, at present, gives us suggestive rather than conclusive evidence that such erosion has taken place.

This work has laid the basic framework for research which could progress in many directions. More work could be done with the improvement of the mass spectrometer design for faster and easier analysis. If more lunar samples became available, there is need for the collection of considerable additional volatilization data. The data could be collected to determine the trends of alkali release according to type of lunar mineral. Work with the electron microprobe shows the most promise for future investigations. An investigator should be extensively trained on the operation of the microprobe so that he can run samples himself without interfering with the work at the Naval Facility (106), and so that he can spend considerably more time on the microprobe, and use it to a greater degree of effectiveness than was possible for this study. The lunar

soils seem to hold the most promise for future investigations. This should include as much microprobe work as possible on the different types of soil fragments and an investigation of the source of the high potassium content in basaltic fragments. Scanning for elements other than alkali or silicon can be used to determine the types of minerals present and to look for signs of alkali metasomatism in alkali-bearing minerals. Ultimately, quantitative measurements with the microprobe of the distribution of the elements in lunar materials is another aspect that should be pursued. Also, more microprobe work is necessary on degraded-terrestrial basalts to further elucidate the alkali attack mechanism.

V. APPENDIXES

Appendix A

Lunar Rock #12002,140 Experiments

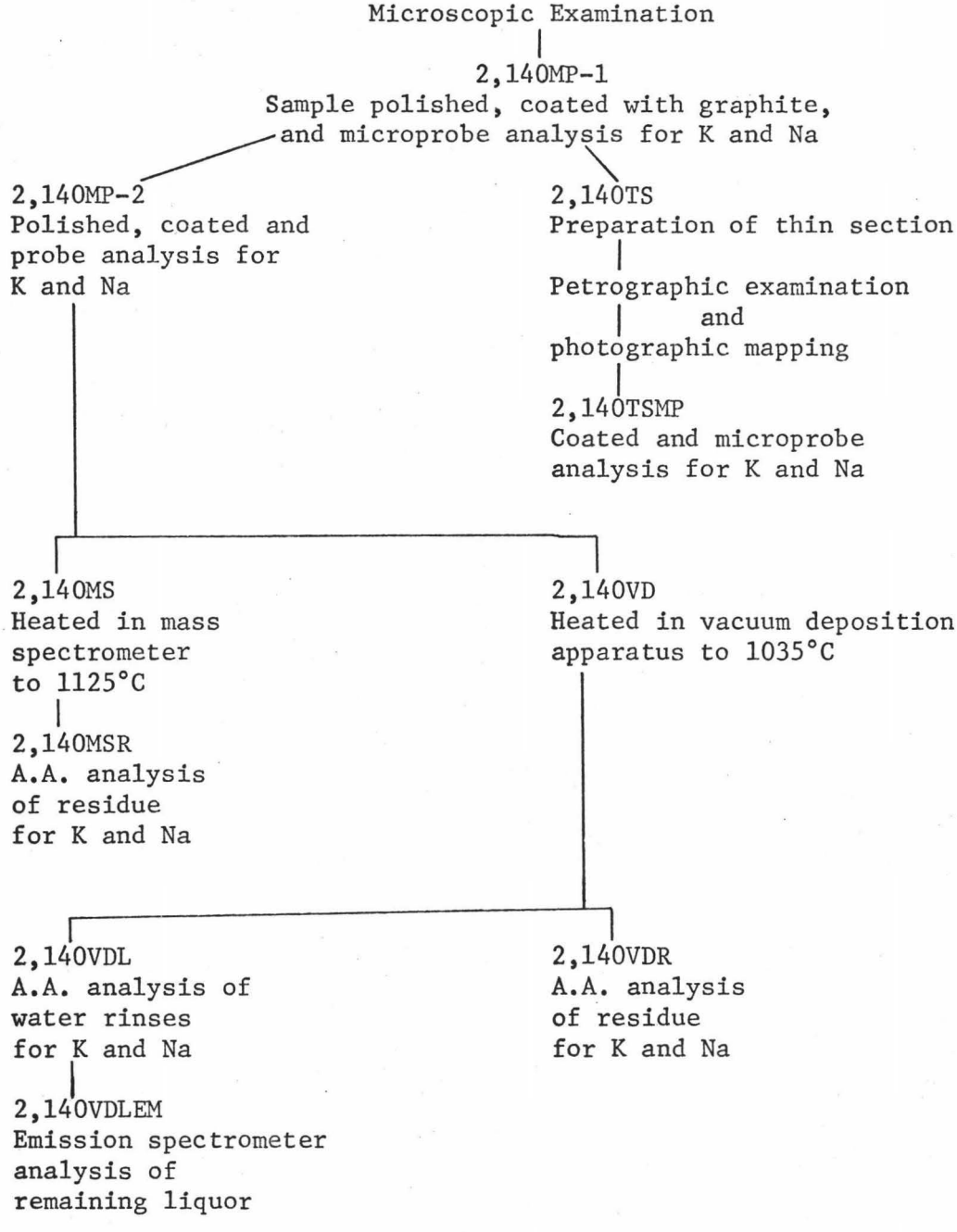

Appendix B

Lunar Rock #12002,144 Experiments

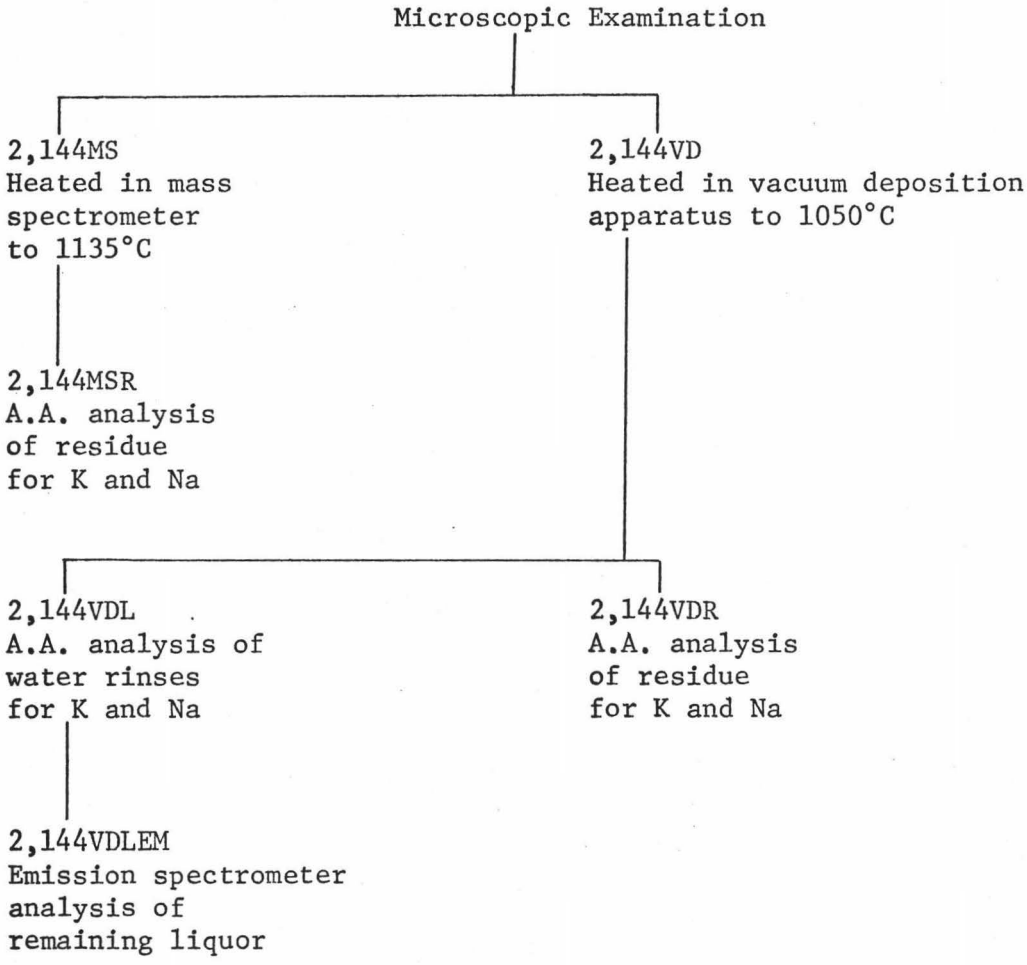

Appendix C

Lunar Rock #12022,47 Experiments

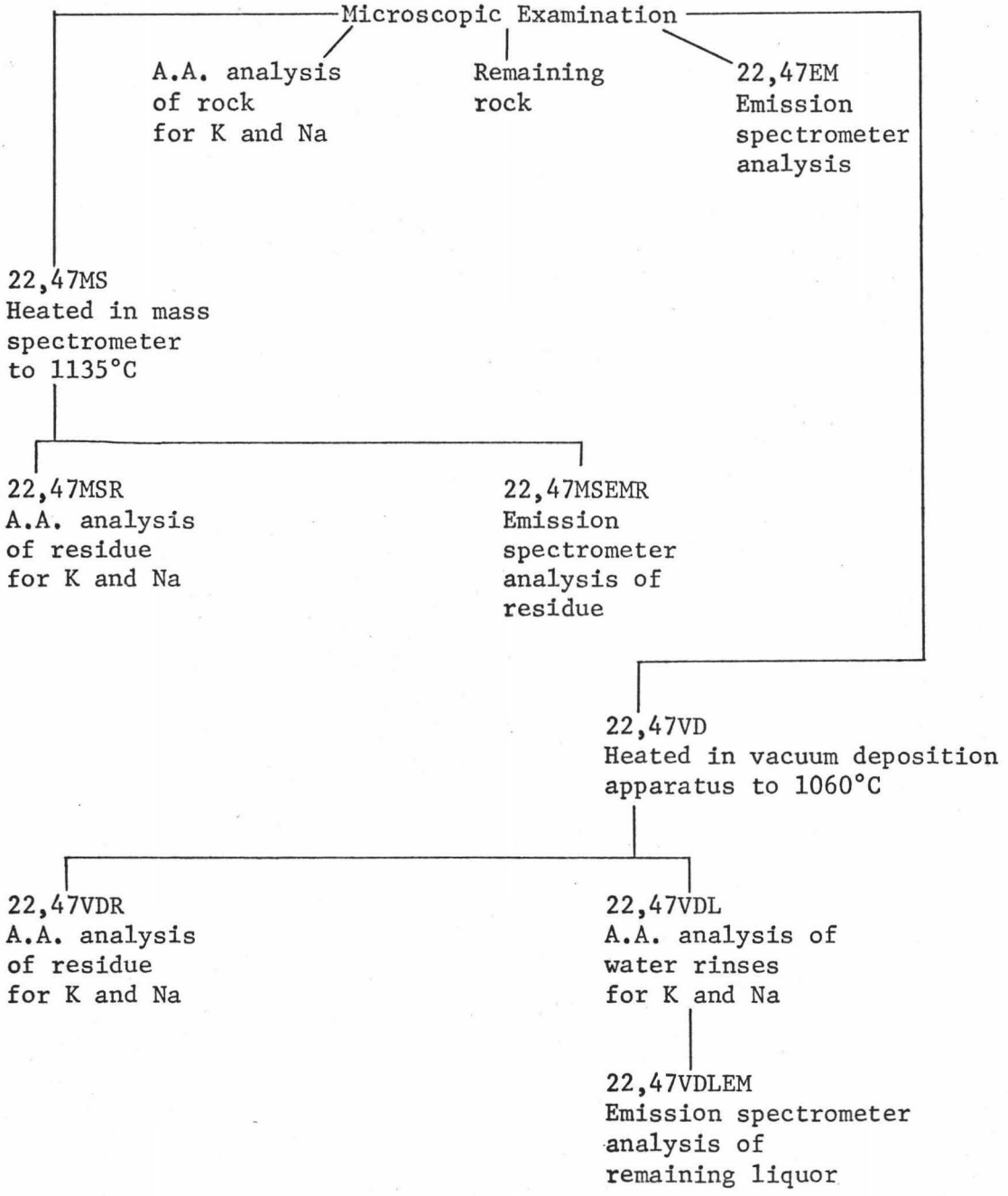

Appendix D

Lunar Rock #12052,34 Experiments

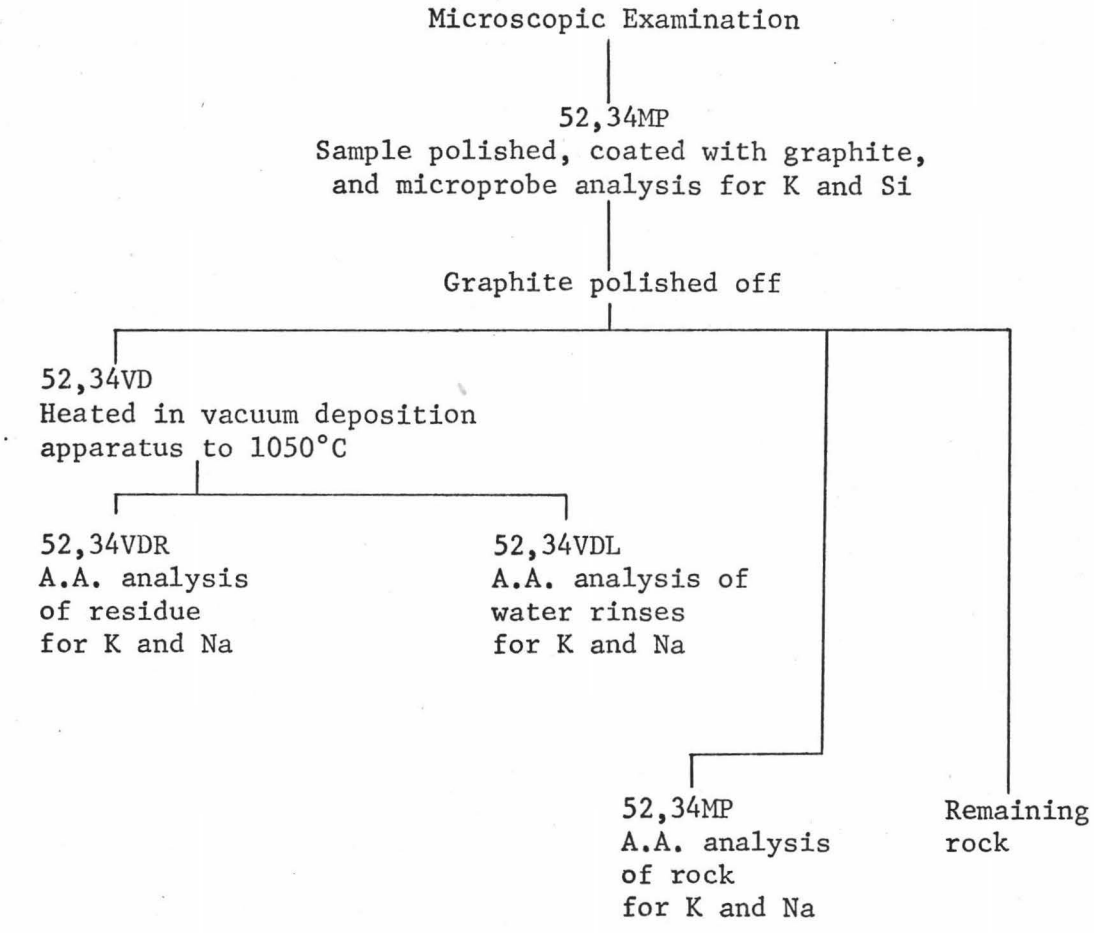

Appendix E

Lunar Rock #12052,63 Experiments

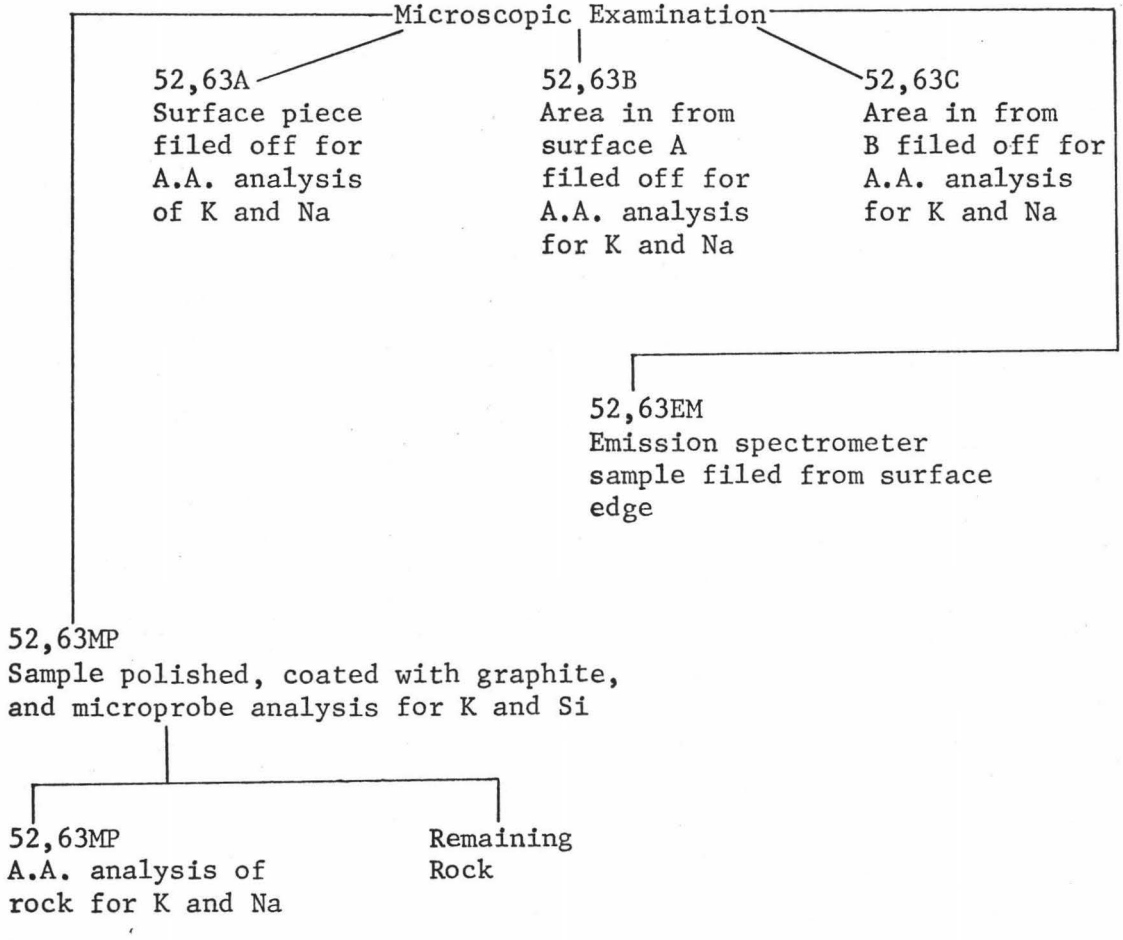

Appendix F

Lunar Fines #12070,164 Experiments

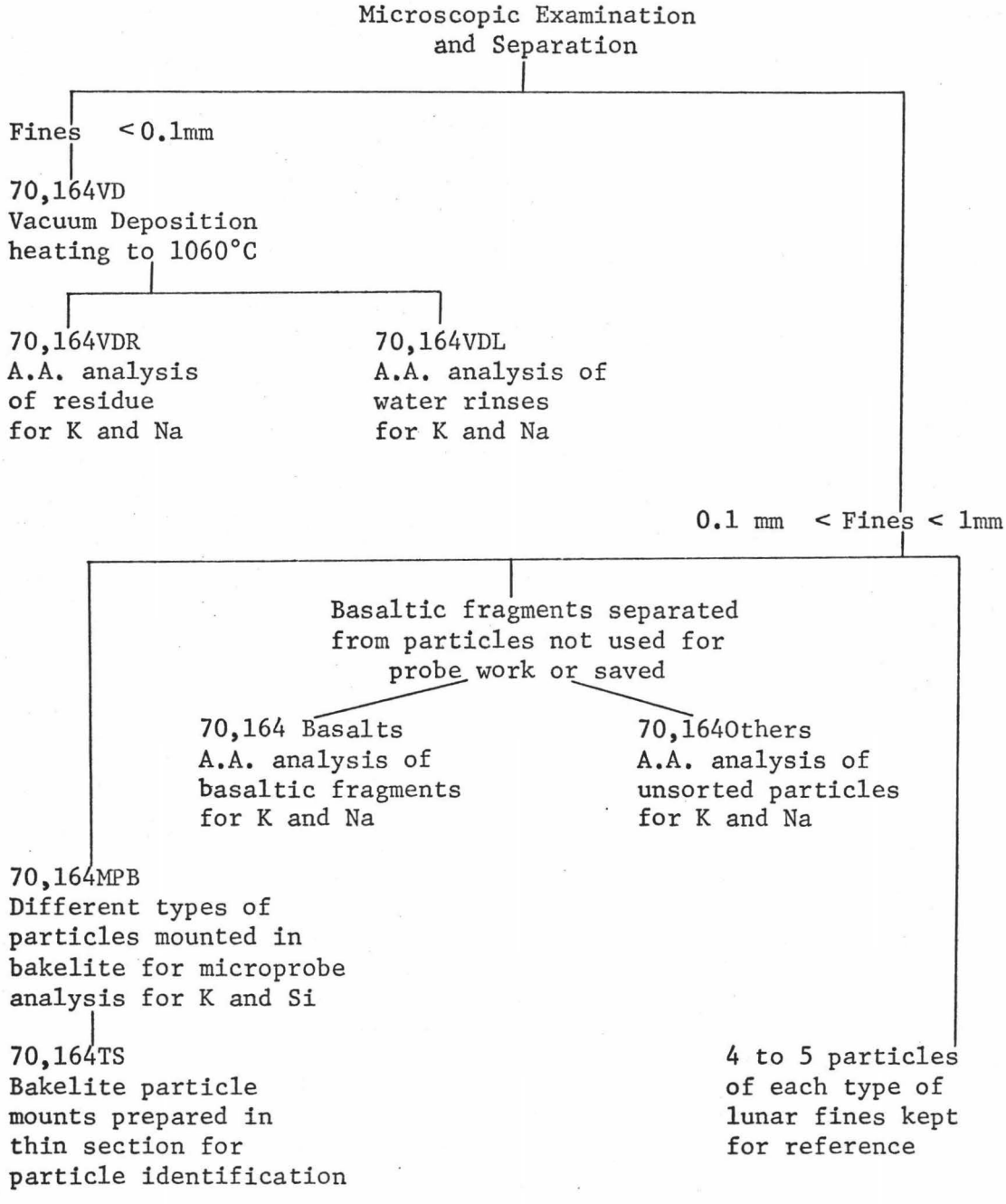

Appendix G

Values Used for Thermodynamic Calculations

Reference	Formula	-fef Values at 1000°K in cal./deg.-mole	$\Delta H_{f(298)}$ in kcal./mole
126	$K_2O_{(c)}$	30.2	-86.4
127	$K_{(g)}$	39.3	21.5
127	$K_{2(g)}$	64.3	30.6
126	$O_{2(g)}$	50.7	00.0
126	$Na_2O_{(c)}$	26.4	-99.4
127	$Na_{(g)}$	37.8	25.8
127	$Na_{2(g)}$	59.6	33.8
		S°_{298} Values in cal./deg.-mole	
130	$KAlSi_3O_{8(c)}$	52.5	-51.0
130	$NaAlSi_3O_{8(c)}$	50.2	-35.9
131	$KAlSi_3O_{8(c)}$	52.5	-947.5
131	$NaAlSi_3O_{8(c)}$	50.2	-938.8

VI. REFERENCES

1. Balwin, R. B., The Measure of the Moon, (1963), p. 188.

2. Trask, N. J., Rowan, L. C., "Lunar Orbiter Photographs: Some Fundamental Observations," Science, 158, 1529(1967).

3. Moore, H. H., Gault, D. E., "Current Tabulation of Data from Hypervelocity Impact Experiments," (Astrogeologic Studies Semiannual Progress Report, 26 Feb. to 24 Aug., 1961), p. 106.

4. Bjork, R. L., "Analysis of the Formation of Meteor, Arizona: A Preliminary Report," J. Geophys. Res., 66, 3379(1961).

5. Whipple, F. L., "The Dust Cloud About the Earth," Nature, 189, 127(1961).

6. The Lunar Sample Preliminary Examination Team, "Preliminary Examination of Lunar Samples from Apollo 12," Science, 167, 1325 (1970).

7. The Lunar Sample Preliminary Examination Team, "Preliminary Examination of Lunar Samples from Apollo 11," Science, 165, 1211 (1969).

8. Gold, T., "The Lunar Surface," Monthly Notices Roy. Astron. Soc., 115, 6, 585(1955).

9. Fairbairn, H. W., Hurley, P., "Radiation Damage in Zircon and Its Relation to Ages of Palezoic Igneous Rocks in Northern New England and Adjacent Canada," Trans. Am. Geophys. Union, 38, 99(1961).

10. Wehner, G. K., "Sputtering Effects on the Moon's Surface," J. Am. Rocket Soc., 31, 438(1961).

11. Fisher, D. E., "Space Erosion of the Grant Meteorite," J. Geophys. Res., 66, 1509(1961).

12. Gilvarry, J. J., "Nature of the Lunar Surface," Nature, 180, 911(1957).

13. Sutton, G., Unpublished Data (Hawaii Institute of Geophysics, Honolulu, Hawaii, 1970).

14. Green, J., "The Geology of the Lunar Base," (North American Aviation, Space, and Information Systems Division, Report 61-358, 1961).

15. Alter, D., "The Atmosphere of the Moon," Proceedings of the Lunar-Planetary Exploration Colloquium, 3, 1, 57(1962).

16. Ryan, J. A., "The Case Against Thermal Fracturing at the Lunar Surface," J. Geophys. Res., 67, 2549(1962).

17. Gilvarry, J. J., Origin and Nature of Lunar Surface Features," Nature, 180, 886(1960).

18. Naughton, J. J., "Discussion of Differences to be Expected between Lunar and Terrestrial Volcanism," Unpublished Report (Hawaii Institute of Geophysics, Honolulu, Hawaii, 1963).

19. Whipple, F. L., in Alperin, M., Gregory, H. F., editors, Vistas in Astronautics, (1959), p. 267.

20. Kuiper, G. P., in Alperin, M., Gregory, H. F., editors, Vistas in Astronautics, (1959), p. 273.

21. Kozynov, N. A., "Observation of a Volcanic Process on the Moon," Sky and Telescope, 18, 184(1959).

22. "Surveyor III, A Preliminary Report," (NASA Technical Report #SP-146, June, 1967).

23. "Surveyor V, A Preliminary Report," (NASA Technical Report #SP-163, December, 1967).

24. "Surveyor VI, A Preliminary Report," (NASA Technical Report #SP-166, March, 1968).

25. Lunar Sample Analysis Planning Team, "Summary of Apollo 11 Lunar Science Conference," Science, 167, 449(1970).

26. Gold, T., "Apollo 11 Observations of a Remarkable Glazing Phenomenon on the Lunar Surface," Science, 167, 1345(1969).

27. Buhl, D., Welsch, W. J., Rea, D. G., "Reradiation and Thermal Emission from Illuminated Craters on the Lunar Surface," J. Geophys. Res., 73, 5281(1968).

28. Gramlich, J., Unpublished Data (Hawaii Institute of Geophysics, Honolulu, Hawaii, 1970).

29. O'Hara, M. J., Biggar, G. M., Richardson, S. W., "Experimental Petrology of Lunar Material: The Nature of Mascons, Seas and the Lunar Interior," Science, 167, 605(1970).

30. Elsmore, B., Whitfield, G. R., "Lunar Occulation of a Radio Star and the Derivation of an Upper Limit for the Density of the Lunar Atmosphere," Nature, 176, 457(1955).

31. Watson, K., Murray, B. C., Brown, A., "The Behavior of Volatiles on the Lunar Surface," J. Geophys. Res., 66, 3033(1961).

32. Buettner, K.J.K., "The Moon's First Decimeter," Planet. Space Sci., 11, 135(1963).

33. Winborne, R. A., Personal Correspondence (Liquid Metals Communication System, Canoga Park, Calif., September, 1967).

34. Miller, E. C., Liquid Metals Handbook (Atomic Energy Commission, 1952), p. 144.

35. Stapleton, R. E., Snavely, W. H., "Alkali Metal Resistant Wire," (Atomic Energy Commission Liquid Metals Information Center, Report No. APL-TDR-64-42, April, 1964).

36. Tarpinian, M., "Effect of Molten Sodium on Thermal Insulation Specimens," (North American Aviation's Atomics International Division Report No. NAA-SR-Memo-1171, November, 1954).

37. Naughton, J. J., Barnes, I. L., Hammond, D. A., "Rock Degradation by Alkali Metals: A Possible Lunar Erosion Mechanism," Science, 149, 630(1965).

38. Wada, K., "Lattice Expansion of Kaolin Minerals by Treatment with Potassium Acetate," Amer. Mineral., 46, 78(1961).

39. Ernsberger, F. M., "Detection of Strength Impairing Surface Flaws in Glass," Proc. Roy. Soc. Ser. A., 257, 219(1960).

40. Grimley, R. F., in Margrave, J. L., editor, The Characterization of High Temperature Vapors, (1967), p. 196.

41. Chupka, W. A., Inghram, M. G., "Molecular Species Evaporating from a Carbon Surface," J. Chem. Phys., 21, 371(1953).

42. Honig, R. E., "On the Heats of Sublimation and Evaporation of Germanium," J. Chem. Phys., 22, 126(1954).

43. Drowart, J., Goldfinger, P., "Investigation of Inorganic Systems at High Temperature by Mass Spectrometry," Ange. Chem. Inter. Ed., 6, 581(1967).

44. Campbell, J. E., Sherwood, E. M., editors, High Temperature Materials and Technology, (1967), p. 63.

45. Carlson, K. D., in Margrave, J. L., editor, The Characterization of High Temperature Vapors, (1967), p. 115.

46. Langmuir, I., "The Vapor Pressure of Tungsten," Phys. Rev., 2, 329(1913).

47. Aldrich, L. T., "The Evaporation Products of Barium Oxide from Various Base Metals and of Strontium Oxide from Platinum," J. Appl. Phys., 22, 1168(1951).

48. Drowart, J., Honig, R. E., "A Mass Spectrometric Method for the Determination of Dissociation Energies of Diatomic Molecules," J. Phys. Chem., 61, 980(1957).

49. Honig, R. E., "Mass Spectrometric Study of the Molecular Sublimation of Graphite," J. Chem. Phys. 22, 1610(1954).

50. Porter, R. F., Schissel, P., Inghram, M. G., "A Mass Spectrometric Study of Gaseous Species in the Al-Al_2O_3 System," J. Chem. Phys., 23, 339(1955).

51. Buchler, A., Berkowitz-Mattuck, J. B., "Gaseous Metaborates, I. Mass Spectrometric Study of the Vaporation of Lithium and Sodium Metaborates," J. Chem. Phys., 39, 286(1963).

52. Kiser, R. W., Introduction to Mass Spectrometry and Its Applications, (1965), p. 37.

53. Hagstrum, H. D., "Ionization by Electron Impact in CO, N_2, NO, O_2," Rev. Mod. Phys., 23, 185(1951).

54. Dempster, A. J., "Positive Ray Analysis of Lithium and Magnesium," Phys. Rev., 18, 415(1921).

55. Bleakney, W., "A New Method of Positive Ray Analysis and Its Application to the Measurement of Ionization Potentials in Mercury Vapor," Phys. Rev., 34, 157(1929); 35, 139(1930).

56. Tate, T., Smith, P. T., "Ionization Potentials and Probabilities for the Formation of Multiply Charged Inos in the Alkali Vapors and in Krypton and Xenon," Phys. Rev., 46, 773(1934).

57. Nier, A. O., "A Mass Spectrometer for Routine Isotope Abundance Measurements," Rev. Sci. Instr., 11, 212(1940).

58. Inghram, M. G., Hayden, R. J., Handbook of Mass Spectrometry, (1954), p. 311.

59. Otvos, J. W., Stevenson, D. P., "Cross Sections of Molecules for Ionization by Electrons," J. Am. Chem. Soc., 78, 546(1956).

60. "Study of Mineral Stability in the Lunar Environment," (NASA Report No. N68-25579, June, 1968).

61. Muenow, D., Chemistry Seminar (University of Hawaii, Honolulu, Hawaii, 1969).

62. Wanless, R. K., Loveridge, W. D., Stevens, R. D., "Age Determinations and Isotopic Abundance Measurements on Lunar Samples," Science, 167, 479(1970).

63. Smales, A. A., Mapper, D., Webb, M.S.W., Webster, R. K., Wilson, J. D., "Elemental Composition of Lunar Surface Material," Science, 167, 509(1970).

64. Marti, K., Lugmair, G. W., Urey, H. C., "Solar Wind Gases, Cosmic Ray Spallation Products and the Radiation History," Science, 167, 548(1970).

65. Abell, P. I., Draffan, G. H., Eglington, G., Hayes, J. M., Maxwell, J. R., Pillinger, C. T., "Organic Analysis of the Returned Lunar Sample," Science, 167, 757(1970).

66. Reynolds, J. H., Hohenberg, C. M., Lewis, R. S., Davis, P. K., Kaiser, W. A., "Isotopic Analysis of Rare Gases from Step-wise Heating of Lunar Fines and Rocks," Science, 167, 545(1970).

67. Wedepohl, K. H., "Untersuchungen zur Geochemie des Zinks," Geochim. et Cosmochim. Acta, 3, 93(1953).

68. Fletcher, M. H., "Determination of Lithium in Rocks by Distillation," Anal. Chem., 21, 173(1949).

69. Edwards, G., Urey, H. C., "Determination of Alkali Metals in Meteorites by a Distillation Process," Geochim. et Cosmochim. Acta, 7, 154(1954).

70. Somorjai, G. A., "Mechanism of Sublimation," Science, 162, 755 (1968).

71. Shewnon, P. G., Diffusion in Solids, (1963), p. 164.

72. Rybach, L., Laves, F., "Sodium Diffusion Experiments in Quartz Crystals," Geochim. et Cosmochim. Acta, 31, 539(1967).

73. Frischat, G. H., "Sodium Diffusion in SiO_2 Glass," J. Amer. Cer. Soc., 51, 528(1968).

74. Frischat, G. H., "Tracer Diffusion of Sodium in the c-axis Direction of Quartz," Physica Status Solidi, 35, K47(1969).

75. Bowen, N. L., "Diffusion in Silicate Melts," J. Geol. XXIX, 295 (1921).

76. Wood, J. A., "Criticism of Paper by H. E. Suess and H. Wanke, 'Metamorphosis and Equilibrium in Chondrites,'" J. Geophys. Res., 72, 6379(1967).

77. Fisher, J. C., "Calculation of Diffusion Penetration Curves for Surface and Grain Boundary Diffusion," J. Appl. Phys., 22, 74 (1951).

78. Sippel, R. F., "Sodium Self-Diffusion in Natural Minerals, Geochim. et Cosmochim. Acta, 27, 107(1963).

79. Gerling, E. K., Levskii, L. K., Morozova, I. M., "On the Diffusion of Radiogenic Argon from Minerals," Geochem., 6, 551(1963).

80. Levskii, L. K., "Diffusion of Helium from Stony Meteorites," Geochem., 6, 556(1963).

81. Pepin, R. O., Reynolds, J. H., Turner, G., "2. A Comparison with Natural Argon in Its Diffusion," J. Geophys. Res., 69, 1406(1964).

82. Fechtig, H., Kalibitzer, S., in Schaeffer, O. A., Zahringer, J., editors, Potassium-Argon Dating, (1966), p. 74.

83. Fechtig, H., Kalibitzer, S., in Schaeffer, O. A., Zahringer, J., editors, Potassium-Argon Dating, (1966), p. 68.

84. Reichenburg, D., "Properties of Ion-Exchange Resins in Relation to their Structure. III. Kinetics of Exchange," J. Am. Chem. Soc., 75, 589(1953).

85. Moore, W. J., Physical Chemistry, (1964), p. 273.

86. Smith, J. V., "X-Ray Emission Microanalysis of Rock-Forming Minerals. I. Experimental Techniques," J. Geol., 73, 830 (1965).

87. Chao, E.C.T., James, O. B., Minkin, J. A., Boreman, J. A., Jackson, E. D., Raleigh, C. B., "Petrology of Unshocked Crystalline Rocks and Shock Effects in Lunar Rocks and Minerals," Science, 167, 644(1970).

88. Fredriksson, K., Nelen, J., Melson, W. G., Henderson, E. P., Anderson, C. A., "Lunar Glasses and Microbreccias: Properties and Origin," Science, 167, 664(1970).

89. Hargraves, R. B., Hillister, L. S., Otalora, G., "Compositional Zoning and Its Significance in Pyroxenes from Three Coarse-Grained Lunar Samples," Science, 167, 631(1970).

90. Richardson, K. A., McKay, D. S., Greenwood, W. R., Foss, T. H., "Alpha-Particle Activity of Apollo 11 Samples," Science, 167, 516 (1970).

91. Adler, I., Walter, L. S., Lowman, P. D., Glass, B. P., French, B. M., Philpotts, J. A., Henrich, K.J.F., Goldstein, J. I., "Electron Microprobe Analysis of Lunar Samples," Science, 167, 590(1970).

92. Castaing, R., "Electron Probe Microanalysis," Advances in Electronics and Electron Physics, 13, 317(1960).

93. Taylor, C. M., "Specimen Preparation Procedures of Minerals for Electron Microprobe Analysis," from his Ph.D. Dissertation (Stanford University, 1965).

94. Birks, L. S., Brooks, E. J., "Electron Probe X-Ray Microanalyzer," Rev. Sci. Instr., 28, 709(1957).

95. Birgensmith, C. E., Personal Correspondence (Materials Analysis Company, Palo Alto, Calif., May, 1970).

96. Seybolt, A. U., Burke, J. E., Experimental Metallurgy, (1953), p. 25.

97. Schaeffer, O. A., "An Improved Mass Spectrometer Ion Source," Rev. Sci. Instr., 25, 660(1954).

98. Moore, L. J., "Isotopic Fractional in Hawaiian Volcanic Gases," Ph.D. Dissertation (University of Hawaii, 1968).

99. Kiser, R. W., Introduction to Mass Spectrometry and Its Applications, (1965), p. 46.

100. Speiser, R., Naiditch, S., Johnston, H. L., "The Vapor Pressure of Inorganic Substances. II. B_2O_3," J. Am. Chem. Soc., 72, 2578(1950).

101. Buchler, A., Berkowitz-Mattuck, J. B., "Gaseous Metaborates. I. Mass Spectrometric Study of Lithium and Sodium Metaborates," J. Chem. Phys., 39, 288(1963).

102. Lewis, V., Chemist (Geochemistry Department, Hawaii Institute of Geophysics, Honolulu, Hawaii, 1970).

103. Bernas, B., "A New Method for Decomposition and Comprehensive Analysis of Silicates by Atomic Absorption Spectrometry," Anal. Chem., 40, 1682(1968).

104. "Operating Instructions for KSE-2 High Vacuum Evaporator," (Kinney Vacuum Division, New York Air Brake Company, Boston, Mass.).

105. "Operating Instructions for MAC Model 400S Electron Microprobe," (Materials Analysis Company, Palo Alto, Calif.).

106. Legrone, H., Metallurgist (Quality Evaluation Laboratory, Lualualei Naval Ammunition Depot, Oahu, Hawaii, 1970).

107. Fischer, R. B., Peters, D. G., Quantitative Chemical Analysis, (1968), p. 86.

108. Blaedel, W. J., Meloche, V. W., Elementary Quantitative Analysis, (1963), p. 627.

109. Hale, D., Director of Applies Sciences Division, (Quality Evaluation Laboratory, Lualualei Naval Ammunition Depot, Oahu, Hawaii, 1970).

110. Bastron, H., Barnett, P. R., Murata, K. J., "Method for the Quantitative Spectrochemical Analysis of Rocks, Minerals, Ores and Other Materials by a Powder D. C. Arc Technique," (U.S. Geol. Surv. Bull., 1084-G, 1960).

111. "Lunar Sample Information Catalog for Apollo 12," (Lunar Receiving Laboratory, Manned Spacecraft Center, Houston, Tex., January 12, 1970).

112. United States Department of the Interior, Geological Survey, Laboratory Report No. 66DC-7, (February 15, 1966).

113. Inghram, M. G., Porter, R. F., Chupka, W. A., "Mass Spectrometric Study of Gaseous Species in the B-B_2O_3 System," J. Chem. Phys., 25, 498(1956).

114. Eitel, W., The Physical Chemistry of Silicates, (1954), p. 283.

115. Garelis, E., Thomson, G. W., in Sittig, M., editor, Sodium, Its Manufacture, Properties, and Uses, (1956), p. 361.

116. Green, J. C., "Alkali Metasomatism in a Thermal Gradient; Two Possible Examples," J. Geol., 71, 653(1963).

117. Orville, P. M., "Alkali Ion Exchange Between Vapor and Feldspar Phases," Amer. Jour. Sci., 261, 201(1963).

118. Reid, A. M., Meyer, C., Harmon, R. S., Bulter, P., Brett, R., "Metallin Two Apollo 12 Igneous Rocks," Trans. Amer. Geophys. Union, 51, 584(1970).

119. Asunmaa, S. K., Liang, S. S., Arrhenius, G., "Primordial Accretion; Inferences from the Lunar Surface," Geochim. et Cosmochim. Acta, 34, 1975(1970).

120. Crozaz, G., Haack, U., Hair, M., Maurette, M., Walker, R., Woolum, D., "Nuclear Track Studies of Ancient Solar Radiations and Dynamic Lunar Surface Processes," Geochim. et Cosmochim. Acta, 34, 2051(1970).

121. Hapke, B. W., Cohen, A. J., Cassidy, W. A., Wells, E. N., "Solar Radiation Effects on Optical Properties of Apollo 11 Samples," Geochim. et Cosmochim. Acta, 34, 2199(1970).

122. Frondel, C., Klein, C., Ito, J., Drake, J. C., "Mineralogical and Chemical Studies of Apollo 11 Lunar Fines and Selected Rocks," Geochim. et Cosmochim. Acta, 34, 445(1970).

123. Lovering, J. F., Ware, N. G., "Electron Probe Microanalysis of Minerals and Glasses in Apollo 11 Lunar Samples," Geochim. et Cosmochim. Acta, 34, 633(1970).

124. McKay, D. S., Greenwood, W. R., Morrison, D. A., "Origin of Small Lunar Particles and Breccia from the Apollo 11 Site," Geochim. et Cosmochim. Acta, 34, 673(1970).

125. O'Hara, M. J., Biggar, G. M., Richardson, S. W., Ford, C. E., Jamieson, B. G., "The Nature of Seas, Mascons, and the Lunar Interior in Light of Experimental Studies," Geochim. et Cosmochim. Acta, 34, 695(1970).

126. Bockris, J.O'M., White, J. L., Mackensie, J. D., editors, Physico-Chemical Measurements at High Temperatures, (1959), p. 365.

127. Stull, D. R., Sinke, G. C., Thermodynamic Properties of the Elements, (1956), p. 157; p. 187.

128. Berkowitz, J., Chupka, W. A., Blue, G. D., Margrave, J. L., "Mass Spectrometric Study of the Sublimation of Lithium Oxide," J. Phys. Chem., 63, 644(1959).

129. Hicks, W. T., "Evaluation of Vapor Pressure Data for Mercury, Lithium, Sodium, and Potassium," J. Chem. Phys., 38, 1873(1963).

130. Clark, S. P., editor, Handbook of Physical Constants, (1966), p. 450.

131. Krauskopf, K. B., Introduction to Geochemistry, (1967), p. 657.

132. Opik, E. J., Singer, S. F., "Escape of Gases from the Moon," J. Geophys. Res., 65, 3065(1960).

133. Herring, J. R., Licht, A. L., "Effect of Solar Wind on the Lunar Atmosphere," Science, 130, 266(1959).

134. Spitzer, L., "The Terrestrial Atmosphere Above 330km," in Kuiper, G. P., The Atmosphere of the Earth and Planets," (1952), p. 239.

135. Johnson, F. S., Evans, D. E., Carroll, J. M., "Cold Cathode Gage (Lunar Atmosphere Detector)," (Preliminary Science Report of Apollo 12, NASA Report SP-235, June 1, 1970), p. 93.

136. Rutten, M. G., The Geological Aspects of the Origin of Life on Earth, (1962), p. 62.